Mechanistic insights into ALK inhibitor resistance in neuroblastoma

Inaugural-Dissertation

to obtain the academic degree

Doctor rerum naturalium (Dr. rer. nat.)

submitted to the Department of Biology, Chemistry, Pharmacy

of Freie Universität Berlin

by

Mareike Katharina Berlak

from Berlin, Germany

2022

This thesis was conducted in the group of Prof. Dr. med. Johannes Hubertus Schulte at the Charité - Universitätsmedizin Berlin, Institute for Paediatric Oncology and Haematology from November 2017 to November 2021. Parts of the following thesis were published in Molecular Cancer [1].

1st reviewer: Prof. Dr. Johannes Hubertus Schulte

2nd reviewer: Prof. Dr. Charlotte Kloft

Date of defence: 19th December 2022

Selbstständigkeitserklärung

Hierdurch versichere ich, dass ich meine Dissertation selbstständig verfasst und keine anderen als die von mir angegebenen Quellen und Hilfsmittel verwendet habe. Die Dissertation ist in keinem früheren Promotionsverfahren angenommen oder abgelehnt worden.

Mareike Katharina Berlak

Acknowledgements

First, I would like to express my gratitude to my supervisor *Prof. Dr. Johannes Hubertus Schulte* for the opportunity to work in his lab at the Charité and the possibility to write my PhD thesis under his supervision. I would like to thank him for the interesting scientific project, for constructive discussions, his support and the freedom to shape this project.

I am deeply thankful to *Prof. Dr. Charlotte Kloft* for the external supervision of my PhD thesis, her guidance, scientific discussions, and support.

I would also like to thank all members of the *AG Kloft* at the Department of Clinical Pharmacy and Biochemistry at the Institute of Pharmacy of the Freie Universitaet Berlin for their feedback on my project from a different scientific perspective. I would especially like to thank *Dr. Johanna Seger* for being a very supportive ˈgo-to-personˈ within the AG Kloft, for her guidance and reviewing this dissertation.

Furthermore, I would like to thank *Prof. Dr. Michael Boettcher* for being my CRISPR mentor, for his great support during my CRISPR screening projects, analysis of the CRISPR knockout screen data and especially for inspiring me.

Thanks to *Dr. Mathurin Dorel,* for computational modelling using STASNet and both, *Prof. Dr. Nils Blüthgen* and *Dr. Mathurin Dorel* for a very fruitful, inspiring, and educational collaboration.

Special thanks to all former and current members of the Schulte lab, who created a welcoming and supportive environment. Thank you, *Aleix*, for your support on RNA isolation and qPCRs as well as for having a great laugh! A huge thank you goes to *Annika* for emotional, scientific and lab support, for always taking the time to help or discuss, for being such a lovely person and for not judging me for my cola, crisps and croissant consumption in stressful times. You always found a way to make me smile.

Thank you, *Louisa* and *Kathi*, for being great office mates during the last months in the Schulte lab and *Kath*i for making weekends in the lab less lonely.

I would also like to thank *Filippos Klironomos, PhD* and *Joern Toedling, PhD* for their bioinformatic support. Thank you, *Joern*, for assisting me in learning *R*, for your important advice in scientific and non-scientific questions, for your moral support and encouragement and for your valuable input on my thesis.

A big thank you to all former and current members of the Eggert group for a cooperative and fun work atmosphere. I would like to thank especially *Prof. Dr. Angelika Eggert* herself for her scientific advice and connecting me with the scientific community. Many thanks to *Prof. Dr. Anton G. Henssen* for his great support on the Molecular Cancer manuscript and for encouraging me to further investigate scientific questions even in downbeat times.

Thank you, *Dr. Nicole Huebener*, for always finding financial ways to enable me to pursue my project and for sharing with me the greatest hiking trails.

I am deeply thankful to my former fellow PhD students *Laura*, *Kerstin* and *Birte* without whom it wouldn't have been half as fun. Thank you for your emotional support, for great hours in tissue culture, your scientific input and your honest joy in times of successes and compassion when things didn't work out. Thank you, *Birte*, for reviewing the present thesis and your helpful input.

I would like to express my deep gratitude to *Dr. Falk Hertwig* for being my mentor. Thank you for your endless support during my PhD life and beyond. I am deeply grateful for your patience, for hearing my ideas and pushing me into the right directions. Thank you for inspiring and believing in me. Philosophising about research with you during coffee breaks brightened up my day.

Furthermore, I would like to thank my friends for their support and for taking my mind off work, especially *Marlene*, *Sekina*, *Robin*, *Asja*, *Safak* and *Stephan*. Thank you for your emotional support and for being great friends.

To my *parents*: Thank you for your endless support during my studies, for always being there for me and for promoting my interest in science. Thank you for making my journey possible.

Finally, and most importantly, I want to thank my wife *Hannah*, who supported me in every way imaginable. I am deeply grateful for your understanding and patience. Thank you for bearing my moods, for taking care of me, for always having my back and for always believing in me.

For my grandparents

Georg, Rosmarie and Gisela.

Abstract

Anaplastic lymphoma kinase (ALK) is a driving oncogene in neuroblastoma and mutated in 8% - 10% of neuroblastoma cases. Despite high-risk neuroblastoma patients being treated with an intensive multimodal therapy, up to 60% of these patients relapse and the 10-year overall survival rate for high-risk cases is less than 40%. Therefore, targeted therapies are under investigation for paediatric use and might be considered as first-line therapy. Many cases of acquired therapy resistance to targeted therapies have been reported, including cases during paediatric clinical trials of ALK inhibitors. Hence a deeper understanding of resistance development is required and investigated within this thesis.

The first part of this thesis focused on the identification of genes associated with ALK inhibitor (ALKi) resistance using *in vitro* neuroblastoma systems. A CRISPR/Cas9 knockout screen in the *ALK*-mutated neuroblastoma cell line SH-SY5Y identified the tumour suppressor gene *NF1* to be associated with resistance to the ALK inhibitors ceritinib and lorlatinib. The hypothesis, whether a loss of *NF1* can confer ALKi resistance in *ALK*-mutated neuroblastoma was investigated by generating isogenic *NF1* knockout (KO) models using the CRISPR/Cas9 system in respective neuroblastoma cell lines. It was observed, that an *NF1* KO leads to an ALKi-resistant phenotype as well as increased RAS/MAPK pathway signalling.

Moreover, gene alterations were also investigated in tumour and liquid biopsy samples of patients with relapsed, *ALK*-driven neuroblastoma, who have been treated with ALK inhibitors in paediatric clinical trials. These patients had initially responded well to the treatment but eventually relapsed and *de novo* inactivating mutations of *NF1* were detected in these relapse tumour samples using sequencing approaches. Thus, genes which were found associated with ALKi resistance in neuroblastoma cell lines were also observed in relapse samples of patients with *ALK*-driven neuroblastoma treated with ALK inhibitors.

The second part of this thesis focused on the role of *NF1* loss in ALKi resistance, its effect on ALK downstream signalling and new collateral sensitivities. This role was investigated by perturbation experiments and subsequent ELISA assays to quantify protein phosphorylation, and thus pathway activity. *NF1* knockout cell line models showed increased downstream signalling of the RAS/MAPK pathway. The perturbation data was used with a prior known signalling network topology to model the downstream signalling response in NF1-deficient neuroblastoma cells. The model indicated an absent ERK-RAF feedback loop and implied a possible MEK inhibitor sensitivity. When NF1-deficient neuroblastoma cells were exposed to the MEK or RAF inhibitors, increased inhibitor sensitivities were observed.

Overall, this thesis employed phenotypic screens as well as isogenic cell lines as suitable models to investigate and elucidate clinical observations. Hence, it was successful in demonstrating an association of genetic *NF1* alterations with ALKi resistance in cell line models, in the same manner as in a functional experimental recapitulation of observed *NF1* alterations in clinical cases of ALKi resistant *ALK*-driven neuroblastoma. This thesis underlined how modelling of signalling pathways can be used to reveal new collateral sensitivities and gives some mechanistic insights as well as new potential therapy options, which may potentially impact clinical practice and clinical trial design. The identified collateral sensitivities represent promising therapy options for patients with relapsed *ALK*-mutated and ALK-inhibitor resistant neuroblastoma harbouring loss of *NF1* mutations, which are worth being investigated in clinical trials, that cover sequential treatment as well as a pre-emptive combination therapy with ALK and MEK inhibitors.

Zusammenfassung

Das *ALK* (anaplastische Lymphomkinase) Gen ist ein bekanntes Onkogen des Neuroblastoms, welches in 8 %-10 % der Patienten/innen mit einer Neuroblastomerkrankung Mutationen aufweist. Trotz einer intensiven und multimodalen Therapie von Patienten/innen mit einem Hochrisiko-Neuroblastom kommt es in bis zu 60 % der Fälle zu einem Rezidiv, was mit einem 10-Jahres-Gesamtüberleben von weniger als 40 % einhergeht. Zielgerichtete Therapien sind daher in den Fokus von pädiatrisch-klinischen Studien gerückt und könnten ebenfalls für eine Erstlinienbehandlung in Betracht gezogen werden. Es wurden bereits einige Fälle von Resistenzentwicklung gegenüber zielgerichteten Therapien beschrieben, einschließlich Fälle aus pädiatrisch-klinischen Studien für ALK-Inhibitoren. Die Identifizierung der grundlegenden Mechanismen dieser Resistenzentwicklung sind daher unerlässlich und waren zentraler Gegenstand der vorliegenden Arbeit.

Der erste Teil dieser Doktorarbeit befasste sich mit der Identifizierung von ALK-Inhibitor vermittelnden Resistenzgenen in *in vitro* Zellmodellen des Neuroblastoms. Mit Hilfe einer genomweiten sgRNA Bibliothek und dem CRISPR/Cas9 Systems wurden Gene in der *ALK*-getriebenen Neuroblastomzelllinie SH-SY5Y ausgeschaltet und das Tumorsuppressorgen *NF1* mit einer Resistenz gegenüber den ALK Inhibitoren Ceritinib und Lorlatinib assoziiert. Die abgeleitete Hypothese, dass inaktivierende Mutationen des *NF1* Gens eine ALK-Inhibitor Resistenz bedingen, wurde durch Generierung von isogenen *ALK*-mutierten Neuroblastomzelllinien mit einem CRISPR/Cas9-vermitteltem Ausschalten von *NF1* untersucht. Es wurde beobachtet, dass das Ausschalten von *NF1* in diesen Zelllinien zu einem ALK-Inhibitor-resistenten Phänotypen führt und dass diese Zellen eine erhöhte Aktivität der RAS/MAPK Signaltransduktionskaskade aufweisen.

Des Weiteren wurden Tumorgewebsproben von Patienten/innen mit einem rezidivierten *ALK*-getriebenen Neuroblastom untersucht, welche in klinischen Studien zur ALK-Inhibitor Therapie behandelt wurden. Zunächst ließ sich unter Therapie eine Tumorregression beobachten, doch im weiteren Therapieverlauf kam es zur erneuten Tumorprogression. In diesen Rezidiv-Proben wurden *de novo* Mutationen detektiert, die zu einem Verlust von NF1 führten. Somit ließen sich *in vitro* identifizierte ALK-Inhibitor Resistenzgene auch in Patientenproben beobachten.

Der zweite Teil dieser Doktorarbeit fokussierte sich auf die Rolle eines NF1-Verlusts während einer ALK-inhibitor Resistenz, die durch einen NF1-Verlust bedingten Veränderungen der ALK-aktivierten Signaltransduktionskaskaden sowie neue begleitende Sensitivitäten. Dazu wurden Perturbationsexperimente durchgeführt und phosphorylierte Proteine mithilfe von ELISA Experimenten quantifiziert. Diese Quantifizierung ließ Rückschlüsse auf die jeweilige Aktivität der ALK-aktivierten Signaltransduktionskaskaden zu. Zelllinienmodelle mit inaktiviertem NF1 zeigten dabei eine gesteigerte Aktivität der RAS/MAPK- Signaltransduktionskaskade.

Die Ergebnisse der Perturbationsexperimente wurden zusammen mit einer literatur-basierten Struktur der Signaltransduktionskaskaden genutzt, um mithilfe eines systembiologischen Ansatzes Aktivitäten der ALK-aktivierten Signaltransduktionskaskaden zu modellieren. Anhand des Modells entstand die Annahme, dass Zelllinienmodelle mit inaktiviertem NF1 keine negative ERK-RAF-Rückkopplung aufweisen, was mit einer einhergehenden Sensitivität für MEK-Inhibitoren beschrieben wurde. Als Neuroblastomzelllinien mit fehlerhaftem NF1 gegenüber MEK und RAF Inhibitoren getestet wurden, konnte eine höhere Sensitivität für diese Inhibitoren beobachtet werden.

Im Rahmen dieser Arbeit wurde demonstriert, dass phänotypische Screens sowie isogene Zelllinienmodelle geeignete Modelsysteme sind, um klinisch getriebene Hypothesen experimentell zu untersuchen. Daher konnte erfolgreich ein Zusammenhang zwischen inaktivierenden NF1 Mutationen und einer ALK-Inhibitor Resistenz in *ALK*-getriebenen Neuroblastomzelllinien aufgezeigt werden, welcher ebenfalls in *ALK*-mutierten, ALK-Inhibitor resistenten Neuroblastomen beobachtet wurde. Die vorliegende Arbeit verdeutlicht, wie systembiologische Ansätze genutzt werden können, um neue Inhibitorsensitivitäten und Resistenzmechanismen zu identifizieren. Damit einhergehende neue Therapieansätze für die Behandlung von Patienten/innen mit einer Neuroblastomerkrankung könnten den klinischen Alltag sowie das Aufsetzen klinischer Studien beeinflussen. Diese neuen Inhibitorsensitivitäten stellen vielversprechende Therapieansätze für Patienten/innen mit einer rezidivierten *ALK*-mutierten und ALK-Inhibitor resistenten Neuroblastomerkrankung dar, die mit einem Verlust von NF1 einhergeht, und sollte in klinischen Studien als sequenzielle Therapie oder als präventive Kombinationstherapie aus ALK- und MEK-Inhibitoren getestet werden.

Table of contents

Abbreviations

^{123}I-mIBG	^{123}iodine-meta-iodobenzylguanidine
^{32}Pi	Orthophosphate
3PL	3-parameter logistic model
4PL	4-parameter logistic model
ABC	ATP binding cassette
ADRN	Adrenergic cells
ALCL	Anaplastic large-cell non-Hodgkin's lymphoma
ALK	Anaplastic lymphoma kinase
A-loop	Activation loop
amp	Ampicillin
ATP	Adenosine triphosphate
AUC	Area under the curve
BCA	Bicinchoninic acid assay
BSA	Bovine serum albumin
CFU	Colony forming unit
C-loop	Catalytic loop
CO_2	Carbon dioxide
CPM	Counts per million
CR	Completely responsive
CRC	Core regulating circuitries
CRISPR	Clustered Regularly Interspaced Short Palindromic Repeats
CSRD	Cysteine-serine-rich domain
ctDNA	Circulating tumour DNA
ddPCR	Digital droplet PCR
DFG-motif	Aspartic acid-phenylalanine-glycine-motif
DIN	DNA Integrity Number
DKFZ	Deutsches Krebsforschungszentrum
D-MEM	Dulbecco's modified Eagle Medium
DMSO	Dimethyl sulfoxide
DSBs	Double-stranded breaks
DSMZ	German Collection of Microorganisms and Cell Cultures
DUSPs	Dual specificity phosphatases
E. coli	Escherichia coli
EGFR	Epidermal growth factor receptor
EGFRi	EGFR-inhibitor
EML4	Echinoderm microtubule-associated protein-like 4
EMT	Epithelial-to-mesenchymal transition
ERK	Extracellular signal-regulated kinase
ETS	E-twenty-six
F	Phenylalanine
FCS	Fetal calf serum
FDA	Food and Drug Administration
FDG-PET scans	[^{18}F] fluorodeoxyglucose-positron emission tomography scans
FDR	False discovery rate
FISH	Fluorescent in situ hybridization
FOXO	Fork head box O
FR	Fold resistance
FRET	Fluorescence resonance energy transfer
FWER	Familywise-error rate
GAPs	GTPase-activating proteins
gDNA	Genomic deoxyribonucleic acid

GDP	Guanosine diphosphate
GEFs	Guanine nucleotide exchange-factors
GPOH	German Society of Paediatric Oncology and Haematology
GRB2	Growth-factor receptor-bound protein-2
GRD	GAP-related domain
GSEA	Gene Set Enrichment Analysis
GTP	Guanosine triphosphate
GTPases	Guanosine triphosphatases
HDAC	Histone deacetylase
HGF	Hepatocyte growth factor
IGF-1	Insulin like growth factor 1
IGF-1R	Insulin-like growth factor 1 receptor
IMT	Inflammatory myofibroblastic tumour
INDEL	Insertions or deletions
INRC	International Neuroblastoma Response Criteria
INRG	International Neuroblastoma Risk Group
INSR	Insulin receptor
INSS	International Neuroblastoma Staging System
KSR1	Kinase suppressor of Ras 1
L	Leucin
LB	Luria Bertani
MAPK	Mitogen-activated protein kinase
MES	Mesenchymal-like cells
Mg^{2+}	Magnesium
MOI	Multiplicity of infection
mRNA	Messenger RNA
mRNA-seq	mRNA-sequencing
MS	Mass spectrometry
NADH	Nicotinamide adenine dinucleotide hydrogen
NEAA	Non-essential amino acids
NES	Normalized enrichment score
NF1	Neurofibromin 1
NGS	Next-generation sequencing
NHEJ	Non-homologous end joining pathway
NMD	Nonsense mediated decay
NPM	Nucleophosmin
NSCLC	Non-small cell lung cancer
O_2	Oxygen
P/S	Penicillin/Streptomycin
PAM	Protospacer adjacent motif
PBS	Phosphate-buffered saline
PCA	Principal component analysis
PCR	Polymerase chain reaction
PDMS	Polydimethylsiloxane
pDNA	Plasmid DNA
PDX	Patient derived xenograft
Ph	Philadelphia chromosome
PH-like domain	Pleckstrin homology-like domain
PI3K	Phosphatidylinositol 3-kinase
PTB domain	Phosphor-tyrosine-binding domain
PVDF	Polyvinylidene fluoride
Q	Glutamine

R	Arginine
RAF	Ras-activated factor
RECIST	Response Evaluation Criteria in Solid Tumours
RIN	RNA Integrity Number
RNA	Ribonucleic acid
RPMI	Roswell Park Memorial Institute
RTK	Receptor tyrosine kinase
SDS-PAGE	Sodium dodecyl sulfate-polyacrylamide gel electrophoresis
Ser	Serine
sgRNA	Single-guide RNA
SH2-domain	Src homology 2 domain
SHC domain	Src homology 2 domain
SNV	Single nucleotide variant
SOC	Super optimal broth
SOS	Son of sevenless
SPR	Surface plasmon resonance
SPRED	Sprouty-related EVH1 domain-containing protein
SRA	NCBI Sequence Read Archive
STASNet	Steady-state analysis of signalling networks
STR	Short tandem repeat
TBD	Tubulin-binding domain
TU	Transducing unit
VST	Variance-stabilising transformation

1 Introduction

1.1 Neuroblastoma

Neuroblastoma (NB) is an embryonal malignancy that originates from incompletely committed sympathoadrenal progenitors of the neural crest and therefore tumours arise in tissues of the sympathetic nervous system, like the adrenal medulla or paraspinal ganglia [2-4]. It accounts for 5.5% (approximately 132 cases) of childhood cancer cases in Germany and the median age at diagnosis is 14 months (2009-2018) [5]. Neuroblastomas are clinically heterogeneous. Some tumours show a spontaneous regression (very low risk cases), caused by unknown mechanisms, while other cases present with a malignant tumour progression and despite an intensive multimodal therapy the 10-year overall survival rate for high-risk cases is less than 40% [6-9].

1.1.1 Clinical presentation and risk classification system of neuroblastoma

It has been reported that 40% of neuroblastoma patients are asymptomatic and diagnosed by chance [6]. Patients can show symptoms such as pain, fever, weight loss and swelling at the primary tumour site [6].

Primary tumours occur in over 40% of neuroblastoma cases in the adrenal glands [10]. Patients may also present with primary tumour sites in the neck, upper chest or along the paraspinal sympathetic ganglia [4, 11]. Furthermore, some patients have a disseminated tumour at diagnosis with metastases in bone marrow, bone, lymph nodes, skin and liver [11].

In order to diagnose neuroblastoma, patients undergo a physical examination, ultrasound of the neck, abdomen and mediastinum as well as X-ray of the chest [6]. In addition, concentrations of unfavourable prognostic serum markers, neuron-specific enolase and lactate dehydrogenase, are determined [6]. Further, urine is tested for catecholamine or catecholamine metabolites as high concentrations are observed in neuroblastoma patients [6, 11, 12]. Further tumour imaging methods, like magnetic resonance imaging, are used if the suspicion of a neuroblastoma diagnosis substantiates [6, 13]. To assess the extent of metastasis ^{123}iodine-meta-iodobenzylguanidine (^{123}I-mIBG) scintigraphy (MIBG scan) is conducted as most neuroblastoma cells express the noradrenaline transporter and therefore ^{123}I-mIBG is transported into the cells [11, 14]. In addition, bone marrow aspirates and biopsies are used for histology and immunohistochemistry [6, 11]. For cytogenomic characterisation of the tumour fluorescent *in situ* hybridization (FISH) is used to detect *MYCN* amplifications and chromosome 1p36 aberrations; next-generation sequencing is performed on biopsy material to identify other genomic alterations [6, 11, 15].

To make profound treatment decisions for neuroblastoma patients, a risk classification system was established accounting for results of the diagnostic methods mentioned. This system assigns patients

to stages based on the degree of surgical tumour resection and tumour dissemination using the International Neuroblastoma Staging System (INSS) as well as the staging system by the International Neuroblastoma Risk Group (INRG) [16-18]. The international neuroblastoma risk group defined 16 different patient subgroups that assign patients to one of the four major risk categories: very low, low, intermediate and high [6, 16]. With this classification system, patients are stratified into risk groups based on tumour localization and dissemination status of the tumour, presence and extent of metastases, and amplification status of the *MYCN* neuroblastoma oncogene. Patients presenting with a *MYCN*-amplified tumour are always assigned to the high-risk group [6].

Except for the *MYCN* status and chromosome 1p aberrations, genomic characterisation of the tumour is currently not considered for risk stratification, and thus does not affect treatment recommendations as stated in the guidelines of the German Society of Paediatric Oncology and Haematology (GPOH) [6]. However, this might be changed in the future and alterations of telomerase maintenance mechanisms as well as RAS/MAPK pathway alterations considered for risk stratification [19-21].

1.1.2 Treatment of high-risk neuroblastoma

Therapy for high-risk neuroblastoma patients comprises an intensive and multimodal treatment. It is divided into three phases, an induction phase, a consolidation phase, and a post-consolidation phase [6].

During the induction phase, high-risk neuroblastoma patients undergo high-dose chemotherapy cycles [6]. Furthermore, for primary tumours a resection may be performed during or after induction chemotherapy, dependent on the patient condition; and the primary tumour tissue used for molecular analysis [6]. Stem-cells are also harvested during the induction phase for infusion in the consolidation phase [6]. Cytotoxic drugs applied to treat high-risk neuroblastoma are combined in the form of chemotherapy cycles [6]. A total of six cycles, with alternating N5 and N6 cycles, is recommended during the induction phase [6]. N5 cycles comprise of the cytotoxic drugs cisplatin, etoposide and vindesine whereas N6 cycles contain vincristine, dacarbacine, ifosfamide and doxorubicin [6, 22, 23].

Drug administration in the form of myeloablative chemotherapy as well as stem-cell infusion are part of the consolidation phase [6, 22-25]. If a patient's tumour cells express the norepinephrine transporter system, ^{131}I-mIBG-treatment is recommended to be scheduled between induction and consolidation chemotherapy [6, 26-28]. Radiotherapy of the primary tumour region is also advised [29]. The last treatment phase, post-consolidation, includes treatment with the anti-GD2 antibody Dinutuximab beta [29, 30]. Dinutuximab targets the tumour-associated antigen disialogangloiside GD2, which is highly expressed in neuroblastoma [31].

Despite this intensive treatment and an initial remission, up to 60% of high-risk patients relapse with tumours that are largely resistant to therapy [32-34]. This further highlights the necessity of alternative treatment options.

1.1.3 Molecular characterisation of neuroblastoma

As outlined above, neuroblastoma is characterised by diverse clinical behaviours while only a few recurrently altered genes and chromosomal aberrations have been described. One of those genes is *MYCN* for which amplifications are observed in 20% of neuroblastoma cases and patients diagnosed with *MYCN* amplifications are at high risk of death [16, 20, 35]. The transcription factor encoded by *MYCN* activates genes involved in, *e.g.*, cell cycle progression, proliferation, self-renewal, angiogenesis, pluripotency and metastasis [11, 36]. It was also described that *MYCN* expression correlates with metastatic behaviour, which might be explained by MYCN mediated downregulation of integrins alpha1 and beta1, supporting detachment from the extracellular matrix and enabling of cell migration [11, 36-38].

Other recurrently altered genes in neuroblastoma are *TERT* (encoding the telomerase catalytic subunit), for which activating genomic rearrangements have been described, as well as inactivating *ATRX* (a helicase with chromatin remodelling activity) mutations [39-43]. Based on reported recurrence of gene alterations and chromosomal aberrations, Ackerman *et al*. defined mechanistic risk groups based on their genetic characterisation, for instance, ultra high-risk neuroblastomas with activated telomere maintenance mechanisms as well as driving oncogene activation and/or loss of tumour suppressor functions, are characterised on the molecular levels as harbouring i) either activating *MYCN* or *TERT* alterations or deleterious *ATRX* alterations with ii) simultaneous occurrence of RAS and/or p53 pathway gene mutations [20].

The anaplastic lymphoma kinase (*ALK)* gene is another recurrently altered gene and oncogenic driver in neuroblastoma, that is mutated in 8%-10% of neuroblastoma cases and shows an increased mutation frequency upon disease relapse [33, 44-52]. Chromosomal aberrations observed in neuroblastoma, that are also associated with *MYCN* amplification and a poor prognosis, are a gain of chromosome arm 17q, observed in 50% of neuroblastoma cases, as well as a loss of chromosome arm 1p in about 33% of neuroblastoma cases [11, 42, 53, 54].

Relapsed neuroblastomas have been described to show a higher frequency of mutations in the RAS/MAPK pathway or *ALK,* in comparison to treatment naïve tumours [33, 34, 52]. The discrepancy of mutations in primary and relapse samples can be described as temporal genetic intratumor heterogeneity (ITH) and is due to tumour evolution. Spatial intratumor heterogeneity with genetically distinct cell clones detected in different regions of a tumour or in metastasis have been reported for

neuroblastoma as well [55]. ITH may lead to selection of treatment resistant clones and therefore has been associated with treatment resistance [56].

In contrast to the stated genomic alterations, another concept potentially leading to relapse and therapy resistance was proposed by two independent research groups and is based on the hypothesis of two physiologically distinct tumour cell types in neuroblastoma [57, 58]. These two cell types are dictated by lineage specific super-enhancers or core regulating circuitries (CRCs) activating a distinct transcription factor network [57, 58]. Consequently, the two different cell types are found either as committed adrenergic cells (ADRN, also defined as sympathetic noradrenergic cells) or as less differentiated mesenchymal-like cells (MES), the latter presenting as chemoresistant *in vitro* and potentially enriched in post-treatment and relapsed tumours [57, 58].

1.2 Anaplastic Lymphoma Kinase (ALK)

1.2.1 ALK is a receptor tyrosine kinase

One of the most commonly altered genes in neuroblastoma is the *ALK* gene that encodes the anaplastic lymphoma kinase (ALK). ALK is a receptor tyrosine kinase (RTK), located in the plasma membrane, and composed of an extracellular ligand-binding domain, a transmembrane domain and an intracellular tyrosine kinase domain [59, 60]. Due to structural homology, it has been categorised into the insulin receptor family, RTK subclass II [59, 60].

The extracellular domain of ALK consists of multiple subdomains: an LDL-A domain, two MAM-domains and a glycine-rich region [59, 61, 62]. The intracellular kinase domain (Figure 1.1) is shaped by an N-terminal N-lobe and a C-terminal C-lobe, which are connected by the hinge region, which is a loop (loops connect secondary structure elements) [61, 63]. The cavity formed between the two lobes as well as the hinge region define the adenosine triphosphate (ATP) binding site [61, 63]. The N-lobe itself is formed by a five-stranded antiparallel β-sheet and an αC-helix, that binds to the α- and β-phosphates of ATP, whereas the C-lobe is mainly α-helical and harbours the catalytic loop (1247-1254) followed by the regulatory activation loop (A-loop) (1270-1299), which begins with the aspartic acid-phenylalanine-glycine (DFG)-motif (activation segment) followed by a short α–helix (αAL,1272-1279) [61]. Within the A-loop lies the autophosphorylation motif **Y**XXX**YY** that is needed for receptor activation [61, 64].

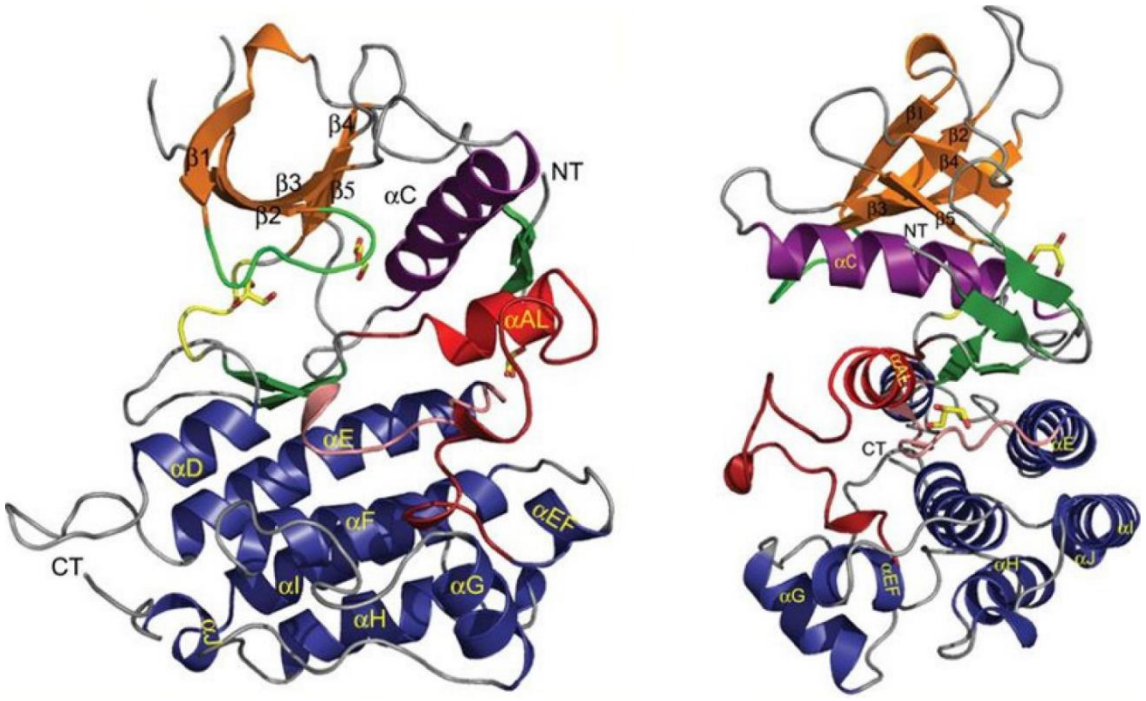

Figure 1.1 Crystal structure of the kinase domain of the anaplastic lymphoma kinase receptor (ALK) (PDB code 3L9P). The structure is shown in two orthogonal orientations. The N-terminus is indicated by NT and the C-terminus with CT. The N-terminal N-lobe is comprised of a five-stranded antiparallel β-sheet (shown in orange) and an αC-helix (shown in purple). The glycine-rich P-loop, shown in bright green, connects the first two β-strands of the β-sheet and coordinates the phosphates of adenosine triphosphate (ATP). The hinge region, which connects the N-lobe and the C-lobe is shown in yellow. The C-lobe is comprised of helices which are shown in blue. Furthermore, the C-lobe harbours the catalytic loop (C-loop, shown in salmon), which is followed by the regulatory activation loop (A-loop, shown in red). In addition, a β-turn is shown in green and displayed in stick representation are three bound glycerol molecules (oxygens are shown in red, carbons in yellow). Reprinted and adapted from Lee *et al*.[61].

In contrast to other RTKs, ALK presents with a DFG-in like conformation in the autoinhibited state, meaning that the proximal A-loop containing the DFG motif, does not obstruct the ATP binding site, and hence the active site is not occluded [61]. Nevertheless, the autoinhibited and unphosphorylated conformation of ALK only approximates an active kinase conformation and is characterised by a relative closure between its two lobes, representing an intermediate state between the open and closed conformation [61, 65, 66]. Furthermore, the autoinhibited conformation is stabilised by hydrophobic interactions of a phenylalanine core and by interactions of the αC-helix and the αAL [67]. Proposed ALK ligands, that were shown to activate the ALK and leukocyte tyrosine kinase receptor, are FAM150A and FAM150B [68, 69]. Furthermore, the growth factors pleiotrophin and midkine are also suggested ALK ligands but were shown to activate other receptors like the receptor protein tyrosine phosphatase β and the receptor protein tyrosine phosphatase ζ, N-syndecan, low-density lipoprotein receptor-related protein and integrins [70-76].

ALK expression has been reported to be very high at the neonatal stage and restricted to the nervous system, suggesting a role in nervous system development [59, 62]. Adult mouse brains showed only

very low mRNA and protein levels of ALK in comparison to neonatal mouse brains and a weak ALK signal was observed in human adult tissue of the nervous system (hypothalamus, basal ganglia, cerebral cortex, cerebellum, thalamic nuclei, erythroid and basal ganglia) consistent with the observations in mice [59, 62, 77]. However, ALK can also play a role in adulthood, as its expression and functionality are well described in malignancies.

1.2.2 *ALK* as a driving oncogene

ALK was first described as an oncogene in anaplastic large-cell non-Hodgkin's lymphoma (ALCL) as part of a nucleophosmin (NPM)-ALK fusion protein [78, 79]. This fusion protein resulted from a chromosomal translocation and led to a constitutively activated ALK kinase [59, 62, 78]. Meanwhile ALK is described in a variety of malignancies like *e.g.*, ALCL, non-small cell lung cancer (NSCLC), inflammatory myofibroblastic tumour (IMT), breast cancer and neuroblastoma [44-46, 49, 78, 80-82]. For these tumour entities ALK fusion proteins were reported as well as overexpression of the *ALK* gene and activating point mutations within *ALK* [83].

Activating point mutations have been described for both hereditary and sporadic neuroblastoma [44-47, 49]. There are three hotspot residues reported that account for 85% of activating kinase domain mutations observed in neuroblastoma, namely arginine (R)1275, phenylalanine (F)1174 and F1245 [50, 67]. R1275 and F1174 are the most common mutated amino acids. R1275 is located within the αAL and provides stability for the autoinhibited kinase by electrostatic interaction and hydrogen-bonding with αC-helix residues, whereas F1174 is part of a hydrophobic phenylalanine core [59, 67]. In neuroblastoma, R1275 is often exchanged to glutamine (Q) and F1174 to leucin (L) due to mutations in *ALK* [44, 47, 50, 67]. Both amino acid exchanges result in a constitutively activated kinase with accelerated autophosphorylation by destabilisation of the autoinhibited conformation [50]. For the F1174L mutation a ligand- and therefore dimerisation-independent activation of ALK has been suggested [84].

1.2.3 ALK downstream signalling

The general activation of RTKs is initiated through ligand binding by two receptor monomers via the N-terminal hydrophilic extracellular domains and leads to an active receptor dimer. This activation induces autophosphorylation of tyrosines within the autophosphorylation motif of the receptor activation loop and subsequent phosphorylation of cytoplasmic proteins from intracellular signalling transduction pathways [59, 61, 85]. Signalling transduction pathways activated by ALK are the PI3K/AKT, JAK/STAT and the RAS/MAPK axis, which are involved in cell transformation, cell growth and antiapoptotic signalling [86-90].

1.2.3.1 RAS

Three *RAS* genes have been identified in the human genome: *HRAS*, *KRAS* and *NRAS* [91]. The encoded RAS proteins are guanosine triphosphatases (GTPases) that possess a high degree of homology in their sequence but are not redundant in their function [92-94]. RAS proteins show an 85% homology in the critical domains for GTPase function and differ in the C-terminal part named hypervariable region [95].

As GTPases RAS proteins cycle between an active guanosine triphosphate (GTP)-bound state and an inactive guanosine diphosphate (GDP)-bound state [96-99]. Guanine nucleotide exchange-factors (GEFs) mediate binding of RAS to GTP by inducing a conformational change in RAS that diminishes the binding affinity for GDP which is released and replaced with GTP [100]. Examples for receptor tyrosine kinases activated GEFs are son of sevenless 1 and 2 (SOS1, SOS2) and growth-factor receptor-bound protein-2 (GRB2) [101].

GTPase-activating proteins (GAPs) on the other hand stimulate the intrinsic GTPase activity of RAS proteins [102]. GAP interaction with RAS stabilises the position of glutamine 61 , which engages with a catalytic water molecule and a specific arginine (GAP arginine finger) [103]. This interaction leads to release of a hydrogen atom from the water molecule and results in a hydroxyl ion that acts as a nucleophile and attacks the γ-phosphate of GTP causing GTP hydrolysis [103]. Examples for GAPs are Neurofibromin 1 (NF1), Sprouty-related EVH1 domain-containing protein 1,2 and 3 (SPRED1, SPRED2 and SPRED3) [101].

RAS proteins themselves activate Ras-activated factor (RAF) serine/threonine kinases (ARAF, BRAF, CRAF/RAF-1), phosphatidylinositol 3-kinase (PI3K) and other effectors that are involved with cell transformation, cell growth and antiapoptotic signalling [104-108].

Same as for *ALK,* the three *RAS* genes are known oncogenes [109]. The most frequently mutated residues are glycine 12 and 13 as well as Q61 [101]. In case one of the glycines is mutated to any amino acid but proline, the arginine finger of the GAPs cannot enter the active site, and GAP-Ras interaction does not result in GTP hydrolysis [102]. As glutamine 61 is important for GTP hydrolysis, a mutation of this residue inhibits the intrinsic RAS GTPase activity and GAP stimulated GTPase activity [102]. In all three cases, mutations result in a constantly active RAS protein [101].

1.2.3.2 RAS/MAPK signalling transduction pathway

As mentioned above, ALK activates the RAS/MAPK pathway (Figure 1.2). This is mediated through the Src homology 2 domain-containing (SHC) proteins SHC1 and 3 [90]. These proteins have two phosphotyrosine-binding domains, a phosphor-tyrosine-binding (PTB) domain and a Src homology 2 (SH2)-domain [110]. SHC1/3 bind phosphorylated Y1507 of ALK with their SH2-domain and are in turn phosphorylated at specific tyrosine residues by ALK or a cytoplasmic kinase [90, 111-113]. This specific

phosphorylation recruits and functions as a docking site for the preformed GRB2-SOS complex [90, 114-117]. Via SOS1/2 this complex is recruited to the plasma membrane to engage with membrane anchored RAS [117, 118]. SOS1/2 in turn activate RAS proteins due to their function as GEFs [119]. Activated RAS-GTP recruits the serine/threonine kinase RAF to the plasma membrane, which induces a conformational change in RAF and allows membrane associated kinases to phosphorylate RAF at activating residues [120]. Activated RAF phosphorylates two serine (Ser) residues (Ser-217/-218 and Ser-221) of MAPK(mitogen-activated protein kinase)/ERK (extracellular signal-regulated kinase)-Kinase 1/2 (MEK 1/2), both kinases bound by the scaffold protein kinase suppressor of Ras 1 (KSR1) [121, 122]. In turn phosphorylated MEK1/2 activates extracellular signal-regulated kinase 1/2 (ERK 1/2), that is also bound to KSR1, by phosphorylation of Threonine-183 and Tyrosine-185 [123, 124]. Activated ERK 1/2 kinases translocate into the nucleus and activate different downstream targets, *e.g*. genes of transcription factors as the E-twenty-six (ETS) transcription factor family, FOS and genes encoding dual specificity phosphatases (DUSPs) and Sprouty proteins [125]. The ALK-induced RAS/MAPK signalling transduction cascade in particular activates members of the transcription factor families fork head box O (FOXO) and ETS as well as genes encoding DUSPs [90, 126-128].

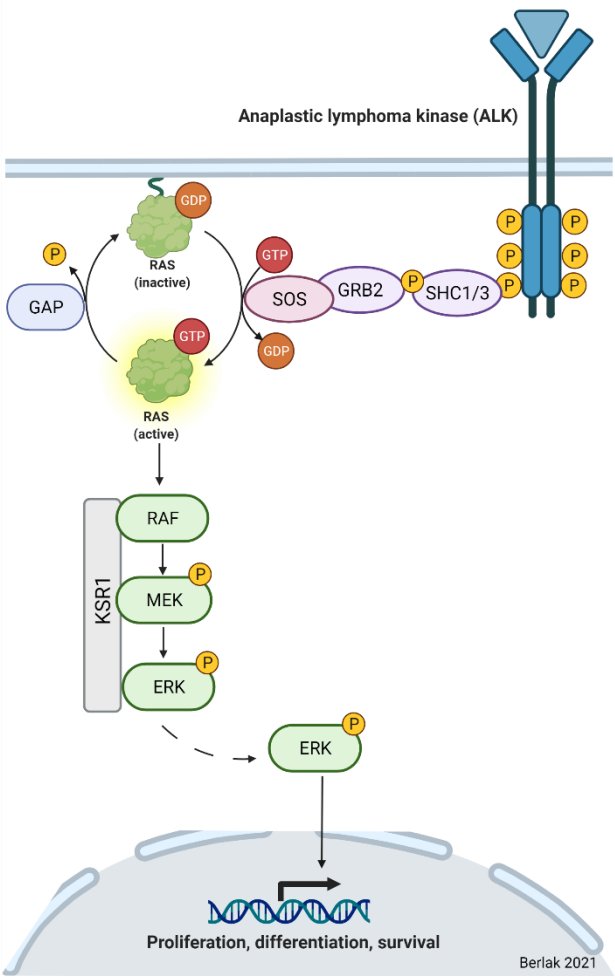

Figure 1.2: Schematic representation of anaplastic lymphoma kinase (ALK)-activated RAS/mitogen activated protein kinase (MAPK) pathway signalling. Src homology 2 domain-containing (SHC) proteins SHC1 and 3 bind to phosphorylated Y1507 of ALK and are in turn phosphorylated. This specific phosphorylation recruits the growth-factor receptor-bound protein-2 - son of sevenless (GRB2-SOS) complex. Via SOS1/2 this complex is recruited to the plasma membrane to engage with membrane anchored RAS protein. SOS1/2 in turn activate RAS due to their function as guanine nucleotide exchange-factor (GEF). Activated RAS-GTP recruits the Ras-activated factor (RAF) to the plasma membrane, which induces a conformational change in RAF and allows membrane associated kinases to phosphorylate RAF at activating residues. Activated RAF phosphorylates MAPK (mitogen-activated protein kinase)/ERK (extracellular signal-regulated kinase)-Kinase 1/2 (MEK 1/2), both kinases bound by the scaffold protein kinase suppressor of Ras 1 (KSR1). In turn phosphorylated MEK1/2 activates extracellular signal-regulated kinase 1/2 (ERK 1/2) by phosphorylation. Activated ERK 1/2 kinases translocate into the nucleus and activate different downstream targets. GTPase-activating protein= GAP, guanosine diphosphate =GDP, guanosine triphosphate =GTP, phosphorylation=P. This figure was generated with BioRender based on information from Emdal *et al*. [90].

NF1 is one of the central regulators of RAS within the RAS/MAPK pathway. It is a tumour suppressor and a GAP that negatively regulates RAS [129-131]. It stimulates the intrinsic GTPase-activity of RAS via its GAP-related domain (GRD) and accelerates GTP to GDP hydrolysis, inactivating RAS [129, 130, 132].

The NF1 protein (size: 320 kDa) is composed of multiple domains: an N-terminal cysteine-serine-rich domain (CSRD) (residues 543 to 909), the GRD (residues 1198 to 1530) that has an N-terminal

tubulin-binding domain (TBD), the bipartite phospholipid-binding module SecPH, composed of an Sec14-like domain (residues 1560 to 1698) as well as a C-terminal pleckstrin homology (PH)-like domain (residues 1715 to 1816) and an C-terminal tubulin-binding domain (residues 2260-2818) [133-138].

The bipartite phospholipid-binding module, in particular the Sec14-like domain, binds glycerolphospholipids (*e.g.*, phosphatidylinositol phosphate), which is thought to regulate the GAP activity of NF1 (GAP activity inhibition) and localises NF1 at the plasma membrane [134, 139-142]. More recently, an interaction of NF1 and SPRED1, which is also a negative regulator of RAS, has been described and suggested to be important for the NF1 translocation to the plasma membrane [143-145].

NF1 is a regulator of protein activity, which in turn is regulated by other proteins. The phosphorylation sites in the CSRD domain can be phosphorylated by protein kinase A and C, and their phosphorylation by protein kinase C increases the GAP activity of NF1 [146, 147]. Protein kinase A is described to phosphorylate the C-terminal domain of NF1 as well and these phosphorylated residues function as 14-3-3 protein binding site that inhibits the GAP activity of NF1 [148].

1.3 Targeted therapies and inhibitor resistance

For most malignancies, first-line treatment is composed of conventional chemotherapy. These cytotoxic drugs mostly cause DNA damage or inhibit cell cycle progression in rapidly dividing cells and therefore do not distinguish between healthy tissue and cancer cells [149]. Targeted therapeutics are an alternative to cytotoxic drugs, which including target-specific small molecule inhibitors and biologicals [150]. Until 2020, 43 small molecule inhibitors have been approved by the US Food and Drug Administration (FDA) for the field of oncology, most of which are kinase inhibitors that bind either in the active site of the kinase (orthosteric site) or allosteric sites [150].

1.3.1 ALK inhibitors (ALKi)

Five small-molecule inhibitors against ALK have been approved by the FDA for treating NSCLC: crizotinib, alectinib, brigatinib, ceritinib and lorlatinib [150]. All five ALK inhibitors are orally available ATP-competitive inhibitors binding to the active site of ALK [151-155]. Despite their high selectivity for ALK other targets/off-targets are reported. In addition to ALK, ROS1 is a reported target of lorlatinib as well as ceritinib [155]. Additional ceritinib off-targets are the insulin-like growth factor 1 receptor (IGF-1R) and the insulin receptor (INSR) [156].

Crizotinib was the first ALK inhibitor, FDA-approved in 2011 for metastatic, ALK-positive NSCLC and paediatric patients with relapsed or refractory, ALK-positive, systemic ALCL. As *ALK* is also an oncogenic driver in neuroblastoma and up to 60% of high-risk neuroblastoma patients relapse after the current

first-line therapy, paediatric clinical studies were conducted [33, 52]. Crizotinib showed only limited success in a phase one study for neuroblastoma patients with the ALK F1174L mutation, which seems to be intrinsically resistant to the inhibitor [157-160]. The usage of ceritinib, a second-generation ALK inhibitor, was investigated in a phase one trial as well and a relevant response was detected in some patients with *ALK*-driven, relapsed neuroblastoma. In contrast, a duration of response with detectable regression was observed before disease progression, indicating a development of therapy resistance for some tumours [161]. A phase I/II trial is currently being conducted for lorlatinib as a second line treatment for relapsed neuroblastoma [162].

1.3.2 MEK inhibitors (MEKi)

Another type of kinase inhibitors are MEKi. Until now, four MEKi have been approved by the FDA [163]. All of these inhibitors target an allosteric site within the dual specificity kinase MEK 1/2 and are ATP-non-competitive [163]. One of these small molecule inhibitors, trametinib (GSK 1120212), was FDA-approved for the indication of *BRAF V600E*- or *V600K*-mutated unresectable or metastatic melanoma as a monotherapy as well as for *BRAF V600E*-mutated metastatic NSCLC in combination with the BRAF inhibitor dabrafenib in 2013 [164, 165]. As stated above it binds to an allosteric site adjacent to the active site (ATP binding site) of MEK1 and MEK2 and interacts with a hydrophobic pocket of MEK [164, 166, 167]. A phenotype resistant to MEK inhibition has been reported for different MEK inhibitors. It was described that MEK inhibition leads to increased level of phosphorylated MEK in wildtype BRAF cells due to a reduced inhibitory ERK to RAF feedback [168-170]. This was not observed in *BRAF V600E*-mutated cell lines, where this negative feedback seems to be disrupted and leads to elevated baseline phosphorylated MEK levels, as MAPK signalling is the driving force of cell proliferation in these cells [170]. Due to the increase of downstream signalling in *ALK*-driven neuroblastoma cell lines, Umapathy *et al*. investigated the use of trametinib and found that trametinib exposure did not affect cell proliferation in *ALK*-mutated neuroblastoma [171].

1.3.3 Therapy resistance

A major challenge for the efficacy of targeted therapies in oncology is that tumour cells develop resistances to small-molecule inhibitors, the reason for which are multifactorial [172]. Resistance can be either intrinsic, *i.e*. tumours are refractory to the treatment, or acquired , which describes an initial partial or nearly complete remission in response to the treatment followed by recurring tumour progression [173]. Resistance can further be classified into resistance caused by on-target mutations and off-target mutations. On-target mutations occur in the gene encoding the target protein and diminish or obviate drug binding to the active site or the allosteric site [174]. An example for such an on-target mutation conveying resistance was observed in a cohort of NSCLC patients treated with crizotinib and lorlatinib [175, 176].

Furthermore, there are bypass mechanisms that lead to resistance, such as increased activation of other proteins signalling through the same signalling pathway, increased activity of proteins further downstream of the driver oncogene or epigenetic mechanisms that alter gene expression [174, 177]. One example for resistance mediated by epigenetic mechanisms was described for cases of NSCLC with an echinoderm microtubule-associated protein-like 4 (*EML4*)-*ALK* rearrangement, where ALKi resistance was associated with remodelled enhancers causing repression of tumour-suppressor micro RNAs and activation of genes like *AXL* [178]. In *ALK*-positive NSCLC patients, resistance to crizotinib was described, caused by on-target mutations in ALK as well as amplification of *ALK* fusion genes leading to target-mediated resistance [179]. In the same patient cohort, bypass mechanisms via increased autophosphorylation of the epidermal growth factor receptor (EGFR) were reported as well [179].

Resistance to targeted therapies can be multifactorial, which is highlighted by the following example. Epithelial-to-mesenchymal transition (EMT) was observed as a mechanism of resistance in two *in vitro* studies using *ALK*-rearranged lung cancer cell lines treated with lorlatinib and in neuroblastoma cell lines treated with ceritinib [180-182]. During EMT, epithelial cells become more fibroblastic, losing their cell-to-cell junctions and cell polarity, reorganising their cytoskeleton which results in increased motility and metastatic potential [182, 183]. Other known resistance mechanisms are based on upregulation of efflux pumps (ATP binding cassette (ABC) transporters), leading to reduced intracellular drug concentrations as a consequence of their active transport out of the cell [184]. The tumour microenvironment can also mediate resistance as reported by Strausmann *et al*. [185]. In this particular case, stromal cells secreted the hepatocyte growth factor (HGF), reactivating the RAS/MAPK and PI3K/AKT pathway through the MET receptor in *BRAF*-mutated RAF inhibitor treated melanoma cell lines [185].

Resistance to anti-cancer therapies is thought to be driven through evolutionary processes which are observed as ITH. The basic assumption of tumour evolution (in agreement with the observation of temporal ITH) is that there is a single cell of origin and acquired genetic alterations lead to sequential selection of more aggressive subclones [186]. Tumour lesions can be genomically heterogenous and some genomic alterations may lead to selection advantages during inhibitor therapy, resulting in the respective cell populations becoming dominant [187]. However, those cells, might be displaced as the dominant population by resilient cells (drug-refractory), that don't harbour a driver mutation but are resilient *e.g*., due to a passenger mutations, once the selective pressure (inhibitor) is absent [186-190]. Due to the increasing number of performed next-generation sequencing (NGS) experiments on tumour biopsies, an increased number of acquired mutations is detected and the major challenge is now to

distinguish between passenger mutations, that occur, but don't enhance cell fitness, and functionally relevant driver mutations, that grant a selective growth advantage to the cells [189, 190].

1.3.3.1 Resistance definition

Partial remission representing therapy resistance is frequently observed for malignant tumours. For neuroblastoma, disease response is assessed using the International Neuroblastoma Response Criteria (INRC) [18, 191]. The latest version (2017) of the INRC suggests assessing response of primary tumour soft tissue and metastatic sites according to Response Evaluation Criteria in Solid Tumours (RECIST), requiring the measurement of lesions in only one dimension (single longest dimension in orthogonal plane), instead of multidimensional measurements, in addition to MIBG scans or [^{18}F] fluorodeoxyglucose-positron emission tomography (FDG-PET) scans to define measurable lesions [191, 192]. Additionally, neuroblastoma cell infiltration into the bone marrow should be assessed by immunohistochemistry or histology and immunocytology or cytology [191]. A total of four bone marrow samples, bilateral aspirates (from both sites) and bilateral trephine (solid core of bone marrow) biopsies should be analysed. Primary tumour response is defined as completely responsive (CR) if a complete resolution in MIBG or FDG-PET scans is observed and residual soft tissue at primary site is smaller than 10 mm [191]. A partial response is defined as a ≥30% decrease in the single longest dimension of the primary tumour and MIBG or FDG-PET uptake at the primary site is stable, improved or not observed in comparison to previous results [191]. Disease progression on the other hand is defined as increase in the single longest dimension of a tumour lesion of at least 5 mm and more than 20% in comparison to a reference [191]. An overall disease progression is observed if any bone marrow metastasis, bone sites or metastatic soft tissue lesions as well as primary tumour sites are defined as a progressive disease according to the INRC criteria [191].

There are no general response criteria or definitions described for assessment of resistance in *in vitro* systems. For investigation of resistance in perturbed *in vitro* systems, a colony formation assay can be used to detect all cells, that are still able to form colonies as they did not lose the ability of unlimited cell division during or after exposure to a drug [193]. Furthermore, cell lines are exposed to different drug concentrations and either cell numbers determined over time using a live cell imaging system or cell viability assays, like the CellTiter-Glo® assay that quantifies ATP, are performed at a defined endpoint [194, 195].

The data generated in these biological assays are then used to fit a concentration-response curve and to determine an IC_{50} value, which is defined as the concentration of a drug causing 50% inhibition [196]. McDermott *et al*. proposed a definition for *in vitro* resistance based on comparison of patient derived cancer cell lines before and after acquired clinical resistance to chemotherapy and defined a parameter called "fold resistance"(FR), which is defined as the ratio of the IC_{50} value of the resistant cell line and

IC_{50} value of the parental cell line [194]. The patient derived cell line pairs described by McDermott *et al*. were used to assess drug responses *in vitro,* performing an acid phosphatase assay to determine cell viability and their FR for cytotoxic drugs [194]. Based on the results McDermott *et al*. defined *in vitro* cell line models with a FR of 2- to 5-fold as clinically relevant resistance models, although for some a FR of 8 to 12 was observed [194]. High-level laboratory models, which they suggest are clinically irrelevant, were defined as *in vitro* cell models with a FR ≥ 12 [194]. One example for a clinically relevant resistance cell model was reported for treatment-naïve patient-derived neuroblastoma cells compared to the corresponding chemotherapy-resistant cells, for which a FR of 3 and 2.7 for different cytotoxic drug was determined *in vitro,* using a colony formation assay [197]. That *in vitro* models, in form of patient derived cell lines, are appropriate models to investigate resistance, was shown by Kim *et al*., reporting treatment responses of cell lines in agreement with tumour response in patients [198].

Fallahi-Sichani *et al*. suggested the use of additional parameters next to the IC_{50} value to define resistance *in vitro*, like E_{max}, the Hill coefficient or slope *m* and the area under the curve (AUC) [199]. Through comparison of CellTiter-Glo® (cell viability assay) derived concentration-response data of 53 breast cancer cell lines treated with 64 different anticancer drugs they observed that the parameter values of E_{max} and the Hill coefficient vary systematically with drug class (based on target or mechanism), *e.g*., EGFR inhibitors had higher Hill coefficient values than PI3K inhibitors and AKT inhibitors as well as PI3K inhibitors had higher Hill coefficient values than mTOR inhibitors [199].

In addition to above mentioned methods, therapy resistance of isogenic cell lines or cell populations should be assessed in comparison to the parental cell line after treatment by western blot or proteomic approaches detecting *e.g*., activating phosphorylation patterns of the drug target or downstream effectors in case of receptors. In general, investigation of the known target interactome on RNA or protein level is useful to assess a resistant phenotype.

1.3.3.2 ALKi resistance

Several resistance mechanisms have been proposed for ALK inhibitor resistance in a variety of malignancies. For *ALK*-positive NSCLC, resistance towards ceritinib was described to be mediated via increased Src kinase activity [200]. A loss of *NF2* as well as EMT have been reported to lead to a lorlatinib resistant phenotype in *ALK*-rearranged lung cancer [180]. Other mechanisms described are the decreased expression of *DUSP6*, a gain of the *KRAS* gene, increased activation of AXL or EGFR as well as reduced expression of tumour suppressor micro RNAs [178, 201, 202].

Resistance to ALK inhibitor treatment in neuroblastoma is a matter of ongoing research. So far, a few resistance mechanisms have been proposed for *in vitr*o models. Activation of the tyrosine kinase AXL

and EMT have been described to mediate resistance in the neuroblastoma cell line SH-SY5Y, after cells had been rendered resistant to the ceritinib parent compound TAE684, by continuous exposure to increasing drug concentrations over a period of 8-12 months [181]. The same methodology was used to investigate ALKi resistance in the *MYCN*-amplified, *ALK*-mutated neuroblastoma cell line Kelly. In this case, investigators reported a loss of *MYCN* expression and an upregulation of *BORIS* leading to a phenotypical reprogramming and an ALK-inhibitor resistant phenotype [203]. Furthermore, by use of a CRISPR-mediated activation screen, leading to overexpression of specific target genes, the PIM1 kinase was identified as a resistance mediator for ceritinib and brigatinib in SH-SY5Y [204].

1.3.4 Collateral sensitivity

Due to tumour evolution, cells can acquire new genetic alterations under drug exposure, which on one hand render them resistant to the drug but, on the other hand, may lead to new drug vulnerabilities [172]. This phenomenon of new drug-specific vulnerabilities developing during the evolution of a resistant phenotype is termed collateral sensitivity [172]. This was first described for the field of microbiology and antibiotics resistance by Szybalski and Bryson *et al*., who observed for example that, resistance of the *E. coli* strain B/r to chloromycetin simultaneously showed an increased sensitivity to polymyxin B in comparison to the parental strain [205]. The concept of collateral sensitivities was then adapted to the field of oncology describing new vulnerabilities in chemotherapy resistant malignancies [206]. One example is the report of a Philadelphia chromosome (Ph)-positive acute lymphoblastic leukaemia mouse model, which acquired resistance to classical BCR-ABL1 inhibitors and at the same time became sensitive to inhibitors targeting other proteins than BCR-ABL1, such as the ALK inhibitor crizotinib [207] .

Therefore, elucidating the resistance mechanisms underlying ALKi resistance in neuroblastoma might lead to the simultaneous identification of collateral sensitivities and could improve patient outcome.

1.4 Objectives

Mutated *ALK* is a well-established oncogenic driver in several malignancies, including the paediatric cancer neuroblastoma, where mutations in *ALK* are described in 8% - 10% of the cases [33, 44-52, 83]. As up to 60% of high-risk neuroblastoma patients relapse despite an intensive multimodal therapy and the 10-year overall survival rate is less than 40%, there is a high, urgent, unmet medical need for alternative treatment options [6-9, 33, 52]. Therefore, small molecule inhibitors against ALK have been investigated in paediatric clinical trials including neuroblastoma patients [159, 160, 162, 208]. As reported for malignancies of adulthood, for some of the paediatric patients disease regression was observed, but the respective patients eventually relapsed during the treatment [161]. Furthermore, genomic data of tumour biopsies from ALK inhibitor-resistant (ceritinib) neuroblastoma of patients treated at the Charité were analysed regarding mutations and inactivating *NF1* mutations were detected. Hence, a deeper understanding of resistance development is required and investigated within this thesis.

The objectives of the first part of this thesis were (1) to identify genes associated with an ALK inhibitor resistant phenotype in *ALK*-driven neuroblastoma cell lines using an unbiased screening approach and (2) to validate the identified genes and their phenotypic effect.

The objectives of the second part of this thesis were (1) to gain a mechanistic understanding of ALK inhibitor resistance in order (2) to prevent or overcome ALK inhibitor resistance.

2 Materials and methods

2.1 Material

2.1.1 Laboratory devices and equipment

All devices used for performance of the experiments are listed in Table 2-1.

Table 2-1: Laboratory devices and equipment used within this project.

Name	Manufacturer
4200 TapeStation System	Agilent, Santa Clara, USA
Analytical balance ABS-N	Kern, Balingen, Germany
Axio Vert.A1 microscope	Carl Zeiss, Jena, Germany
Balance EW-N	Kern, Balingen, Germany
Bio-Plex MAGPIX multiplex reader	BioRad, Hercules, USA
C1000 Touch Thermal Cycler	BioRad, Hercules, USA
Cell counter TC20	BioRad, Hercules, USA
Centrifuge 5415R	Eppendorf, Hamburg, Germany
Centrifuge 5427R	Eppendorf, Hamburg, Germany
Centrifuge 5810 R	Eppendorf, Hamburg, Germany
D300e Digital Dispenser	Tecan Group Ltd., Männedorf, Switzerland
DOC-PRINT-VX5	Vilber Lourmat, Eberhardzell, Germany
Duomax 1030, platform shaker	Heidolph Instruments, Schwabach, Germany
Erlenmeyer flask (250 mL and 1 L)	Carl Roth, Karlsruhe, Germany
Freezer (-80°C), HeraFreeze T series HFU400TV63	Thermo Fisher Scientific, Waltham, USA
Freezer -20°C	Liebherr, Bulle, Switzerland
Freezing container 5100 Cryo 1. (Mr. Frosty)	Thermo Fisher Scientific, Waltham, USA
Fridge 4°C	Liebherr, Bulle, Switzerland
Fusion Fx Spectra	Vilber Lourmat, Eberhardzell, Germany
Gene Pulser Xcell electroporation system	BioRad, Hercules, USA
Glass beads, 5 mm	Merck, Darmstadt, Germany
HERACELL VIOS 250i 230V CU GS	Thermo Fisher Scientific, Waltham, USA
Heratherm™ Compact Microbiological Incubator	Thermo Fisher Scientific, Waltham, USA
Ice machine Manitowoc SOTTO	Manitowoc
Incubator shaker KS 4000 i control	IKA, Staufen, Germany

Incucyte® S3 Live-Cell Analysis System	Sartorius, Göttingen, Germany
Laminar Airflow Bench maxisafe 2020 1.8, Class II	Thermo Fisher Scientific, Waltham, USA
Luminometer GloMax®-Multi+Microplate Multimode Reader with Instinct® E8032	Promega, Madison, USA
Magnetic separation stand, Two-position	Promega, Madison, USA
MCO-230AICUV IncuSafe CO2 Inkubator	PHC Europe B.V., Etten-Leur, Netherlands
Microwave HMT72M420	Bosch, Gerlingen, Germany
Millipore Barnstead MicroPure	Thermo Fisher Scientific, Waltham, USA
Mini-PROTEAN tetra system	BioRad, Hercules, USA
MiniSeq system	Illumina, San Diego, USA
MiniStar silverline Microcentrifuge	VWR, Darmstadt, Germany
NanoDrop 2000	Thermo Fisher Scientific, Waltham, USA
NextSeq 550 sequencer	Illumina, San Diego, USA
PerfectBlue Horizontal Midi S Gel system,15x25 cm	Peqlab Biotechnologie, Erlangen, Germany
PerfectBlue Midi S combs, 1.5 mm, 10 or 20 teeth	Peqlab Biotechnologie, Erlangen, Germany
PerfectBlue Midi S gel tray	Peqlab Biotechnologie, Erlangen, Germany
pH Meter, five easy	Mettler-Toledo, Gien, Germany
Phoenix RS-TR 5 tube roller	Phoenix Instrument, Garbsen, Germany
Pipette filler pipetus®	Hirschmann Labortechnik, Eberstadt, Germany
Pipette ResearchR Plus Multichannel	Eppendorf, Hamburg, Germany
Pipettes (2.5 – 1000 µL) Research (Plus)	Eppendorf, Hamburg, Germany
PowerPac Basic Power supply	BioRad, Hercules, USA
Qubit 2.0 Fluorometer	Thermo Fisher Scientific, Waltham, USA
Reax top Vortexer	Heidolph Instruments, Schwabach, Germany
RH basic magnetic stirrer	IKA, Stauffen, Germany
Sorvall Lynx 4000 super speed centrifuge	Thermo Fisher Scientific, Waltham, USA
Sorvall SLA-3000 rotor	Thermo Fisher Scientific, Waltham, USA
Spectrophotometer, Epoch	BioTek Instruments, Winooski, USA
Suction pump AC02	Carl Roth, Karlsruhe, Germany

SW 32 Ti Swinging-Bucket Rotor	BeckmanCoulter, Brea, USA
ThermoMixer comfort	Eppendorf, Hamburg, Germany
Trans-Blot Turbo Transfer system	BioRad, Hercules, USA
Ultracentrifuge Optima L90K	BeckmanCoulter, Brea, USA
Waterbath GFL 1086	GFL Technology, Noida, India
XCell SureLock™ Mini-Cell	Thermo Fisher Scientific, Waltham, USA

2.1.2 Consumables

Table 2-2: Consumables used within this project.

Name	Supplier (catalog no.)
0.2 µm PVDF membranes	Roche, Basel, Switzerland (#3010040001)
8 Well PCR tube strips plus 8 domed caps	Sarstedt, Nümbrecht, Germany (strips#72.985.002, caps #65.989.002)
96 Well Plate Advanced TC (flat bottom)	Greiner Bio-one, Kremsmünster, Austria (#655983)
Blotting paper (Whatman), 0.35 mm	Carl Roth, Karlsruhe, Germany (#0043.1)
Cell culture Assay Plate 96 well white, flat bottom, sterile	Corning, Corning, USA (#3917)
Cell culture multiwall plate, 6 well, PS, clear, sterile	Greiner Bio-one, Kremsmünster, Austria (#657160)
Cell scraper	Corning, Corning, USA (#3011)
Counting slides for TC10™/TC20™ Cell Counter, Dual chamber	BioRad, Hercules, USA (#1450011)
CryoPure Tube 1.6 mL yellow	Sarstedt, Nümbrecht, Germany (#72.380.004)
Dispenser head Cassettes HP T8	Tecan Group Ltd., Männedorf, Switzerland (#30097370)
Disposable needles Sterican® long bevel facet, 0.30x12mm	B. Braun, Melsungen, Germany (#4656300)
Disposable scalpel	Swann-Morton, Sheffield, United Kingdom (#0503)
Falcon® 10 mL Serological Pipet	Corning, Corning, USA (#357551)
Falcon® 100 mm TC-treated Cell Culture Dish	Corning, Corning, USA (#353003)

Falcon® 12-well Clear Flat Bottom TC-treated Multiwell Cell Culture Plate	Corning, Corning, USA (#353043)
Falcon® 15 mL High Clarity PP Centrifuge Tube	Corning, Corning, USA (#352096)
Falcon® 150 mm TC-treated Cell Culture Dish	Corning, Corning, USA (#353025)
Falcon® 24-well Clear Flat Bottom TC-treated Multiwell Cell Culture Plate	Corning, Corning, USA (#353047)
Falcon® 25 mL Serological Pipet	Corning, Corning, USA (#357525)
Falcon® 35 mm TC-treated Easy-Grip Style Cell Culture Dish	Corning, Corning, USA (#353001)
Falcon® 40 µm Cell Strainer	Corning, Corning, USA (#352340)
Falcon® 48-well Clear Flat Bottom TC-treated Multiwell Cell Culture Plate	Corning, Corning, USA (#353078)
Falcon® 5 mL Serological Pipet	Corning, Corning, USA (#357543)
Falcon® 50 mL High Clarity PP Centrifuge Tube	Corning, Corning, USA (#352070)
Falcon® 50 mL Serological Pipet	Corning, Corning, USA (#357550)
FrameStar Fast Plate 96-well semi skirted	Azenta, Chelmsford, USA (#4Ti-0910)
Gene Pulser/MicroPulser Electroporation Cuvettes, 0.1 cm gap	BioRad, Hercules, USA (#1652083)
Nunc EasYFlasks 225 cm^2 (T225)	Thermo Fisher Scientific, Waltham, USA (#159934)
NuPAGE 3-8% Tris-Acetate Protein Gels	Thermo Fisher Scientific, Waltham, USA (#EA0375)
Open-Top Thinwall Ultra-Clear Tube, 25 x 89 mm	BeckmanCoulter, Brea, USA (#344058)
Pasteurpipette glass, 145 mm	BRAND, Wertheim, Germany (#500635)
Pasteurpipette glass, 230 mm	BRAND, Wertheim, Germany (#500636)
Petri dish, 94x16, with vents	Greiner Bio-one, Kremsmünster, Austria (#633180)
Qubit Assay tubes	Thermo Fisher Scientific, Waltham, USA (#Q32856)
Reaction tube (1.5 mL, 2 mL)	Sarstedt, Nümbrecht, Germany (#72.706.200, #72.695.200)
Reagent Reservoirs, 25 mL	Carl Roth, Karlsruhe, Germany (#EKT8.1)
Rotilab®-syringe filters, CA, sterile, 0.45 µm	Carl Roth, Karlsruhe, Germany (#KC71.1)
Spitzen Filter SurPhob 10 µL lang (10x96)	Biozym, Hessisch Oldendorf, Germany (#VT0200)

Spitzen Filter Surphob 100 µL (10x96)	Biozym, Hessisch Oldendorf, Germany (#VT0230)
Spitzen Filter Surphob 1250 µL (10x96)	Biozym, Hessisch Oldendorf, Germany (#VT0270)
stericup quick release durapore 0.45 µm, PVDF	Merck, Darmstadt, Germany (#SCHVU05RE)
TapeStation 4200 loading tips	Agilent, Santa Clara, USA (#5067-5598)
TapeStation 4200 optical Tubes, 8x Strip	Agilent, Santa Clara, USA (#401428)
Tissue culture flask 300 cm^2 (T300)	VWR International GmbH, Dresden, Germany (#90301)
Vasco® Nitril blue glove S	B. Braun, Melsungen, Germany (#9205518)

2.1.3 Chemicals and Reagents

Table 2-3: Chemicals and Reagents used within this project.

Name	Supplier (catalog no.)
20% SDS solution	Serva, Heidelberg, Germany (#39575.02)
4% Formaldehyde in PBS	Neolab, Heidelberg, Germany (#LC-6470.1)
4x Laemmli buffer	BioRad, Hercules, USA (#161-0747)
Albumin from bovine serum Fraktion V	Carl Roth, Karlsruhe, Germany (#8076.3)
Ammonium Persulfate (APS)	Carl Roth, Karlsruhe, Germany (#9178.3)
ampicillin	Carl Roth, Karlsruhe, Germany (#K029.2)
Aprotinin	Merck, Darmstadt, Germany (#10236624001)
Biozym LE Agarose	Biozym, Hessisch Oldendorf, Germany (#840004)
Ceritinib	Axon Medchem, Groningen, Netherlands (#Axon224)
Chloroform	Serva, Heidelberg, Germany (#39553.01)
cOmplete™ Mini EDTA free protease inhibitor	Roche, Basel, Switzerland (#11836170001).
Crystal violet	Merck, Darmstadt, Germany (#C0775)
Dimethyl sulfoxide (DMSO)	Carl Roth, Karlsruhe, Germany (#A994.1)
DNA loading dye (6x Orange)	Thermo Fisher Scientific, Waltham, USA (#R0631)

EDTA	Carl Roth, Karlsruhe, Germany (#1E23.1)
Ethanol Rotipuran 99.8% p.a.	Carl Roth, Karlsruhe, Germany (#9065.2)
Ethanol, Absolute (200 Proof), Molecular Biology Grade, Fisher BioReagents™	Fisher Scientific, Waltham, USA (#BP2818-500)
Ethidiume bromide solution	Carl Roth, Karlsruhe, Germany (#2218.1)
FETAL BOVINE SERUM (FBS) Superior	Merck, Darmstadt, Germany (#S0615)
GeneRuler 1 kb DNA ladder	Thermo Fisher Scientific, Waltham, USA (#SM0311)
GeneRuler 100 bp DNA ladder	Thermo Fisher Scientific, Waltham, USA (#SM0321)
Genetic (G-418)	Merck, Darmstadt, Germany (#G8168)
GlutaMAX	Thermo Fisher Scientific, Waltham, USA (#35050061).
Glycine Pufferan® ≥ 99% p.a.	Carl Roth, Karlsruhe, Germany (#3908.3)
Glycogen, RNA grade	Thermo Fisher Scientific, Waltham, USA (#R0551)
HEPES	Carl Roth, Karlsruhe, Germany (#6763.3)
High Sensitivity D1000 Reagents	Agilent, Santa Clara, USA (#5067- 5585)
HiMark Pre-stained Protein Standard	Thermo Fisher Scientific, Waltham, USA (#LC5699)
Isopropanol	Serva, Heidelberg, Germany (#39559.02)
LB media	Carl Roth, Karlsruhe, Germany (#X968.2)
LB-Agar	Carl Roth, Karlsruhe, Germany (#X969.1)
Leupeptin	Merck, Darmstadt, Germany (#L8511-5MG)
Lorlatinib	Axon Medchem, Groningen, Netherlands (#Axon2600)
Methanol ROTIPURANR ≥99.8%	Carl Roth, Karlsruhe, Germany (#4627.4)
Minimum Essential Medium Non-Essential Amino Acid Solution (100x)	Lonza, Basel, Switzerland (#BE13-144E)
NaF	Merck, Darmstadt, Germany (#S6776-100G)
Nuclease-free water	Thermo Fisher Scientific, Waltham, USA (#10977035)
NuPAGE Antioxidant	Thermo Fisher Scientific, Waltham, USA (#NP0005)

PageRuler™ Prestained Protein Ladder	Thermo Fisher Scientific, Waltham, USA (#26617)
Penicillin-Streptomycin (10,000 U/mL)	Thermo Fisher Scientific, Waltham, USA (#15140122).
Phenylmethanesulfonyl fluoride solution (PMSF)	Merck, Darmstadt, Germany (#93482-50ML-F)
PhosSTOP™	Roche, Basel, Switzerland (#4906845001)
Pictilisib	Axon Medchem, Groningen, Netherlands (#Axon1377)
Polyacrylamid Rotiphorese, 30%	Carl Roth, Karlsruhe, Germany (#3029.1)
Polybrene	Merck, Darmstadt, Germany (#TR-1003-G).
Powdered milk, blotting grade	Carl Roth, Karlsruhe, Germany (#T145.3)
Protector RNase Inhibitor of Transcriptor First Strand cDNA Synthesis Kit	Roche, Basel, Switzerland (#04379012001)
Puromycin	Thermo Fisher Scientific, Waltham, USA (#A1113803)
Rapamycin	Axon Medchem, Groningen, Netherlands (#Axon2069)
ROTI®Phenol/Chloroform/Isoamyl alcohol	Carl Roth, Karlsruhe, Germany (#A156.3)
SDS	Carl Roth, Karlsruhe, Germany (#CN30.3)
Sodium acetate (3 M), pH 5.5, RNase-free	Thermo Fisher Scientific, Waltham, USA (#AM9740)
Sodium butyrate	Merck, Darmstadt, Germany (#B5887)
Sodium Chloride (NaCl)	Merck, Darmstadt, Germany (#1.06404.5000)
Sodium pyruvate	Merck, Darmstadt, Germany (#S8636)
Tetramethylethylenediamine (TEMED)	Carl Roth, Karlsruhe, Germany (#2367.1)
Trametinib	Axon Medchem, Groningen, Netherlands (#Axon1761)
TRIS-HCL	Carl Roth, Karlsruhe, Germany (#9090.3)
Triton X-100	Carl Roth, Karlsruhe, Germany (#3051.3)
Trizma base	Merck, Darmstadt, Germany (#T1503)
Trypan Blue Solution 0.4%	Thermo Fisher Scientific, Waltham, USA (#15250061)
Tween®20	Carl Roth, Karlsruhe, Germany (#9127.2)

Western blotting luminol reagent	Santa Cruz Biotechnology, Dallas, USA (#sc-2048)
β-mercaptoethanol 99% p.a.	Carl Roth, Karlsruhe, Germany (#4227)

2.1.4 Enzymes

Table 2-4: Enzymes used within this project.

Name	Supplier (catalog no.)
*Acc*65I	NEB, Ipswich, USA (#R0599S)
*Bam*HI	NEB, Ipswich, USA (#R0136S)
*Bbs*I	NEB, Ipswich, USA (#R0539S)
KAPA2G Fast HotStart ReadyMix,	Roche, Basel, Switzerland (#KK5603)
RQ1 RNase-Free DNase	Promega, Madison, USA (#M6101)
T4 DNA ligase	NEB, Ipswich, USA (#M0202S)
T4 polynucleotide kinase	NEB, Ipswich, USA (#M0201)
T7 Endonuclease	NEB, Ipswich, USA (#M0302S)
Ultra II Q5 Master Mix Polymerase	NEB, Ipswich, USA (#M0544L)

2.1.5 Ligands

Table 2-5: Ligands used within this project.

Name	Supplier (catalog no.)
EGF	R&D systems, Minneapolis, USA (#AFL236-200)
IGF-1	R&D systems, Minneapolis, USA (#291-G1-200)

2.1.6 Kits

Table 2-6: Kits used within this project.

Name	Supplier (catalog no.)
AMPure XP	BeckmanCoulter, Brea, USA (#63880).
Bio-Plex Pro Cell signalling reagent kit	BioRad, Hercules, USA (#171304006M)
CalPhos™ Mammalian Transfection Kit	Takara, San Jose, USA (#631312)
CellTiter-Glo® Luminescent Cell Viability Assay 10x10 mL	Promega, Madison, USA (#G7571)
High Sensitivity D1000 ScreenTape	Agilent, Santa Clara, USA (#5067- 5584)
HiSeq 3000/4000 PE Cluster Kit	Illumina, San Diego, USA (#FC-410-1001)
Illumina Stranded mRNA Prep	Illumina, San Diego, USA (#20040534)
Lipofectamine LTX Reagent with PLUS Reagent	Thermo Scientific, Waltham, USA (#A12621)
NucleoBond PC 10000EF kit	Macherey-Nagel, Dueren, Germany (#740548)
NucleoBond Xtra Maxi kit	Macherey-Nagel, Dueren, Germany (#740414.50)
NucleoSpin Gel and PCR-Clean Up kit	Macherey-Nagel, Dueren, Germany (#740609.50)
NucleoSpin Tissue kit	Macherey-Nagel, Dueren, Germany (#740952.50)
paired-end 150 High Output kit	Illumina, San Diego, USA (#20024907)
paired-end 150 MiniSeq Mid Output kit	Illumina, San Diego, USA (#FC-420-1004)
Pierce ™ BCA Protein assay kit	Thermo Scientific, Waltham, USA (#23225)
PlasmoTest kit	InvivoGen, San Diego, USA (#rep-pt1)
QIAprep Spin Miniprep kit	Qiagen, Hilden, Germany (#27104)
Qubit dsDNA BR Assay 500	Thermo Scientific, Waltham, USA (#Q32853)
RNA Screen tape	Agilent, Santa Clara, USA (#5067-5576)
TOPO™ TA Cloning™ Kit for Sequencing	Thermo Scientific, Waltham, USA (#45-0030)
ZymoResearch Quick-gDNA MidiPrep	ZymoResearch, Irvine, USA (#D4075)

2.1.7 Plasmids

Table 2-7: Bacterial and lentiviral plasmids used within this project.

Name	Origin	Supplier (catalog no.)
human CRISPR knockout library Brunello	Doench *et al*. [209]	Addgene, Watertown, USA (#73179)
lentiCas9-EGFP	Chen *et al*. [210]	Addgene, Watertown, USA (#63592)
pMD2.G	gift from Didier Trono to Addgene	Addgene, Watertown, USA (#12259)
pMDLg/pRRE	Dull *et al*. [211]	Addgene, Watertown, USA (#12251)
pRSV-REV	Dull *et al*. [211]	Addgene, Watertown, USA (#12253)
pSpCas9(BB)-2A-GFP (PX458)	Ran *et al*. [212]	Addgene, Watertown, USA (#48138)
pSpCas9(BB)-2A-Puro (PX459)	Ran *et al*. [212]	Addgene, Watertown, USA (#48139)
pUC19	-	Thermo Fisher Scientific, (#SD0061)
TOPO® vector	TOPO™ TA Cloning™ Kit for Sequencing	Thermo Scientific, Waltham, USA (#45-0030)

2.1.8 Bacterial strains

Table 2-8: Bacterial strains used within this project.

Name	Supplier (catalog no.)
MegaX DH10B T1R Electrocomp™ cells	Thermo Fisher Scientific, Waltham, USA (#C640003)
One Shot TOP10 Chemically Competent *E. coli*	Thermo Fisher Scientific, Waltham, USA (#C404003)
XL10-Gold ultracompetent *E. coli* cells	Agilent Santa Clara, USA (#200314)

2.1.9 Oligonucleotides

Table 2-9: Sequences of single-guide RNAs to introduce knockouts using the CRISPR/Cas9 system in *NF1.*

Name	Single-guide RNA (sgRNA) sequence (5'-3')	Supplier
NF1_E1_1_top	CACCgCTCGTCGAAGCGGCTGACCA	Eurofins, Luxembourg, Luxembourg
NF1_E1_1_bot	AAACTGGTCAGCCGCTTCGACGAGc	Eurofins, Luxembourg, Luxembourg
NF1_E1_2_top	CACCGCGCGCACAGGCCGGTGGAAT	Eurofins, Luxembourg, Luxembourg
NF1_E1_2_bot	AAACATTCCACCGGCCTGTGCGCGC	Eurofins, Luxembourg, Luxembourg
NF1_E30_1_top	CACCgTCATCTGAAGGAGGTTCCGC	Eurofins, Luxembourg, Luxembourg
NF1_E30_1_bot	AAACGCGGAACCTCCTTCAGATGAc	Eurofins, Luxembourg, Luxembourg
NF1_E30_2_top	CACCgTGGCACACACTTCGAAGTTG	Eurofins, Luxembourg, Luxembourg
NF1_E30_2_bot	AAACCAACTTCGAAGTGTGTGCCAc	Eurofins, Luxembourg, Luxembourg

Table 2-10: PCR primers for regions flanking the expected Cas9 cut site in *NF1*.

Name	Sequence (5'-3')	Supplier
NF1_Exon1_forward	GTGGAAAGGATCCCACTTCCG	Eurofins, Luxembourg, Luxembourg
NF1_Exon1_reverse	GGGAGGGGCGGAATGTTATC	Eurofins, Luxembourg, Luxembourg
NF1_Exon30_forward	GTCTACACGTTGCACTTGGCTTAATG	Eurofins, Luxembourg, Luxembourg
NF1_Exon30_reverse	AGACCCGCCTCAACTGTGAAAC	Eurofins, Luxembourg, Luxembourg

Table 2-11: Primer sequences to prepare the sequencing library of the CRISPR/Cas9 knockout screen using the Brunello library.

Name	Sequence (5'-3')	Supplier
P5 0 nt	AATGATACGGCGACCACCGAGATCTACACTCTTTCCCTACACGACGCTCTT CCGATCTTTGTGGAAAGGACGAAACACCG	IDT, Coralville, USA
P5 1 nt	AATGATACGGCGACCACCGAGATCTACACTCTTTCCCTACACGACGCTCTT CCGATCTCTTGTGGAAAGGACGAAACACCG	IDT, Coralville, USA
P5 2 nt	AATGATACGGCGACCACCGAGATCTACACTCTTTCCCTACACGACGCTCTT CCGATCTGCTTGTGGAAAGGACGAAACACCG	IDT, Coralville, USA
P5 3 nt	AATGATACGGCGACCACCGAGATCTACACTCTTTCCCTACACGACGCTCTT CCGATCTAGCTTGTGGAAAGGACGAAACACCG	IDT, Coralville, USA
P5 4 nt	AATGATACGGCGACCACCGAGATCTACACTCTTTCCCTACACGACGCTCTT CCGATCTCAACTTGTGGAAAGGACGAAACACCG	IDT, Coralville, USA
P5 6 nt	AATGATACGGCGACCACCGAGATCTACACTCTTTCCCTACACGACGCTCTT CCGATCTTGCACCTTGTGGAAAGGACGAAACACCG	IDT, Coralville, USA
P5 7 nt	AATGATACGGCGACCACCGAGATCTACACTCTTTCCCTACACGACGCTCTT CCGATCTACGCAACTTGTGGAAAGGACGAAACACCG	IDT, Coralville, USA
P5 8 nt	AATGATACGGCGACCACCGAGATCTACACTCTTTCCCTACACGACGCTCTT CCGATCTGAAGACCCTTGTGGAAAGGACGAAACACCG	IDT, Coralville, USA
P7_A01	CAAGCAGAAGACGGCATACGAGATCGGTTCAAGTGACTGGAGTTCAGAC GTGTGCTCTTCCGATCTCCAATTCCCACTCCTTTCAAGACCT	IDT, Coralville, USA
P7_A02	CAAGCAGAAGACGGCATACGAGATGCTGGATTGTGACTGGAGTTCAGAC GTGTGCTCTTCCGATCTCCAATTCCCACTCCTTTCAAGACCT	IDT, Coralville, USA
P7_A03	CAAGCAGAAGACGGCATACGAGATTAACTCGGGTGACTGGAGTTCAGAC GTGTGCTCTTCCGATCTCCAATTCCCACTCCTTTCAAGACCT	IDT, Coralville, USA
P7_A04	CAAGCAGAAGACGGCATACGAGATTAACAGTTGTGACTGGAGTTCAGAC GTGTGCTCTTCCGATCTCCAATTCCCACTCCTTTCAAGACCT	IDT, Coralville, USA
P7_A05	CAAGCAGAAGACGGCATACGAGATATACTCAAGTGACTGGAGTTCAGAC GTGTGCTCTTCCGATCTCCAATTCCCACTCCTTTCAAGACCT	IDT, Coralville, USA
P7_A06	CAAGCAGAAGACGGCATACGAGATGCTGAGAAGTGACTGGAGTTCAGA CGTGTGCTCTTCCGATCTCCAATTCCCACTCCTTTCAAGACCT	IDT, Coralville, USA
P7_A07	CAAGCAGAAGACGGCATACGAGATATTGGAGGGTGACTGGAGTTCAGA CGTGTGCTCTTCCGATCTCCAATTCCCACTCCTTTCAAGACCT	IDT, Coralville, USA

Table 2-12: Primer for sanger sequencing used within this project.

Name	Sequence (5'-3')	Supplier
Human U6 promoter forward primer	GAGGGCCTATTTCCCATGATT	LGC Genomics GmbH, Berlin, Germany
M13-24 forward primer	CCAGGGTTTTCCCAGTCACG	LGC Genomics GmbH, Berlin, Germany
M13-24 reverse primer	CGGATAACAATTTCACACAGG	LGC Genomics GmbH, Berlin, Germany

2.1.10 Antibodies

Table 2-13: Antibodies used within this project.

Antigen	Dilution	Supplier (catalog no.)
Goat polyclonal anti-mouse-Horseradish Peroxidase (HRP)	1:5,000	Dianova, Hamburg, Germany (#115-035-003)
Goat polyclonal anti-rabbit- Horseradish Peroxidase (HRP)	1:500	Dianova, Hamburg, Germany (#111-035-003)
Mouse monoclonal anti-MEK1/2 (L38C12)	1:1,000	Cell Signaling Technology, Danvers, USA (#9122)
Mouse monoclonal anti-β-Actin (C4)	1:1,000	Santa Cruz Biotechnology, Dallas, USA (#sc-47778)
Rabbit monoclonal anti-Neurofibromin 1 (D7R7D) NF1	1:500	Cell Signaling Technology, Danvers, USA (#14623)
Rabbit monoclonal anti-p44/42 MAPK (Erk1/2) (137F5)	1:1,000	Cell Signaling Technology, Danvers, USA (#4695),
Rabbit monoclonal anti-Phospho-Akt (Ser473) (D9E) XP®	1:1,000	Cell Signaling Technology, Danvers, USA (#4058)
Rabbit monoclonal anti-Phospho-MEK1/2 (Ser217/221) (41G9)	1:1,000	Cell Signaling Technology, Danvers, USA (#9121)
Rabbit monoclonal anti-Phospho-p44/42 MAPK (Erk1/2) (Thr202/Tyr204) (D13.14.4E) XP®	1:1,000	Cell Signaling Technology, Danvers, USA (#4370),

Rabbit polyclonal anti-AKT	1:1,000	Cell Signaling Technology, Danvers, USA (#2938)
Rabbit polyclonal anti-NF1	1:3,000	Abcam, Cambridge, United Kingdom (#17963)
Rabbit polyclonal anti-Vinculin	1:1,000	Cell Signaling Technology, Danvers, USA (#4650)

2.1.11 Buffer and media

Table 2-14: Buffer and media used within this project.

Name	Supplier (catalog no.)
Accutase®	Merck, Darmstadt, Germany (#A6964)
Dulbecco's modified Eagle Medium (D-MEM), high glucose, GlutaMAX™ supplement	Thermo Fisher Scientific, Waltham, USA (#61965026)
NEBuffer 2.1	NEB, Ipswich, USA (#B7202)
NEBuffer 3.1	NEB, Ipswich, USA (#B7203)
NuPAGE Tris-Acetate SDS Running Buffer (20x)	Thermo Fisher Scientific, Waltham, USA (#NP0007)
Opti-MEM	Thermo Fisher Scientific, Waltham, USA (#31985062)
Phosphate buffered saline (PBS)	Thermo Fisher Scientific, Waltham, USA (#10010023)
Roswell Park Memorial Institute (RPMI) 1640-based medium	Thermo Fisher Scientific, Waltham, USA (#21875034)
Super optimal broth (SOC) medium	Thermo Fisher Scientific, Waltham, USA (#15544034)

Table 2-15: Self-made buffers used within this project.

Buffer	Components
1x Separation gel buffer SDS-PAGE	1.5 M Tris 250 mL dH2O pH 8.8
1x Stacking gel buffer SDS-PAGE	1 M Tris-HCL 250 mL dH2O pH 6.8
1x TE-buffer	0.001 M Tris-HCl pH7.4 0.1 mM EDTA pH8
1x TRIS-Glycine SDS running buffer	25 mM Trizma base 192 mM Glycine 1% SDS
1xTAE-buffer	40 mM Tris-base 20 mM acetic acid 1 mM EDTA
Cell lysis buffer BioRad	cell lysis buffer of Bio-Plex Pro Cell signaling kit, cell lysis factor QG (1:100), PMSF (1:250)
Cell lysis buffer I	15 mM HEPES 150 mM NaCl 10 mM EDTA 2% Triton X-100 pH 7.5
Cell lysis buffer II	15 mM HEPES 150 mM NaCl 10 mM EDTA 2% Triton X-100 pH 7.5 1xPhosSTOP™ 1xcOmplete™ Mini EDTA free protease inhibitor 10 µg/mL Leupeptin

	10 µg/mL Aprotinin 200 µM PMSF 25 mM NaF
Semi-dry blot transfer buffer	25 mM Trizma base 192 mM Glycine 20% methanol
TBS-T	1xTBS Tween-20
Wet blot transfer buffer	25 mM Tris 192 mM glycine 10% Methanol 0.05% SDS pH 8.3

2.1.12 Cell lines

Table 2-16: Cell lines used within this project.

Name	Cell origin	Supplier (catalog no.)
HEK293FT	*Homo sapiens,* female, embryonal kidney	Thermo Fisher Scientific, Waltham, USA (#R7007)
Kelly	*Homo sapiens,* female, neuroblastoma, [213]	DSMZ-German Collection of Microorganisms and Cell Cultures GmbH (#ACC 355)
LAN-5	*Homo sapiens,* male, neuroblastoma,[214]	DSMZ-German Collection of Microorganisms and Cell Cultures GmbH (#ACC 673)
SH-SY5Y	*Homo sapiens*, female, neuroblastoma, [215]	DSMZ-German Collection of Microorganisms and Cell Cultures GmbH (#ACC 209)

2.1.13 Software

Table 2-17: Software used within this project.

Name	Reference or producer	URL
Adobe Illustrator 2021	Adobe, San Jose, USA	-
BioRender	BioRender, Toronto, Canada	BioRender.com
D300eControl, version 3.2.5	HP Development Company, L.P.,	-
DESeq2		https://bioconductor.org/packages/release/bioc/html/DESeq2.html
EMBOSS Needle	[216]	https://www.ebi.ac.uk/Tools/psa/emboss_needle/
FastQC		https://www.bioinformatics.babraham.ac.uk/projects/fastqc/
ggplot2		https://ggplot2.tidyverse.org/
GraphPad Prism (version 9)	Graphpad Software, San Diego, USA	-
GSEA_4.1.0	[217, 218]	https://www.gsea-msigdb.org/gsea/index.jsp
IGV_2.8.2	[219]	https://software.broadinstitute.org/software/igv/
Incucyte Plate Map Editor 2019B Rev2	Sartorius, Göttingen, Germany	-
IncuCyte-2019BRev2	Sartorius, Göttingen, Germany	-
MultiQC		
PANTHER classification tool_17.0	[220]	http://www.pantherdb.org/
R Studio Desktop (version 1.1.463)	RStudio, Boston, USA	-
R version 4.1.2	R: A language and environment for statistical	https://www.R-project.org

	computing. R Core Team, R Foundation for Statistical Computing, Vienna, Austria.	
SnapGeneViewer, version 4.1.9	SnapGene, San Diego, USA	-
STAR		https://github.com/alexdobin/STAR
subread featureCounts		http://subread.sourceforge.net/
Vision-Capt (version 16.11a)	Vilber Lourmat	-

2.2 Methods

2.2.1 CRISPR/Cas9 knockout screens

In order to perform Clustered Regularly Interspaced Short Palindromic Repeats (CRISPR)/Cas9 knockout screens to identify genes associated with an ALK inhibitor resistant phenotype in *ALK*-driven neuroblastoma cell lines, a sequence of experiments had to be performed (Figure 2.1). The single-guide RNA (sgRNA)-containing plasmid library named Brunello was amplified, validated, sequenced to investigate the distribution of all the different plasmids and packed in lentiviral particles. The *ALK*-driven neuroblastoma cell line of choice, SH-SY5Y, was infected and positively infected cells selected for using puromycin. The cells were then exposed to the ALK inhibitors ceritinib or lorlatinib, as well as DMSO (vehicle control) for 13 days. Genomic deoxyribonucleic acid (gDNA) was isolated of surviving cells and amplicon sequencing performed to quantify sgRNA abundance using next generation sequencing. The sequencing data was analysed using MAGeCK.

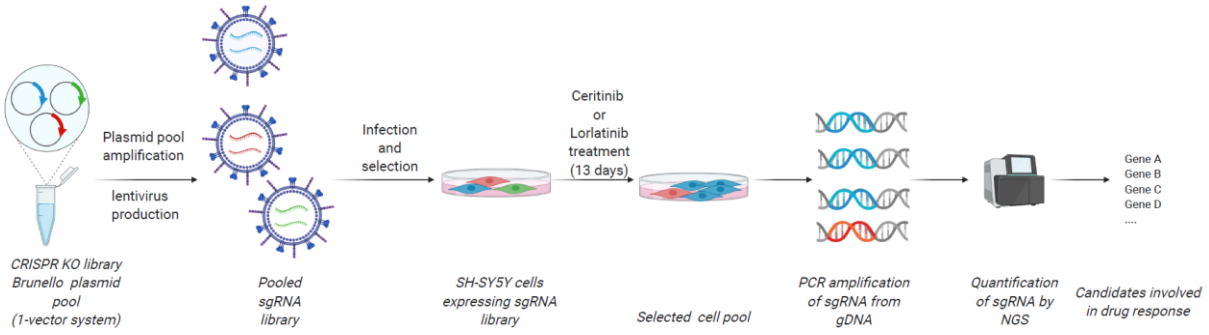

Figure 2.1: Schematic showing the workflow of the performed CRISPR/Cas9 knockout screens. Previously published in Berlak *et al*. [1].

2.2.1.1 Amplification and validation of Brunello library plasmid pool

2.2.1.1.1 Library amplification

To perform CRISPR/Cas9 knockout screens viral particles had to be produced, containing the Brunello library plasmids. Therefore, the sgRNA-containing plasmid library called Brunello, which is composed of DNA plasmids encoding 76,441 sgRNAs that potentially target 19,114 genes (average of 4 sgRNAs per gene) was amplified by bacterial transformation (electroporation) followed by bacterial expansion [209]. Therefore, 25 µL megaX DH10B T1R electrocomp™ Escherichia coli (*E. coli)* cells and 100 ng plasmid DNA (pDNA) were mixed, pipette into a 0.1 cm gap electroporation cuvette and electroporation performed with the Gene Pulser Xcell electroporation system and settings 2.0 kV, 200 ohms and 25 µF. Pre-warmed super optimal broth (SOC) medium was added to the cells and the suspension transferred into a tube. This was performed for a total of 2 reactions. As an electroporation control sample, 25 µL megaX DH10B T1R electrocomp™ cells were electroporated with 100 ng pUC19 plasmid. The cell suspensions were incubated for 1 h at 30°C. Subsequently 6x 100 mL Luria-Bertani (LB) media supplemented with 50 µg/mL ampicillin (amp) were inoculated with equal amounts of cell suspension electroporated with Brunello library pDNA in 1 L Erlenmeyer flasks and incubated at 30°C overnight in an incubator shaker at 250 rpm. A 10 µL aliquot of Brunello library pDNA electroporated cell suspension was used to assess the number of electroporated cells, assuming that one *E. coli* cell takes up only one plasmid. Therefore, the 10 µL aliquot was used for a 1:1,000, 1:10,000 and 1:100,000 dilution which were all spread using glass beads on LB-agar plates (50 µg/mL amp). Plates were incubated at 30°C in a Heratherm™ Compact Microbiological Incubator overnight. The same was performed for the pUC19 control sample. Colony forming units (CFU) were counted the next day to assess the number of electroporated cells in order to draw conclusions about each plasmid's coverage, assuming that one *E. coli* cell takes up only one plasmid.

The inoculated culture of *E. coli* cells with the Brunello library pDNA was centrifuged for 20 min, 4,000 x *g* at 4°C the day after electroporation using a Sorvall SLA-3000 rotor centrifuge. PDNA was isolated using the Macherey-Nagel NucleoBond PC 10000EF kit according to manufacturer's instructions [221]. Each pDNA pellet was dissolved in in 500 µL of kit water under a tissue culture hood and frozen at -20°C.

2.2.1.1.2 Restriction enzyme digest

To confirm that the amplified and isolated pDNA was the Brunello library construct the sample was control digested using restriction enzymes. The reaction was performed as listed in Table 2-18 at 37°C for 15 min.

Table 2-18: Setup restriction digest reaction.

Component	Amount/final concentration
pDNA	1 µg
NEBuffer 3.1	1x
BamHI	20 Units
Acc65I	10 Units

2.2.1.1.3 Agarose gel electrophoresis

Digested pDNA was analysed using an agarose gel electrophoresis. With respect to the expected DNA fragment sizes a 0.6% agarose gel with 0.3% ethidium bromide in 1xTAE buffer was prepared. DNA loading dye Orange G (6x) was added to the digested and to an undigested control sample to reach a 2x concentration. Samples as well as 10 µL GeneRuler 1 kb DNA ladder were loaded on the agarose gel and gel electrophoresis performed with 100 V for 90 min. Gels were documented using the UV Transilluminator ECX-F20.C. For gel extraction after polymerase chain reaction (PCR) experiments (2.2.1.1.5) samples were loaded on 2.7% agarose gels. The gel electrophoresis was performed as described above.

2.2.1.1.4 Nucleic acid quantification

Plasmid DNA was quantified and quality assessed using the Qubit 2.0 Fluorometer with the Qubit double-stranded (ds) DNA broad range assay kit and the 4200 TapeStation System using the High Sensitivity D1000 ScreenTape, both according to manufacturer's instructions [222, 223]. The TapeStation is an automated electrophoresis system, which separates samples based on their molecular weight and detects them using a laser-induced fluorescence detection [224]. Sample bands are then quantified as the amount of nucleic acid correlates with the amount of measured fluorescence [224]. The ScreenTapes as well as the Qubit use fluorescent dyes that, assay dependent, specifically bind DNA or ribonucleic acid (RNA) [225]. Furthermore, the TapeStation enables to assess RNA or DNA quality by calculating the RNA Integrity Number (RIN) or DNA Integrity Number (DIN), respectively [224]. The RIN and DIN are classified in categories from 1 to 10, 10 indicating intact RNA or DNA [224, 226].

As nucleic acids can also be quantified using a UV spectrophotometer due to their absorption maximum at 260 nm pDNA concentrations and purity were also assessed using 1 µL sample on the NanoDrop [227, 228]. The absorption maximum at 260 nm for nucleic acids is observed due to the nucleobases and their conjugated double bonds [227, 228]. Using the Beer-Lambert law, the nucleic acid concentration can be calculated using the measured absorbance, the optical pathlength and the

extinction coefficient [229, 230]. Furthermore, the purity of nucleic acids can be assessed by calculation of the absorbance ratio at 260 nm and 280 nm, to check for protein contamination [231]. A 260 nm/280 nm ratio of 1.8 is considered for pure DNA and 2.0 for pure RNA [231].

2.2.1.1.5 Polymerase chain reaction (PCR)

To confirm the maintenance of the library representation after amplification of the pDNA pool, the Brunello pDNA library was amplified by PCR. Reagents and sample were mixed according to Table 2-19 and the PCR performed on 5 reactions using the cycling conditions stated in Table 2-20 .

Table 2-19: PCR reaction mix for Brunello pDNA pool amplification.

Component	Volume/amount
Brunello pDNA pool	200 ng
Equimolar P5 primer mix	1 µM
P7 A01 primer	1 µM
Ultra II Q5 Master Mix Polymerase	1x
H_2O	to a final volume of 100 µL

Table 2-20: Cycling conditions for amplification of Brunello pDNA library.

Step	Temperature	Time	Cycles
Initial Denaturation	95°C	1 min	1
Denaturation	95°C	30 s	
Annealing	53°C	30 s	28
Extension	72°C	30 s	
Final Extension	72°C	10 min	1
Hold	4°C	∞	1

All five PCR reactions were pooled and loaded on an agarose gel as described in 2.2.1.1.3.

The PCR amplified Brunello pDNA library loaded on an agarose gel was gel extracted using a scalpel and gel purification performed using the NucleoSpin Gel and PCR-Clean Up kit according to manufacturer's instructions [232]. Subsequently, the sample was further purified using AMPure XP beads according to manufacturer's instructions to prepare the pDNA library for NGS [233].

2.2.1.1.6 Next generation sequencing- DNA sequencing

The purified, quantitated and quality assessed PCR amplified Brunello pDNA library sample was sequenced to assess sgRNA distribution in the plasmid pool. The sample was submitted for sequencing at the Berlin Institute of Health sequencing core facility and sequenced using the paired-end 150 MiniSeq Mid Output kit with 10% PhiX on a MiniSeq system. To assess sgRNA distribution in the plasmid pool the respective sequencing data was analysed using MAGeCK-VISPR [234].

2.2.1.2 Lentiviral packaging of Brunello library plasmid pool

2.2.1.2.1 Cell lines

For CRISPR/Cas9 knockout screens to investigate genes associated with ALK-inhibitor resistance, the *ALK*-mutated, human neuroblastoma cell line SH-SY5Y was chosen. It was obtained from the German Collection of Microorganisms and Cell Cultures (DSMZ) and cultured in a Roswell Park Memorial Institute (RPMI) 1640-based medium, supplemented with 10% fetal calf serum (FCS) and 1% penicillin/streptomycin (P/S) at 37°C, 5% carbon dioxide (CO_2) and 21% oxygen (O_2) in humid atmosphere. The cell line was authenticated by short tandem repeat (STR) DNA typing at the DSMZ. Tests for mycoplasma contamination were performed regularly using the PlasmoTest kit. The HEK293FT cell line was purchased from Thermo Fisher and cultivated in Dulbecco's modified Eagle Medium (D-MEM) supplemented with 10% FCS, 1% P/S, 1 mM non-essential amino acids (NEAA), 1mM sodium pyruvate and 500 µg/mL Geneticin and kept in the same atmosphere as the SH-SY5Y cells.

2.2.1.2.2 Cell thawing

Cell stock aliquots stored at -187°C or at -80°C were rapidly thawed in a water bath at 37°C. Cells were transferred into pre-warmed complete growth medium in a collection tube and spun at 300 x *g* for 5 min. The supernatant was discarded, cells resuspended in complete growth medium and transferred to an appropriate tissue culture vessel.

2.2.1.2.3 Cell passaging

For general maintenance of cell lines, cells were passaged once they were 80% confluent. Old growth medium was discarded, and cells washed once with 1x phosphate buffered saline (PBS). To detach cells Accutase was added for 5 min and cells incubated at 37°C until cells detached from the tissue culture vessel. The reaction was stopped using complete growth medium and the cell suspension transferred into an appropriate collection tube and cells centrifuged at 300 x *g* for 5 min. The supernatant was discarded, and cells resuspended in complete growth medium. Depending on subsequent experiments, a certain number of cells were seeded in complete growth medium on an appropriate tissue culture vessel.

2.2.1.2.4 Cell counting

To assess cell viability and cell density, detached cells were pre-diluted in complete growth medium to be in the optimal range of the TC20 cell counter (1 x 10^5 cells to 5 x 10^6 cells). Next, cells were mixed 1:1 with 0.4% trypan blue solution. Trypan blue was used to stain dead cells or cells with a compromised cell membrane [235]. After a one-minute-incubation the mixture was pipetted into the counting slide and counted using the TC20 cell counter and default settings.

2.2.1.2.5 Transfection

In order to perform a CRISPR/Cas9 knockout screen, the validated pDNA pool had to be packed into lentiviral particles using a third-generation lentiviral system. A high viral titer (a total of 76,441,000 transducing units (TU)) had to be produced to meet the coverage criterium of 1,000x of each sgRNA. Therefore 8x 19*10^6 HEK293FT cells were seeded one day prior to transfection on T225 flasks and transfected using the CalPhos™ mammalian transfection kit according to manufacturer's instructions [236]. The following envelope and packaging plasmids as well as the lentiviral transfer plasmid lentiCRISPRv2 (Brunello library) were used in a 1:2:2:3 ratio: pMD2.G, pMDLg/pRRE, pRSV-REV and the Brunello plasmid library. One additional T225 flask was transfected with the lentiCas9-EGFP lentiviral transfer plasmid as transfection control. A medium change was performed approximately 16 h after transfection and the medium supplemented with 6 mM sodium butyrate. Virus was harvested 48 h after sodium butyrate treatment. Therefore, the supernatant (30 mL/T225 flask) was removed from the cells and centrifuged for 10 min, 1,321 x *g* and 4°C. The supernatant gained after centrifugation was then filtered using stericups durapore 0.45 µm on ice and ultracentrifugated at 103,000 x *g* and 4°C for 1 h and 30 min using the ultracentrifuge Optima L90K. The supernatant was discarded, and viral pellets resuspended in 1,120 µL D-MEM medium. This viral solution was transferred to a 1.5 mL tube and incubated for 2 h at 4°C under agitation. The virus containing solution was then aliquoted, to avoid freeze-thaw cycles and resulting titer reduction, and stored at -80°C.

2.2.1.2.6 Virus titer (TU/µL) determination

To perform the CRISPR/Cas9 knockout screen with a low multiplicity of infection (MOI), to aim for only one viral genome integration event per cell, the virus titer (TU/µL) had to be determined for the cell line of interest. 0.7*10^6 SH-SY5Y cells were seeded per well on a 6-well plate one day prior to infection. On the day of transduction different volumes of virus were used to infect the cells. The medium was supplemented with 5 µg/mL polybrene. 24 h post transduction the medium was changed. 48 h post transduction the medium was changed again to select for positively infected cells using 0.8 µg/mL puromycin. The optimal puromycin concentration was determined in a titration experiment beforehand. Cells were kept in selection medium until all cells in the control well (not transduced) were dead. Cells were then stained using crystal violet, as this dye binds to proteins and DNA and

enables the detection of adherence cells [237]. The old medium was discarded, and 4% paraformaldehyde added for 15 min and left on a plate shaker. Afterwards cells were washed once with water. 1% crystal violet staining solution (dissolved in 10% ethanol) was added to the cells for 20 min. After incubation the staining solution was aspirated, and cells washed three times with water. The water was discarded, and samples left to dry. Stained cell colonies were counted for each condition using a Axio Vert.A1 microscope and the viral titer in TU/µL calculated.

2.2.1.3 Performance and evaluation of the CRISPR/Cas9 knockout screens

2.2.1.3.1 Performance of CRISPR/Cas9 knockout screens

CRISPR/Cas9-based knockout screens were performed in the neuroblastoma cell line SH-SY5Y. To achieve one viral genome integration event per cell an MOI of 0.3 was used, which should result in an infection rate of 30% infected cells. To maintain a 1,000x representation of each sgRNA at the timepoint of transduction, 76,441,000 cells had to be infected with an MOI of 0.3. Therefore 7x $36.4*10^6$ SH-SY5Y cells were transduced per T300 flask. One transduction control sample was prepared infecting $36.4*10^6$ SH-SY5Y cells with lentiCas9-EGFP virus and one selection control sample prepared with $36.4*10^6$ not infected SH-SY5Y cells. 24 h post transduction medium was changed. 48 h post transduction puromycin selection medium (0.8 µg/mL puromycin) was added to the cells and selection stopped after 6 days (once all cells of the selection control sample were dead). Positively selected cells were expanded for 14 days to perform the screen with a 1,000x coverage per sgRNA. On the day of selection start one sample was harvest as baseline sample (t_0) and the other samples treated in two technical replicates with DMSO, 0.3 µM ceritinib or 0.1 µM lorlatinib for a total of 13 days. The inhibitor or DMSO containing medium was changed every third day. Cells were passaged as described in the section 2.2.1.2.3 and counted as described in 2.2.1.2.4. For each condition a total of 76,441,000 cells were seeded on 5x T300 flasks to keep the representation of 1,000x coverage per sgRNA. Cells were harvested on day 13 to have a coverage of at least 500x cells per sgRNA per condition.

2.2.1.3.2 DNA isolation

After 13 days of selection using ceritinib, lorlatinib or DMSO, cells were harvested, and gDNA isolated of all samples using the ZymoResearch Quick-gDNA MidiPrep kit according to manufacturer's instructions [238]. Quantity and quality of the genomic DNA was assessed as described in 2.2.1.1.4.

2.2.1.3.3 Polymerase chain reaction (PCR)

Isolated gDNA of CRISPR/Cas9 screening samples was used for PCR amplification. A total of 26 µg gDNA was used as input to maintain a sufficient library representation and 12 PCR reactions per condition performed. For each condition another P7 primer (Table 2-11) was used in the PCR reaction to allow sample demultiplexing of next generation sequencing data.

Table 2-21: PCR reaction mix for 1 reaction to gDNA of Brunello screen samples.

Component	Volume/amount
gDNA Brunello screen per condition	2.2 µg
Equimolar P5 primer mix	1 µM
Specific P7 primer per condition	1 µM
Ultra II Q5 Master Mix Polymerase	1x
H_2O	to a final volume of 100 µL

The same PCR cycling conditions were used as described for the PCR of the pDNA pool (see 2.2.1.1.5, Table 2-20). The input amount of 26 µg gDNA was isolated from $58.3*10^6$ cells and represented a coverage of 763x per sgRNA.

2.2.1.3.4 Agarose gel electrophoresis

For gel extraction after PCR experiments samples were loaded on 2.7% agarose gels. The gel electrophoresis was performed as described in 2.2.1.1.3.

2.2.1.3.5 Gel purification

Genomic DNA of Brunello screen samples that was PCR amplified and pooled per condition, was loaded on an agarose gel and gel extracted as described for the pDNA library in 2.2.1.1.3.

2.2.1.3.6 Next generation sequencing of CRISPR/Cas9 knockout screen derived gDNA

Genomic DNA of Brunello screen samples was pooled in equimolar concentrations before the pooled sample was sent to the German Cancer Research Center (Deutsches Krebsforschungszentrum, DKFZ) sequencing facility. The sample was sequenced on a NextSeq 550 sequencer using the paired-end 150 High Output kit and 10% PhiX. The amount of sequencing reads aimed for per sample was $38.28*10^6$ reads to have a 500x coverage of sgRNAs per condition.

2.2.1.3.7 Data analysis

Sequencing data derived from samples of the CRISPR/Cas9 knockout screens were analysed using MAGeCK-VISPR [234]. A MAGeCK-VISPR derived list of genes which had enriched sgRNAs in all ALK inhibitor treated samples with a *P*-value ≤ 0.01 was subjected to a Gene Set Enrichment Analysis (GSEA). The GSEA [217, 218] was performed using the "c2" gene set from the MsigDB database and specific significance cut-offs (FDR<0.25 (false discovery rate), NES>1.5 (normalized enrichment score) and FWER<0.1 (familywise-error rate)) used. Furthermore, the results of the GSEA were used for a leading-edge analysis. 19 of the 5508 gene sets were again chosen based on the above stated cut offs. Those were the following gene sets:

REACTOME_MITOCHONDRIAL_TRANSLATION;REACTOME_TRANSLATION;REACTOME_NONSENSE_MEDIATED_DECAY_NMD;REACTOME_COMPLEX_I_BIOGENESIS;REACTOME_RESPIRATORY_ELECTRON_TRANSPORT;REACTOME_RESPIRATORY_ELECTRON_TRANSPORT_ATP_SYNTHESIS_BY_CHEMIOSMOTIC_COUPLING_AND_HEAT_PRODUCTION_BY_UNCOUPLING_PROTEINS;REACTOME_SRP_DEPENDENT_COTRANSLATIONAL_PROTEIN_TARGETING_TO_MEMBRANE;REACTOME_MITOCHONDRIAL_TRNA_AMINOACYLATION;WP_MITOCHONDRIAL_COMPLEX_I_ASSEMBLY_MODEL_OXPHOS_SYSTEM;REACTOME_EUKARYOTIC_TRANSLATION_INITIATION;MALONEY_RESPONSE_TO_17AAG_DN;BIOCARTA_EIF_PATHWAY;WP_ELECTRON_TRANSPORT_CHAIN_OXPHOS_SYSTEM_IN_MITOCHONDRIA;REACTOME_REGULATION_OF_EXPRESSION_OF_SLITS_AND_ROBOS;REACTOME_EUKARYOTIC_TRANSLATION_ELONGATION;RHODES_CANCER_META_SIGNATURE;REACTOME_TRNA_AMINOACYLATION;SCHLOSSER_MYC_TARGETS_REPRESSED_BY_SERUM;BIOCARTA_PROTEASOME_PATHWAY

The CRISPR/Cas9 knockout screen datasets are available as FASTQ Files in the NCBI Sequence Read Archive (SRA) with the BioProject accession number PRJNA765129 and SRA accession numbers SRR16003117 to SRR16003122.

2.2.2 CRISPR/Cas9 gene editing

2.2.2.1 Generation and validation of *NF1* knockout cell lines

2.2.2.1.1 CRISPR/Cas9 sgRNA design and preparation

In order to knockout the *NF1* gene in human neuroblastoma cell lines two sgRNAs were designed to target exon 1 and two sgRNAs to target exon 30 of *NF1* using the web tool CHOPCHOP [218]. Oligos were ordered as listed in Table 2-9 following the design recommendations described in Ran *et al*. [212]. Oligos were dissolved in 0.1xTE-buffer to have a concentration of 50 µM. Each sgRNA pair was mixed using 200 nM of each oligo, sgRNA-top and sgRNA-bottom, in a total volume of 500 µL 0.1xTE-buffer. This mixture was then incubated for 5 min at 95°C and afterwards left at room temperature for 30 min.

2.2.2.1.2 Restriction enzyme digest of CRISPR/Cas9 backbone and ligation with sgRNAs

The PX458 and PX459 backbones were digested using the reaction mix stated in Table 2-22 . The digest reaction was incubated overnight at 37°C.

Table 2-22: Restriction digest of PX458 and PX459 for vector linearization.

Component	Volume/amount
PX458 or PX459 pDNA	5 µg
Buffer 2	1x
BbsI	30 Units
H_2O	to a final volume of 50 µL

The digested vector was loaded on an agarose gel and gel electrophoresis performed as described in 2.2.1.1.3 using a 1% agarose gel. The linearized plasmid bands were gel-extracted as described in 2.2.1.3.5. PDNA concentrations and their purity were assessed as described in 2.2.1.1.4. The linearized vectors were then ligated with the annealed oligo pairs. This was performed for all four sgRNAs with both backbones. Annealing reactions (as outlined Table 2-23) were incubated at 16°C overnight.

Table 2-23: Ligation reaction for cloning of CRISPR/Cas9 sgRNA containing plasmids.

Component	Volume/amount
PX458 or PX459 pDNA	2 µL
annealed oligo pair	1 µL
T4 ligase Buffer	1x
T4 ligase	1 µL
H_2O	to a final volume of 20 µL

For each backbone a water control without annealed oligos was prepared to evaluate after a transformation in *E. coli* cells, how many colony forming units contain re-circularized backbones. This would indicate the background signal of the vector and oligo ligation reaction. Resulting plasmids were PX458-E1-1, PX458-E1-2, PX458-E30-1, PX458-E30-2 as well as PX459-E1-1, PX459-E1-2, PX459-E30-1, PX459-E30-2.

2.2.2.1.3 Transformation

Ligation reactions were transformed into XL10-Gold ultracompetent *E. coli* cells. Therefore, 200 µL of XL10-Gold cells were added to each ligation reaction. A heat shock was performed at 42°C in a water bath for 1 min and 30 s. Samples were placed on ice immediately afterwards for 2 min. 800 µL of pre-warmed SOC medium were added and samples incubated for 1 h at 37°C while shaking. This incubation was followed by a short centrifugation of 2 min at 2,700 x *g*. The supernatant was discarded, and cells resuspended in 50 µL SOC medium. The total volume of each sample was spread on 50 µg/mL amp-containing agar plates using glass beads. Plates were incubated overnight at 37°C. For each construct one CFU was picked to inoculate 4 mL of LB-medium supplemented with 100 µg/mL amp.

2.2.2.1.4 Plasmid DNA isolation

For pDNA isolation of low volume cultures inoculated with transformed *E. coli* cells buffers from the QIAprep Spin Miniprep kit were used. 1.5 mL of overnight cultures were transferred to 1.5 mL tubes and centrifuged for 2 min with 2,350 x *g*. Pellets were resuspended in 200 µL buffer P1 and placed on ice. 200 µL of buffer P2 were added and samples mixed by inversion. This step was followed by addition of 200 µL of buffer P3. Samples were mixed again and spun for 10 min at 4°C and 25,000 x *g*. 600 µL of

supernatant were then mixed with 800 µL isopropanol and incubated on ice for 10 min. Samples were again spun at 4°C using 25,000 x *g* for 30 min. The supernatant was discarded, and pellets resuspended in 500 µL of 70% ethanol. Subsequently samples were centrifuged for 10 min at 4°C and 25,000 x *g*. Again, the supernatant was discarded, and remaining pDNA-pellets air-dried. In a final step pDNA-pellets were dissolved in 30 µL 0.1% TE-buffer. DNA concentrations were determined as described in 2.2.1.1.4.The different constructs were then sent for sanger sequencing to validate the correct sequence, using the human U6 promoter forward primer (Table 2-12) according to service provider recommendations (LGC Genomics GmbH).

For high volume cultures pDNA was isolated using the NucleoBond Xtra Maxi kit according to manufacturer's instructions [221].

2.2.2.1.5 Cell lines

Cell lines used to generate *NF1* knockout cell lines were obtained, cultivated, authenticated, and tested for mycoplasma as described in 2.2.1.2.1. The human neuroblastoma cell line LAN-5 was cultured in RPMI 1640-based medium supplemented with 20% FCS, 1% P/S at 37°C and 1 mM NEAA. The neuroblastoma cell line Kelly was cultured as SH-SY5Y described in 2.2.1.2.1 . Cell lines were thawed, passaged and counted as described in 2.2.1.2.2 , 2.2.1.2.3 and 2.2.1.2.4.

2.2.2.1.6 Cell stock preparation

Cells were detached and prepared as described in 2.2.1.2.3. Cells were then resuspended in complete growth medium containing 10% DMSO. Cell suspension was aliquoted, and stocks frozen using a Mr Frosty (freezing container) at -80°C. For long-term storage cell stocks were kept at -187°C.

2.2.2.1.7 Transfection

The neuroblastoma cell lines SH-SY5Y, LAN-5 and Kelly were seeded with 150,000 cells per well on a 12-well plate and transfected with each plasmid listed in 2.2.2.1.2 using Lipofectamine™ LTX according to manufacturer's instructions [239]. After 24 h control cells transfected with PX458-constructs were checked for GFP signals using a microscope. If GFP was detected cells were successfully transfected and therefore the medium changed and supplemented with 0.7 µg/mL puromycin to select for positively transfected cells until all cells in control wells, not transfected cells and all cells transfected with PX458-constructs, were dead. Puromycin selected cell pools were expanded to confluence in 15 cm tissue culture dishes for subsequent experiments.

2.2.2.1.8 Generation of isogenic cell lines

Once positively transfected cell pools were expanded and investigated for edits, isogenic cell lines were isolated. This was done using serial dilution. To this end, cell pools of transfected cells were passed through a 40 µm cell strainer to get single cell suspensions, which were diluted and transferred to a

96-well plate. Dilutions and transfer volumes were chosen to ensure a theoretical transfer of half a cell per single well of that plate. 24 h after seeding wells were checked for cells using a microscope. Wells with one cell were marked and cells with no cell or more than one cell crossed. Single cell clones were expanded to generate isogenic cell lines that were further investigated.

2.2.2.1.9 DNA isolation

Genomic DNA of cell bulk populations and isogenic cell lines was isolated using the NucleoSpin Tissue kit according to manufacturer's instructions [240].

2.2.2.1.10 Polymerase chain reaction (PCR)

DNA of positively transfected cell bulk as well as of single cell clones was used to investigate editing of the CRISPR/Cas9-targeted *NF1* sequences using PCR with primers flanking the region of the expected double strand break, which is mediated by Cas9 nuclease to be 3 bp upstream of the protospacer adjacent motif (PAM) [212]. The sequences of the respective primers used for PCR analyses are described in Table 2-10.

Table 2-24: PCR reaction for INDEL detection.

Component	Volume/amount
gDNA	60 ng
NF1 forward primer	1.67 µM
NF1 reverse primer	1.67 µM
KAPA2G Fast HotStart ReadyMix	1x
H_2O	to a final volume of 15 µL

PCRs were performed using the cycling conditions stated in Table 2-25.

Table 2-25: Cycling conditions for amplification of CRISPR cut site region.

Step	Temperature	Time	Cycles
Initial Denaturation	95°C	5 min	1
Denaturation	95°C	10 s	35
Annealing	62°C	15 s	
Extension	72°C	10 s	
Final Extension	72°C	5 min	1
Hold	4°C	∞	1

2.2.2.1.11 T7 assay

A T7 assay was performed as a first screening experiment to detect editing events in cell bulk and later for isogenic cell lines. The T7 endonuclease catalyses the cleavage of mismatched DNA [241]. 200 ng of PCR products from cell bulk populations or isogenic cell lines generated as described in 2.2.2.1.10 were mixed with 1 µL NEB buffer 2.1 and water in a total volume of 10 µL. Samples were then incubated using the conditions listed in Table 2-26.

Table 2-26: Rehybridization of PCR products for T7 assay performance.

Temperature	Time
95°C	5 min
85°C	ramp down -2°C/s
25°C	ramp down -0.1°C/s
4°C	∞

Each reaction was then supplemented according to Table 2-27.

Table 2-27: Reaction mixture for T7 endonuclease I DNA cleavage of mismatched DNA.

Component	Volume/amount
Rehybridized mix	10 µL
T7 endonuclease I	5 Units
NEB buffer 2.1	1x
H_2O	to a final volume of 15 µL

Samples were incubated for 30 min at 37°C. Subsequently digested and undigested control samples were loaded on a 2% agarose gel as described in 2.2.1.1.3. For some samples PCR products of edited pools or isogenic cell lines were mixed in equimolar ratios with PCR product of the respective parental cell line before the rehybridization step.

2.2.2.1.12 Protein isolation

To investigate cell bulk populations and isogenic cell lines for an *NF1* knockout, western blot experiments were performed. For protein lysate preparation cell pellets were resuspended in cell lysis buffer I supplemented with 1x PhosSTOP™ phosphatase inhibitor cocktail and 1x cOmplete™ Mini EDTA free protease inhibitor cocktail. Samples were incubated for 30 min on ice at 4°C, vortexed for 10 s and centrifuged for 30 min at 4°C and 25,000 x *g*. The supernatant was transferred on ice into new tubes and protein concentrations determined using a bicinchoninic acid assay (BCA).

2.2.2.1.13 Protein quantification using a BCA assay

Protein concentrations were determined using the Pierce™ BCA Protein assay kit according to manufacturer's instructions [242]. Absorbance was measured using the Epoch microplate spectrophotometer at 562 nm.

2.2.2.1.14 Sodium dodecyl sulfate-polyacrylamide gel electrophoresis (SDS-PAGE)

To detect NF1 protein using western blot, 15 µg of sample were prepared for SDS-PAGE. Samples were supplemented with 4x Laemmli buffer containing 355 mM β-mercaptoethanol and denatured at 95°C for 5 min. Samples were loaded on NuPAGE 3-8% Tris-Acetate Protein Gels and electrophoresis performed in NuPAGE Tris-Acetate SDS Running Buffer (1x). Before performance of the SDS-PAGE the buffer was supplemented with NuPAGE Antioxidant (0.25%). 15 µL HiMark Pre-stained Protein Standard or 3 µL PageRuler™ Prestained Protein Ladder were used as size standard. SDS-PAGE experiments were performed at 80 V for 4 h.

2.2.2.1.15 Western Blot

In order to investigate NF1 protein, proteins were transferred from SDS-PAGE gels onto a polyvinylidene fluoride (PVDF) membrane using a wet blot method. Wet blot experiments were performed using the wet blot transfer buffer (Table 2-14) at 4°C, 30 V/90 mA for 16 h. Subsequently, membranes were blocked in 10% milk in TBS-T (Table 2-14) for 1 h and 30 min. Afterwards membranes were washed 3x for 10 min in 1xTBS-T. Membranes were then incubated with respective primary antibodies diluted in 5% milk-TBS-T (see Table 2-13) overnight at 4°C. The next day membranes were again washed 3x for 10 min in 1xTBS-T. Membranes were incubated with secondary antibodies diluted in 5% milk-TBS-T for 1 h and 30 min at room temperature. Membranes were again washed 3x for 10 min in 1xTBS-T. Subsequently blots were developed using a western blotting luminol reagent and documented with a Fusion FX imaging system. Antibodies used for NF1 detection were the rabbit monoclonal anti-Neurofibromin 1 (D7R7D) as primary antibody and goat polyclonal anti-rabbit as secondary antibody. As loading control Vinculin was detected using a rabbit polyclonal anti-Vinculin primary antibody.

2.2.2.1.16 INDEL identification in *NF1* knockout cell lines

Isogenic cell lines were further validated by identification of sequences resulting from insertions or deletions (INDEL) in *NF1* due to Cas9 induced double-stranded breaks (DSBs) and the subsequent DNA damage repair at the targeted locus by the error-prone non-homologous end joining pathway (NHEJ) [212]. Therefore, gDNA was isolated as described in 2.2.2.1.9. The region of interest was amplified as described in 2.2.2.1.10. The PCR product was then used for TOPO cloning using the TOPO™ TA Cloning™ kit for sequencing with one shot™ TOP10 chemically competent *E. coli*. 10 ng PCR product

were mixed with 1 µL salt solution and water to a final volume of 5 µL. Then 1 µL of TOPO® vector was added, the reaction mixed and incubated for 60 min at room temperature. A water control was prepared as well. After the incubation samples were placed on ice. The ligation reaction was then transformed into one shot™ TOP10 chemically competent *E. coli* cells and incubated on ice for 30 min. As a transformation control pUC19 was transformed as well. A short heat shock was performed at 42°C for 30 s. Pre-warmed SOC medium was added, and this pre-culture incubated at 37°C for 1 h while shaking. Different volumes were spread on agar plates (50 µg/mL amp) using glass beads. These agar plates were then incubated at 37°C overnight. The next day multiple CFU were used to inoculate 4 mL of LB-medium supplemented with 100 µg/mL amp. Plasmid DNA was isolated as described in 2.2.2.1.4. Plasmids were control digested as described in

Table ***2-28***.

Table 2-28: Control digest TOPO cloning.

Component	Volume/amount
pDNA	1 µg
NEB buffer 2.1	1x
EcoRI	10 Units
H_2O	to a final volume of 30 µL

Samples were incubated for 2 h at 37°C and analysed using gel electrophoresis as described in 2.2.1.1.3. Samples with a confirmed PCR product insertion were send for sanger sequencing using the M13-24 reverse primer (Table 2-12) according to service provider recommendations (LGC Genomics GmbH). Sequencing data was analysed and compared to the parental control using SnapGeneViewer and the online tool for pairwise sequence alignment EMBOSS Needle.

2.2.2.2 Functional analysis of *NF1* knockout cell lines

2.2.2.2.1 CellTiter-Glo® ATP quantification assay

Effects of cell line exposure to ALK inhibitors as well as other inhibitors was assessed using the luminescent cell viability assay CellTiter-Glo®. This assay quantifies ATP. It was shown, that the amount of ATP is directly proportional to the amount of living cells in the sample [243]. The measured luminescent signal is proportional to the amount of ATP as this bioluminescent signal is one of the products in the oxidation of luciferin catalysed by the recombinant luciferase, that requires ATP (Figure 2.2) [244].

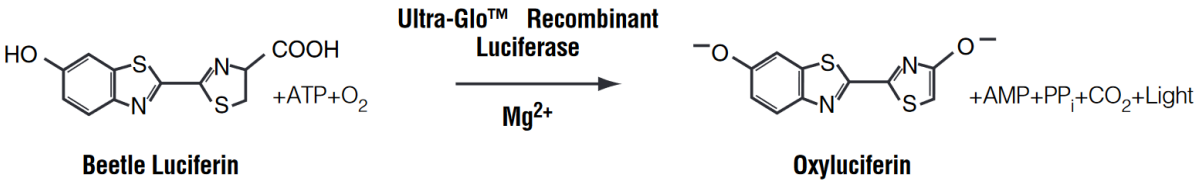

Figure 2.2: Schematic showing the basis of the CellTiter-Glo® reaction to quantify adenosine triphosphate (ATP). Luciferin is oxidized, a reaction catalysed by the luciferase in the presence of magnesium (Mg^{2+}) and oxygen (O_2) [244].

For inhibitor treatments the cell lines LAN-5 (5,000 cells/well), SH-SY5Y (3,000 cells/well) and respective model systems were seeded in white 96-well plates 24 h before the inhibitor treatment to reach a confluence of approximately 30%. Inhibitors dissolved in DMSO were applied using a Tecan D300e digital dispenser and each concentration applied in triplicates. Cell viability was assessed after 72 h performing the CellTiter-Glo® assay according to manufacturer's instructions [244].The luminescent signal was measured using the multi-plate reader GloMax® (Promega). Each experiment was performed at least three times. Each data point was subtracted by background signals of blank controls and normalized to untreated controls. Median values of each biological replicate for each tested concentration were used for evaluation of data with GraphPad Prism 9.0.

2.2.2.2.2 Incucyte

Cell numbers over and after 72 h of exposure to inhibitors were investigated using the live-cell analysis system Incucyte® S3. Therefore, LAN-5, SH-SY5Y and respective model systems were seeded with initial cell numbers according to their specific growth rate in clear 96-well plates 24 h before addition of inhibitors (LAN-5 15,000 cells/well, LAN-5 *NF1* KO #1 17,000 cells/well, LAN-5 *NF1* KO #2 17,000 cells/well, SH-SY5Y 15,000 cells/well, SH-SY5Y *NF1* KO #1 19,000 cells/well, SH-SY5Y *NF1* KO #2 8,000 cells/well). Inhibitors dissolved in DMSO were applied using a Tecan D300e digital dispenser and each concentration applied in triplicates. For each well of the 96-well plate 4 images using a 10x objective were taken and analysed using the cell-by-cell module, which allows counting of individual cells. For each well the median cell number was calculated of the 4 images taken. Subsequently, the median of the three technical replicates was calculated per concentration. Each data point was normalized to a blank control as well as to the untreated control. Median values of each biological replicate for each tested concentration were used for evaluation of data with GraphPad Prism 9.0.

2.2.2.2.3 Modelling of concentration-response data

To describe CellTiter-Glo® and Incucyte derived concentration-response data the statistics software GraphPad Prism 9.0 was used. Outlier were defined to have a viability or response value >100% and were excluded from the data set. The least square method was used to fit the respective model to the data. Two different models were tested to describe the data, the 3- and the 4-parameter logistic model (3PL and 4PL respectively). The 4PL is defined in Equation 2.1 [245-248].

$$Y = \frac{a-d}{1+\left(\frac{X}{c}\right)^{b}} + d \qquad (2.1)$$

X= concentration

Y= response

b= slope factor, Hill slope, determines steepness of the curve

d= top plateau, response when concentration=0, baseline effect

a= bottom plateau, maximum response, E_{max}

c= inhibitory dose or concentration, that results in a response halfway between the top and bottom plateau, relative IC_{50}

In GraphPad Prism 9.0 the 3PL was defined with the Hill slope set to 1. The goodness of fit of the model to describe the data was assessed by standard deviation of the residuals. Furthermore, a D'Agostino-Pearson omnibus K2 normality test was performed to test whether the distribution of residuals follows a Gaussian distribution. This is assumed by a least-square regression [249]. Additionally, a QQ residual plot was generated to further assess the assumption of Gaussian distribution. For some analysis, the Top was constraint at 100%. For comparison of concentration-response data, all settings were kept consistent between cell lines to be compared.

2.2.2.2.4 Differential gene expression in *NF1* knockout cell lines

To investigate differential gene expression in *NF1* knockout cell lines in comparison to the parental cell line messenger RNA (mRNA) sequencing experiments of chemically perturbed cell line models were performed as shown in Figure 2.3.

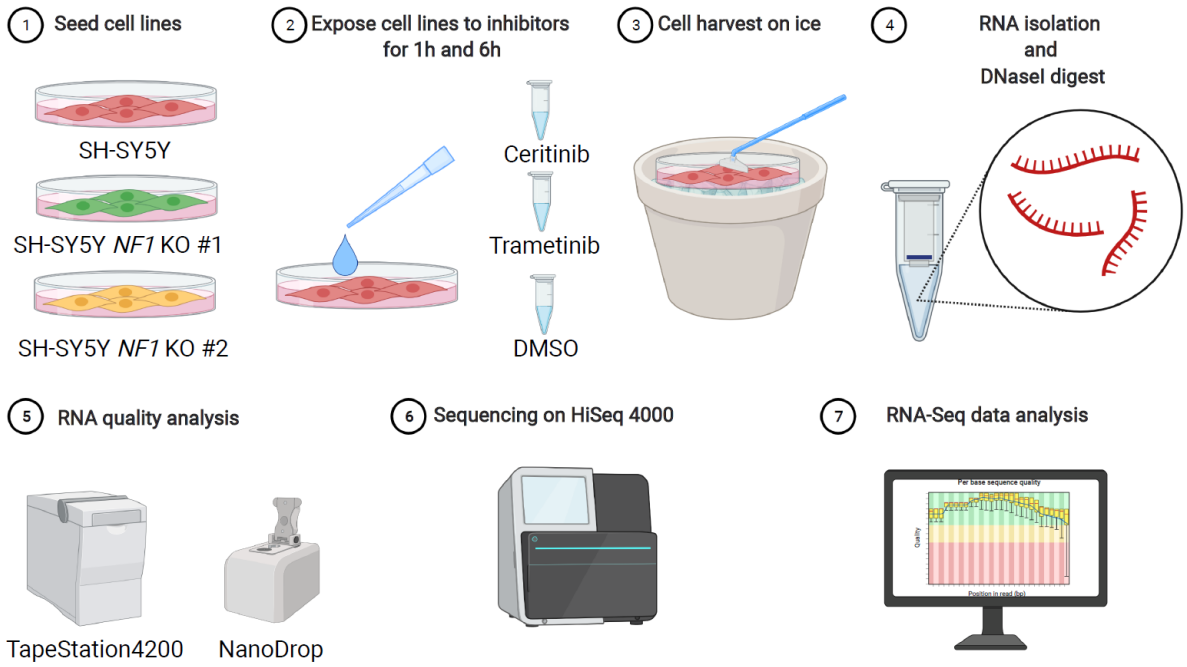

Figure 2.3: Schematic showing the experimental workflow of the performed messenger ribonucleic acid (mRNA)-sequencing experiments of perturbed *NF1* knockout cell lines and the parental cell line. Cells were exposed to the ALK inhibitor ceritinib, to the MEK 1/2 inhibitor trametinib and to DMSO (vehicle control) for 1 hour and 6 hours. Cells were harvested on ice to isolate RNA. Quality control was performed using the NanoDrop and TapeStation to assess RNA concentration, purity, and integrity. RNA meeting the quality criteria was used for sequencing and respective sequencing data analysed to assess differential gene expression.

For the experiments $4.2*10^6$ SH-SY5Y cells and respective *NF1* knockout clones were seeded 24 h before inhibitor exposure to reach 70%-80 % confluence at the time of exposure. Each cell line was incubated with 605 nM ceritinib, 49 nM trametinib, 605 nM ceritinib and 49 nM trametinib or DMSO for 1 h and 6 h. Before adding inhibitors to the cells one t_0 control sample was taken for each cell line. All experiments were performed in three biological replicates.

The cells were harvested on ice and washed with ice cold PBS and detached using a cell scraper. Cells were spun down at 300 x *g* and 4°C for 5 min. Half of each cell pellet was resuspended in TRIzol™ reagent and frozen on dry ice. Samples were stored at -80°C before the RNA isolation was continued. To continue RNA isolation, frozen cell pellets in TRIzol™ were thawed on ice and left for 5 min at room temperature. The RNA was further isolated according to manufacturer's guidelines [250]. Due to low material input 10 µg RNase-free glycogen were added to the samples during RNA precipitation. Furthermore, after glycogen addition samples were vortexed and incubated at -20°C overnight. The protocol was continued. Precipitated RNA samples were then treated with RQ1 RNase-free DNAse I for cleavage of potential residual DNA in the sample. The DNase I digestion reaction was performed as listed in Table 2-29.

Table 2-29: DNase I digest of RNA samples.

Component	Volume/amount
RNA in water or TE buffer	1–8 µL
RQ1 RNase-Free DNase reaction buffer	1x
RQ1 RNase-Free DNase	1 U/µg RNA
Protector RNase inhibitor	1 U/µL
RNA nuclease-free water	to a final volume of 10 µL

The digest was incubated at 37°C for 1 h. Afterwards a phenol:chloroform extraction was performed using equal volumes of phenol-chloroform-isoamyl alcohol and RNA sample. Samples were shaken for 15 s, incubated for 3 min at room temperature and spun for 15 min at 12,000 x *g* and 4°C. The aqueous phase was transferred into a reaction new tube and equal amounts of aqueous solution and chloroform mixed. This was shaken for 15 s and spun for 5 min at 12,000 x *g* and 4°C. Again, the aqueous phase was used for further processing. Sodium acetate was added to a final concentration of 0.3 M to the samples. Afterwards two volumes of 100% isopropanol and 10 µg RNase-free glycogen were added, and samples incubated overnight at -20°C. After the incubation, the samples were centrifuged for 10 min at 25,000 x *g* and 4°C. The supernatant was discarded, and 1 mL 75% ethanol added. After samples were vortexed for 1 min, they were again centrifuged for 10 min at 4°C with 25,000 x *g*. The steps of ethanol addition, vortexing and spinning were repeated once. The ethanol was discarded, and samples spun again for a few seconds to discard residual ethanol. Resulting RNA pellets were air dried for 10 min and resuspended in nuclease free water. RNA concentration and quality were assessed using the NanoDrop and 1 µL sample. Furthermore, the TapeStation 4200 was used with an RNA Screen tape according to manufacturer's instructions [251]. Samples with confirmed quality were sent to FASTERIS for library preparation using the Illumina Stranded mRNA Prep. Samples were then sequenced on an Illumina HiSeq4000 using 75 bp paired-end sequencing by FASTERIS.

2.2.2.2.5 Analysis of mRNA-seq data

The mRNA-sequencing (mRNA-seq) data FASTQ files were transferred from FASTERIS. The data was further processed and analysed as shown in Figure 2.4.

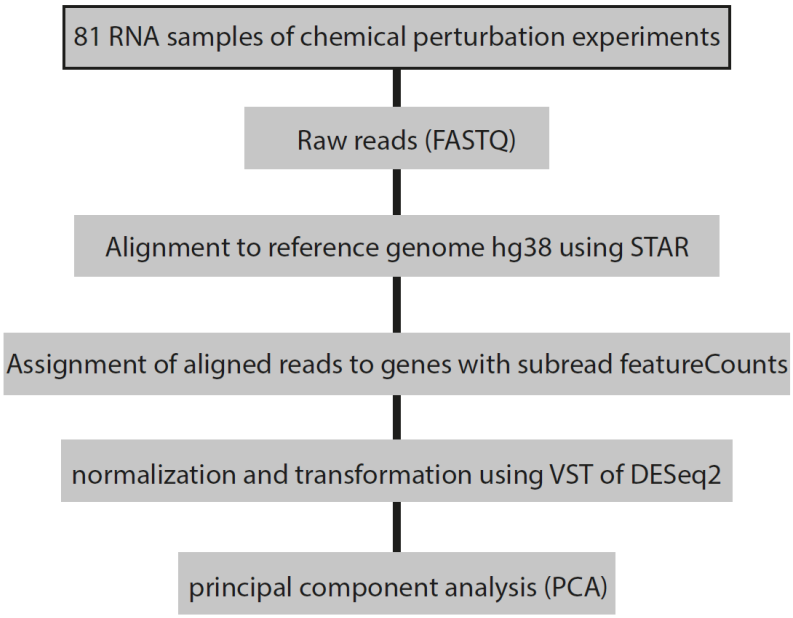

Figure 2.4: Schematic showing the bioinformatic pipeline to analyse mRNA-sequencing data regarding differential gene expression. Raw sequencing reads were aligned to the reference genome using STAR and subsequently assigned to genes using subread featureCounts. The R package DESeq2 was then used to normalise reads-per-gene and to transform these via variance-stabilising transformation. DESeq2 was also used to perform principal component analysis (PCA).

In brief, raw reads were aligned to the human reference genome (hg38) using STAR [252]. The transcriptome annotation was obtained from Gencode (v31) (RefSeq assembly accession: GCF_000001405.38). The aligned reads were assigned to genes on the same strand at the same position using subread featureCounts [253]. Reads-per-gene counts were normalised and transformed using the variance-stabilising transformation (VST) from the R package DESeq2 [254]. The quality of reads was verified using FastQC and results summarized and visualized using MultiQC [255]. A principal component analysis (PCA) was performed using the plotPCA function of DESeq2 and visualized using ggplot2 [256].

To assess differential gene expression between sample groups a linear model was used which takes into account various factors influencing gene expression: cell type, treatment type and duration of the treatment. By inclusion of an interaction term between cell types and treatment the model allowed that each cell type reacts differently to a certain treatment.

2.2.2.2.6 Perturbation experiments and computational modelling

A systems biology approach was used to investigate the effect of different perturbations on downstream signalling in *NF1* knockout cell lines in comparison to the parental cell line. The experimental workflow is shown in Figure 2.5 and is described in Berlak *et al.* [1].

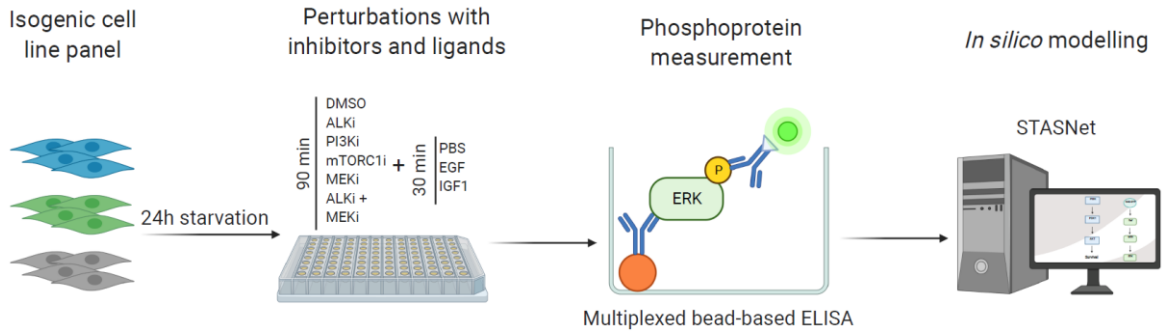

Figure 2.5: Schematic showing the experimental workflow of perturbation experiments. Isogenic cell lines with a knockout of the *NF1* gene and respective parental cell lines, were serum starved for 24 h and then exposed to ceritinib (anaplastic lymphoma kinase (ALK) inhibitor), trametinib (MAPK (mitogen-activated protein kinase)/ERK (extracellular signal-regulated kinase)-Kinase 1/2 (MEK 1/2) inhibitor), rapamycin (mammalian target of rapamycin (mTOR) inhibitor), pictilisib (phosphatidylinositol 3-kinase (PI3K) inhibitor) or DMSO (vehicle control) and subsequently stimulated for 30 min with epidermal growth factor (EGF), insulin-like growth factor-1 (IGF1) or phosphate-buffered saline (PBS) (carrier). Cells were harvested on ice and lysed. Protein lysates were then used to quantify phosphoproteins of certain target proteins using a bead-based ELISA assay. This perturbation data together with a prior network knowledge was used to model ALK downstream signalling using the R package of steady-state analysis of signalling networks (STASNet). This figure is based on Berlak *et al*. [1].

SH-SY5Y and LAN-5 as well as the respective *NF1* knockout cell lines were seeded with $0.35*10^6$ cells and $0.5*10^6$ cells per 12well plate, and serum-starved for 24 h. Then the cells were exposed to different inhibitors (see Table 2-30) inhibiting ALK downstream signalling or DMSO for 90 min. Ceritinib as well as lorlatinib were also used for a combined exposure with trametinib. The cells were incubated at 37°C.

Table 2-30: Chemical perturbations of neuroblastoma cell lines.

Inhibitor	Molecular target	SH-SY5Y	LAN-5
ceritinib	ALK	600 nM	337 nM
lorlatinib	ALK	experiment not performed	478 nM
trametinib	MEK	49 nM	31 nM
pictilisib	PI3K	1 µM	31 nM
rapamycin	mTORC	100 nM	100 nM

Subsequently cells were stimulated with 25 ng/mL EGF, 100 ng/mL insulin like growth factor 1 (IGF-1) or PBS for 30 min. The cells were harvested on ice and subsequently washed twice with ice-cold PBS, supplemented with 1x PhosSTOP™ and 1x cOmplete™ Mini. The supplemented PBS was discarded, and cell lysis buffer BioRad (see Table 2-14) was added. The cells were harvested using a cell scraper, the sample plates frozen on dry ice and stored at -80°C. Protein concentrations were determined using a BCA assay as described in 2.2.2.1.13. Subsequently samples were used for Bio-Plex Pro™ cell signalling assay experiments, which enable phosphoprotein and total target detection, according to manufacturer's instructions [257]. Protein lysates were incubated with antibody-coated magnetic

beads (fluorescently dyed microspheres) as described by Klinger *et al*. [258].These magnetic beads bind proteins of interest via their capture antibodies. Biotinylated detection antibodies specific for phosphorylated analytes of AKT (Ser^{473}), ERK1/2 (Thr^{202}/Tyr^{204}, Thr^{185}/Tyr^{187}), MEK1 (Ser^{217}/Ser^{221}) and RPS6KB1 (Thr^{389}) were added to quantify analytes. These were then bound by a streptavidin-phycoerythrin conjugate, which functioned as a fluorescent reporter. The samples were measured using the Bio-Plex MAGPIX multiplex reader. Subsequently perturbation data was used for computational modelling using the R package STASNet [259]. Model parameters of isogenic cell line triplets were constrained such that they were identical between the isogenic cell line triplets and allowed divergence of parameters between these cell lines only if it was necessary to fit the data, as quantified by a likelihood ratio test [1].

2.2.2.2.7 Perturbation experiments and western blots to investigate ALK downstream signalling

To investigate ALK downstream signalling with a complementary approach to the systems biology experiments, *NF1* knockout cell lines and respective parental cell lines were perturbed with different inhibitors. Similar to the experiments described in 2.2.2.2.6 , cells were seeded on 10 cm dishes according to Table 2-31 to reach 80% confluence at the time of inhibitor exposure, and serum starved for 24 h.

Table 2-31: Cell numbers used for perturbation experiments and subsequent western blot.

SH-SY5Y	**SH-SY5Y *NF1* KO #1**	**SH-SY5Y *NF1* KO #2**	**LAN-5**	**LAN-5 *NF1* KO #1**	**LAN-5 *NF1* KO #2**
$3*10^6$ cells	$2.3*10^6$ cells	$1*10^6$ cells	$3*10^6$ cells	$3*10^6$ cells	$3*10^6$ cells

Cells were treated with trametinib or ceritinib as stated in Table 2-30 or DMSO for a total 1 h which included 30 min of stimulation with 25 ng/mL EGF or PBS (carrier). Afterwards the cells were washed twice with ice cold PBS, supplemented with 1x PhosSTOP™ and 1x cOmplete™ Mini. The supplemented PBS was discarded, and cells harvested on ice using a cell scraper in cell lysis buffer II. Cell lysis and protein concentration determination were performed as described in 2.2.2.1.12 and 2.2.2.1.13. Proteins were separated using hand casted SDS-PAGE gels (Table 2-32).

Table 2-32: Components of hand casted SDS-PAGE gels.

Component	4% Stacking gel	10% Resolving gel
Polyacrylamide (30%)	3.3 mL	330 µL
Buffer	2.5 mL	250 µL
H_2O	4 mL	1.4 mL
SDS (20%)	50 µL	10 µL
APS (10%)	100 µL	20 µL
TEMED	4 µL	2 µL

10 µg of sample were supplemented with 4x Laemmli buffer containing 355 mM β-mercaptoethanol and denatured at 95°C for 10 min. Samples were loaded on self-made 10% Tris-Glycine-SDS polyacrylamide gels and electrophoresis performed in 1x TRIS-Glycine SDS running buffer. 5 µL PageRuler™ Prestained Protein Ladder were used as size standard. SDS-PAGE experiments were performed at 80 V for approximately 4 h. Proteins were then transferred from SDS-PAGE gels onto a PVDF membrane using a semi-dry blot method. Semi-dry blots were performed using 1x semi-dry blot transfer buffer and a trans-blot turbo transfer system at 25 V for 30 min. Membranes were developed as described in 2.2.2.1.15. For the detection of phosphoproteins, membranes were blocked and incubated with antibodies using 10% bovine serum albumin (BSA) or 5% BSA in TBS-T. Antibodies used are listed in Table 2-13.

2.2.3 Statistics

The arithmetic mean and the median were calculated with Microsoft Excel. Model fitting to describe concentration-response data was performed using GraphPad Prism 9.0.

As described in 2.2.1.3.7 data of CRISPR screens was analysed using MAGeCK. For ALK inhibitor treated samples the correlation was investigated by calculating the Pearson correlation coefficient *r* based on beta scores for respective genes and associated sgRNAs. The null hypothesis, that there is no trend in the population was tested using a two-tailed t-test. This analysis was also performed using GraphPad Prism 9.0.

Concentration-response data was evaluated using the software GraphPad Prism 9.0 as described in 2.2.2.2.3.

3 Results

The results presented in the following sections are published in Berlak *et al*. [1].

3.1 Identification of ALK inhibitor resistance associated genes in *ALK*-driven neuroblastoma cell lines

As up to 60% of high-risk neuroblastoma patients relapse despite intensive multimodal therapy and as ALK pathway activation is recurrently found in relapsed neuroblastoma, small molecule inhibitors against ALK have been the subject of paediatric clinical trials [33, 52, 159-162, 208]. In those clinical trials, it was observed that some neuroblastoma patients first experienced disease regression but eventually relapsed during the treatment [161]. To investigate resistance mechanisms to ALK inhibitors in neuroblastoma, genome-wide CRISPR/Cas9 knockout screens were performed to identify ALK inhibitor resistance associated genes in the neuroblastoma cell line SH-SY5Y.

3.1.1 Amplification of a CRISPR plasmid library

In order to perform CRISPR/Cas9 negative selection screens in the *ALK*-driven neuroblastoma cell line SH-SY5Y, the plasmid pool of the genome-wide Brunello sgRNA library had to be expanded and its sequence had to be validated before lentiviral packaging. To sequence this plasmid pool for determination of sgRNA containing plasmid distribution in the pool a PCR protocol was optimized. The recommended settings by Doench *et al*. yielded a distinct DNA band at about 350 bp as shown in Figure 3.1 in the sample PCR1 [209]. The expected band size was 290 bp.

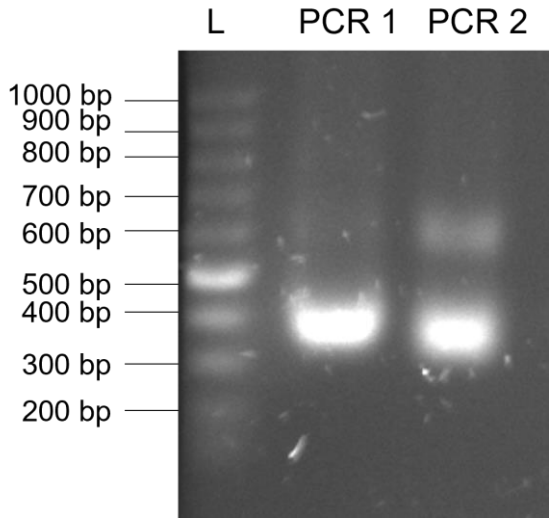

Figure 3.1: Agarose gel image of a test PCR experiment to amplify the region of interest using the Brunello plasmid DNA pool. GeneRuler 100 bp was used as a DNA ladder (L). Two different PCR programs were used for the experiment. PCR 1= PCR program as reported by Doench *et al*., PCR 2= PCR program recommended by New England BioLabs for the use of the NEBNext Ultra II Q5® Master Mix PCR.

The quality of the plasmid DNA pool, that was amplified by transfer into ultracompetent *E. coli* cells using electroporation and subsequent bacterial expansion, was verified by restriction enzyme digest

using *Bam*HI and *ACC*65I. This was performed as a quality control before next generation sequencing to verify the sequence of the plasmids. An undigested as well as the digested sample were loaded on an agarose gel and expected bands at ~5,000 bp (expected 4,829 bp) and ~8,500 bp (expected 8,188 bp) were observed in the digested samples confirming sequence identity (see Figure 3.2).

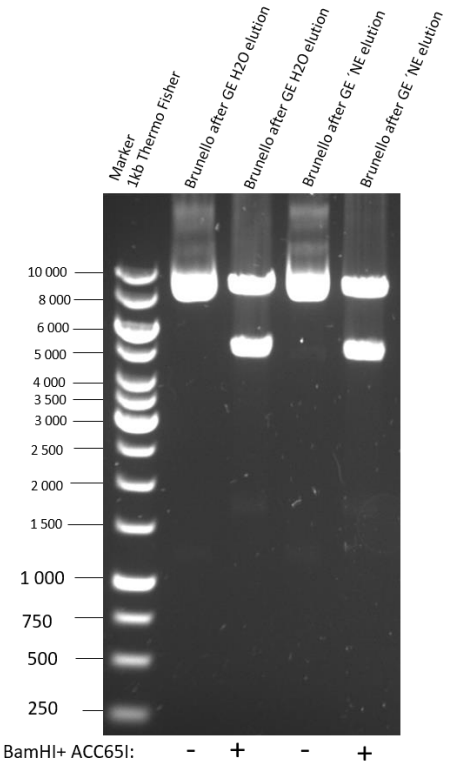

Figure 3.2: Agarose gel image of a control restriction digest. The amplified plasmid DNA pool containing the sgRNAs of the Brunello library was digested using *Bam*HI and *ACC*65I. An undigested control sample was also loaded onto the agarose gel and samples eluted in different solutions compared. For the digested plasmid pools expected DNA bands were observed. Digestion of the samples is indicated below the image with a +.

The PCR product of the sequencing library generation PCR with the plasmid pool as a template showed additional DNA bands in the sample (see Figure 3.3). As these unspecific PCR products would lead to an incorrect quantification of the actual sequencing library samples and therefore would have resulted in an incorrect loading of those samples to the flow cell and subsequently compromised the sequencing read coverage of the correct plasmid library derived amplicons, the band of interest at ~300 bp was extracted after agarose gel electrophoresis.

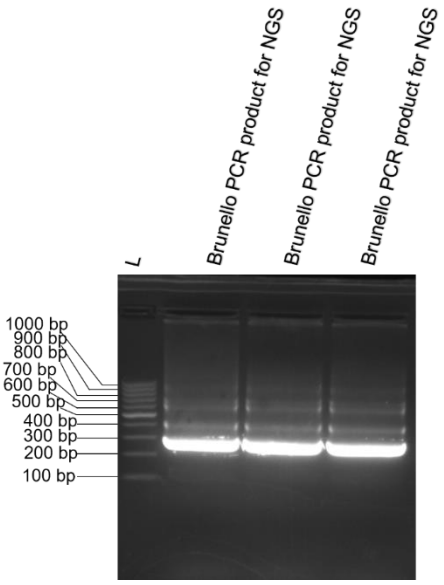

Figure 3.3: Agarose gel image of the PCR product of the sequencing library generation PCR using the amplified plasmid DNA pool as template. The expected 300 bp DNA amplicon was observed but additional DNA bands as well. The 300 bp band was extracted to be submitted for next generation sequencing to determine the distribution of constructs within the plasmid pool. GeneRuler 100 bp was used as a DNA ladder (L).

After quality control experiments the gel-extracted sequencing library sample was sent for NGS to check for even distribution of the constructs in the pool. Furthermore, it allowed to compare the data of the plasmid pool with the data of the t_0 sample to evaluate if essential genes or if sgRNAs have been lost during virus production or infection. The distribution of the plasmid DNA library was assessed by frequency plots and a Lorenz curve (see Figure 3.4). An ideal distribution would resemble a diagonal line with an AUC of 0.5 [260-262]. For the Lorenz curve of the pDNA pool an AUC of 0.646 was calculated indicating a library that is not ideally distributed [260-262]. This was in agreement with the observation that seven genes were represented by less than the four sgRNAs per gene designed. Those genes were *SPHAR*, *ZNF502*, *CT45A2*, *CT45A1*, *DEFB107B*, *DEFB106B* and *MTRNR2L1*. As the abundance of sgRNAs of actual CRISPR/Cas9 library screens is always evaluated relative to the t_0 sample the distribution of sgRNA containing plasmids in the pDNA pool should be considered if sgRNAs dropped out during the screen before interpretation but does not prevent the performance of meaningful selection screens. In the CRISPR/Cas9 knockout screens described in this thesis an uneven distribution might have prevented the identification of further genes associated with a resistant phenotype. Analysis of sequencing data for sgRNA containing plasmid distribution was kindly provided by Dr. Filippos Klironomos.

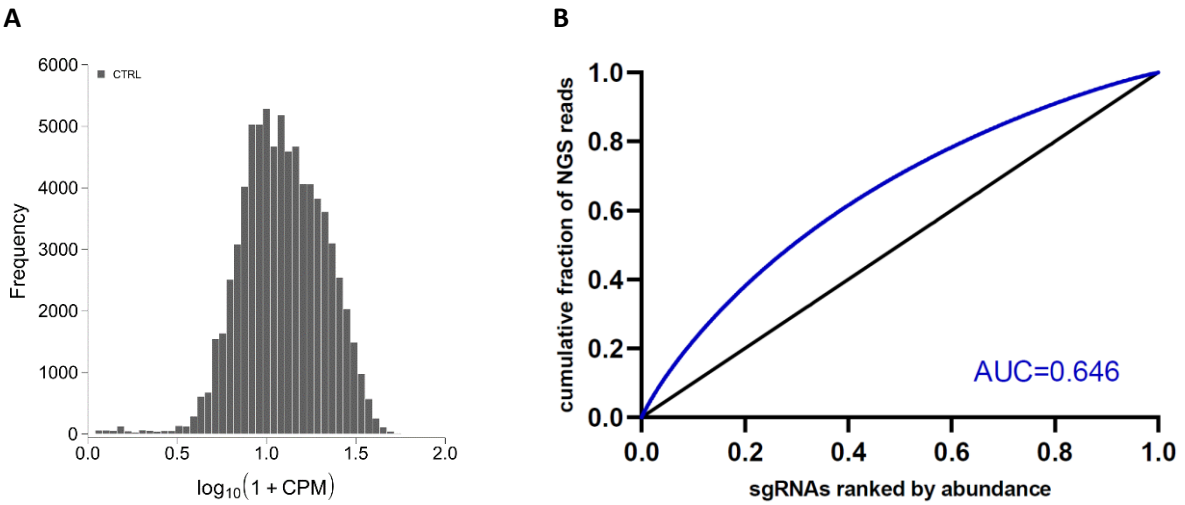

Figure 3.4: Distribution of sgRNA containing plasmids. (**A**) Frequency plot showing the distribution of individual sgRNA containing plasmids (Brunello library) in the plasmid DNA pool that was used for lentivirus production to perform CRISPR/Cas9 knockout screens. Normalized sequencing read counts were multiplied by 10^6 and a pseudocount of one added and then log10-transformed. CPM= counts per million. (**B**) The distribution of individual sgRNA containing plasmids was also assessed by plotting the cumulative fraction of next generation sequencing (NGS) reads and the sgRNAs ranked by abundance as a Lorenz curve. The black diagonal line indicates an ideal distribution with an AUC of 0.5 [260, 261]. The sample is shown in blue with an area under the curve (AUC) of 0.646.

3.1.2 Performance of CRISPR/Cas9 negative selection screens

To identify ALK inhibitor resistance associated genes CRISPR/Cas9 knockout screens were performed in SH-SY5Y by exposure to ceritinib, lorlatinib or DMSO for 13 days. A t_0 sample was harvested before exposure of the cell pool to ceritinib, lorlatinib or DMSO as distribution reference. The Sequencing data derived from the performed CRISPR/Cas9 knockout screens was used to quantitate the abundance of sgRNA sequences and retrieved read count matrices were analysed using MAGeCK-VISPR [234]. Analysis of CRISPR/Cas9 knockout screens derived sequencing data using MAGeCK-VISPR was kindly provided by Jun.-Prof. Dr. Michael Boettcher.

The reproducibility of technical screen replicates for samples exposed to a certain ALK inhibitor was high, indicated by high correlation ($r \geq 0.98$) (Figure 3.5). Based on MAGeCK-VISPR 'β' scores 109 genes with significantly enriched sgRNAs (P-value ≤ 0.01) were identified in both ALK inhibitor-treated samples (Table 8.1). Overall, the correlation of 'β' scores for respective sgRNAs between ALK inhibitor exposed samples was high ($r>0.89$) (Figure 3.6).

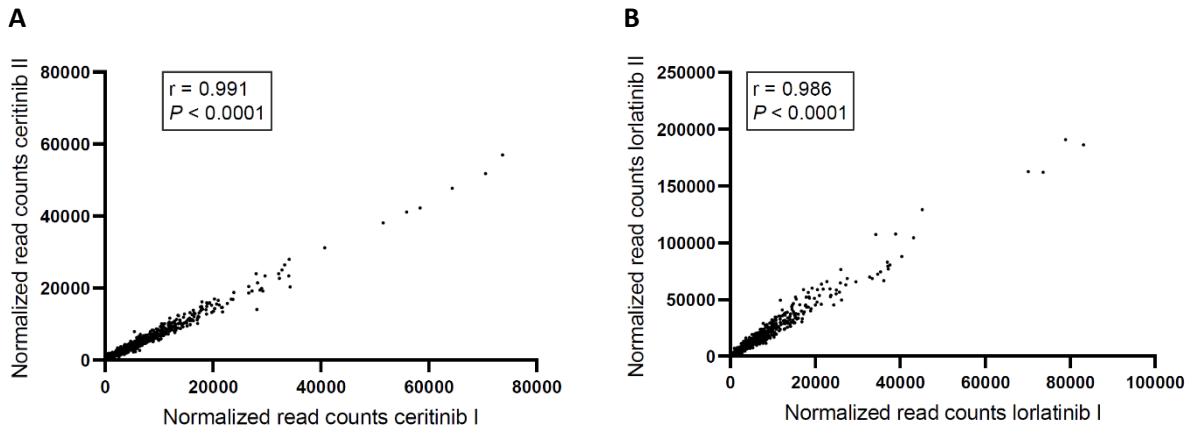

Figure 3.5 Quality control of CRISPR/Cas9 knockout screen. **(A and B)** The correlation between sgRNA phenotypes from two technical screen replicates based on normalized read counts per sgRNA for each ALK inhibitor is shown. The correlation coefficients (r) were calculated using Pearson correlation and tested using a two-tailed t-test; *P*<0.0001. Previously published in Berlak *et al*.[1].

In order to identify pathway and molecular function annotations for the 109 genes with significantly enriched sgRNAs the gene list was uploaded to the PANTHER classification tool to perform a functional classification analysis [220]. Therefore, the PANTHER GO- *Slim Molecular Function* annotation set, and the PANTHER-Pathway annotation set were used. Several genes with significantly enriched sgRNAs were associated with various ALK downstream signalling pathways, like PIAS3 protein being part of the JAK/STAT pathway, inhibiting the DNA-binding activity of STAT3 [263]. The overexpression of *PIAS3* was described to lead to cell growth suppression in human lung cancer cells and its loss suggested to drive high-grade serous ovarian carcinoma [264, 265]. Other interesting candidate genes were *CSK* and *RACK1* (also known as *GNB2L1*) encoding proteins that regulate Src activity [266-272]. The tyrosine kinase Src is described to interact with the ALK receptor [90].

Furthermore, a GSEA was performed querying the entire data set for enrichment of sgRNAs targeting certain genes based on beta scores between both ALK inhibitor treated samples and the DMSO control. The GSEA was performed using the C2 curated gene sets from the MsigDB database [218, 219, 273-275]. This analysis revealed enriched gene sets associated with translation, nonsense mediated decay (NMD) and the respiratory electron transport (Table 8.2). Using the GSEA tool 4.1.0 a leading-edge analysis was performed to determine the gene sets within the defined cut off criteria that showed the highest enrichment and the corresponding genes. The Set-to-Set comparison (Figure 3.7) indicated an overlap of leading-edge genes between subsets.

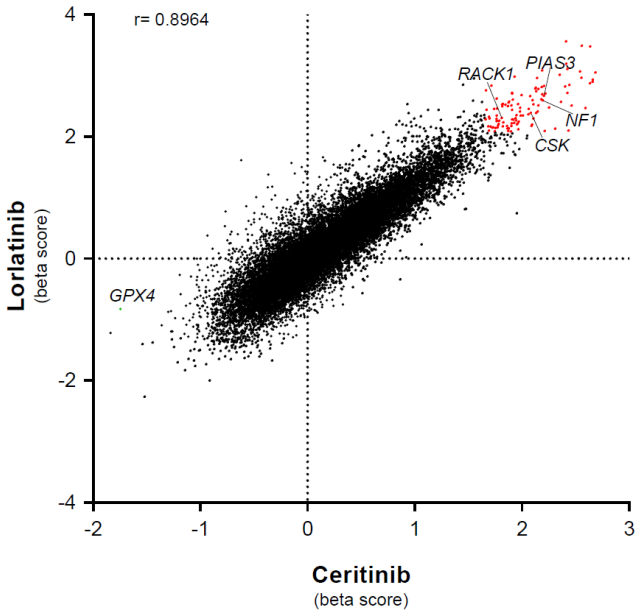

Figure 3.6 Overview of results of genome-wide CRISPR/Cas9 knockout screens. Negative beta scores, derived from the MAGeCK-VISPR analysis, indicate a depletion of sgRNAs targeting denoted genes during treatment, whereas positive beta scores indicate an enrichment of sgRNAs targeting a respective gene. Significant candidate genes (P<0.01) with highly abundant sgRNAs during treatment are highlighted in red. Genes identified to influence ALK downstream signalling pathways are labelled. Previously published in Berlak *et al*.[1].

For the three gene sets representing genes of the respiratory chain (reactome respiratory electron transport, reactome respiratory electron transport ATP synthesis by chemiosmotic coupling and heat production by uncoupling proteins, WP electron transport chain oxphos system in mitochondria signal), an overlap of leading-edge genes was observed only within this group of respiratory chain gene sets, indicating a result specific to this biological process. Identified genes were *NDUFA1, NDUFA2, NDUFA6*, *NDUFB2, NDUFB3, NDUFB4*, *NDUFS1, NDUFS2, NDUFS6, NDUFC2, NDUFU3, NDUFAB1* and *NDUFB6.* These genes all encode subunits of the NADH:ubiquinone oxidoreductase (complex I), which is composed of 45 subunits and the first enzyme of the respiratory chain, oxidizing nicotinamide adenine dinucleotide hydrogen (NADH) [273].

In addition to the functional classification analysis and the GSEA a literature search was performed on the 109 genes with significantly enriched sgRNAs. Thereby the NF1 gene, encoding the Ras-GTPase Activating Protein (Ras-GAP) NF1, which is also a negative regulator of RAS signalling, was identified as a mediator of ALK inhibitor response (Figure 3.6) [129, 274].

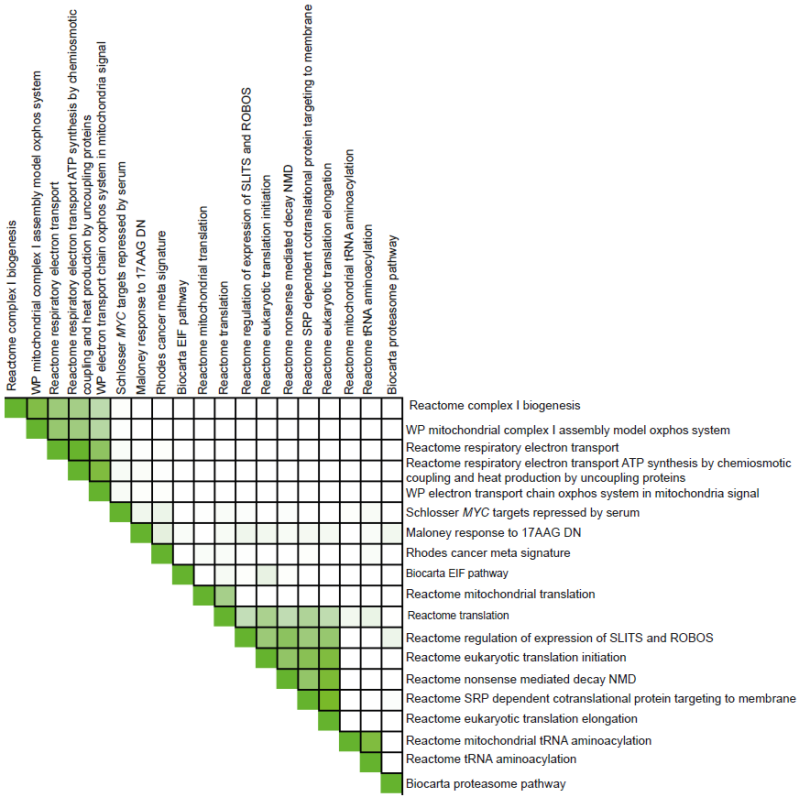

Figure 3.7 A gene set enrichment analysis (GSEA) was performed comparing enrichment of sgRNAs targeting certain genes based on beta scores between both ALK inhibitor treated samples and the DMSO control. The GSEA was performed using the C2 curated gene sets from the MsigDB database. A GSEA leading edge analysis was performed to determine the gene sets within the defined cut off criteria that showed the highest enrichment and the corresponding genes. These gene sets are shown in this set-to-set map. The extent of overlap between gene sets is indicated with darker colour. White squares indicate that gene sets have no overlapping leading edge genes.

Data indicated that cells expressing one of the four sgRNAs against *NF1*, enrich over time when treated with lorlatinib or ceritinib, suggesting a role for NF1 in ALK signalling in neuroblastoma cell lines and an association with ALK inhibitor resistance (Figure 3.8). Interestingly, NF1 was also described to be inactivated in some neuroblastoma tumours [42, 274].

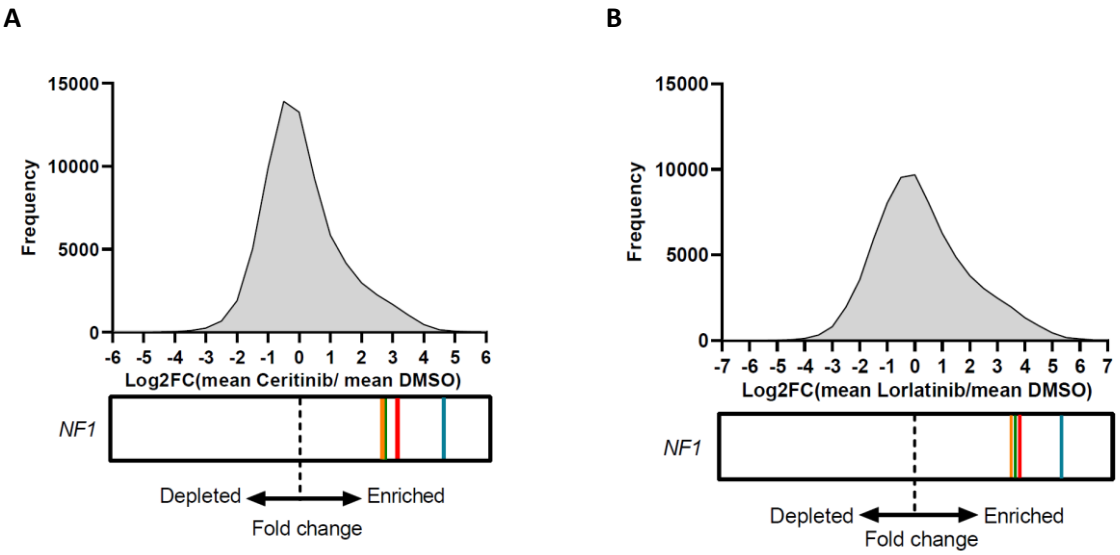

Figure 3.8 Histograms depicting the abundance distribution of all sgRNAs to their log2 fold change (mean ALK inhibitor/mean DMSO) for both ALK inhibitors. The enrichment of sgRNAs targeting *NF1* is shown below, with each colored line representing one of the four sgRNAs targeting *NF1*. The enrichment of sgRNAs is consistent between both ALK inhibitors. Previously published in Berlak *et al*.[1].

Taken together, some of the genes identified, with enriched sgRNAs overtime in ALK inhibitor exposed samples using a genome-wide CRISPR/Cas9 knockout screen, encode proteins modulating ALK downstream signalling. A knockout of the respective genes may lead to ALK inhibitor resistance.

3.2 Generation and validation of *NF1* knockout cell lines using the CRISPR/Cas9 system

A loss of NF1 function was reported to confer resistance against a variety of targeted therapies, such as EGFR-inhibition in lung cancer, BRAF-inhibition in melanoma, BCR-ABL-inhibition in chronic myeloid leukaemia and endocrine therapies in advanced breast cancer [275-278]. Furthermore, genomic data of tumour biopsies from ALK inhibitor-resistant neuroblastoma of patients treated at the Charité in a paediatric phase 1 study for ceritinib were analysed regarding mutations. This data was compared with genomic data of tumour biopsies of the same patients before resistance development. In the biopsies of ALK inhibitor-resistant neuroblastoma inactivating *NF1* mutations were detected as reported in Berlak *et al*.[1]. Therefore, isogenic cell lines with an *NF1* knockout were generated, to investigate whether a knockout of *NF1* mediates ALK inhibitor resistance in neuroblastoma cell lines.

Respective *ALK*-driven neuroblastoma cell lines of interest were shown to be authentic upfront. Furthermore, the cell lines SH-SY5Y and LAN-5 were investigated for mutations in ALK downstream signalling pathways using NGS and no mutations in ALK downstream signalling pathways were identified (see Berlak *et al*.[1]). Isogenic cell lines were generated as described in the methods section. In the following example data for one cell line will be shown.

Respective cell line bulk populations were analysed for editing events after transfection with the sgRNA containing plasmids, targeting exon 1 or exon 30 of the *NF1* gene, using a T7 assay. T7 endonuclease digested samples of SH-SY5Y bulk populations showed additional DNA bands in comparison to the undigested sample and the parental samples indicating editing events (Figure 3.9).

Cell line pools found positive for editing events were used for limited dilution experiments. Isolated single cell clones were also analysed for INDELS using the T7 assay (Figure 3.10).

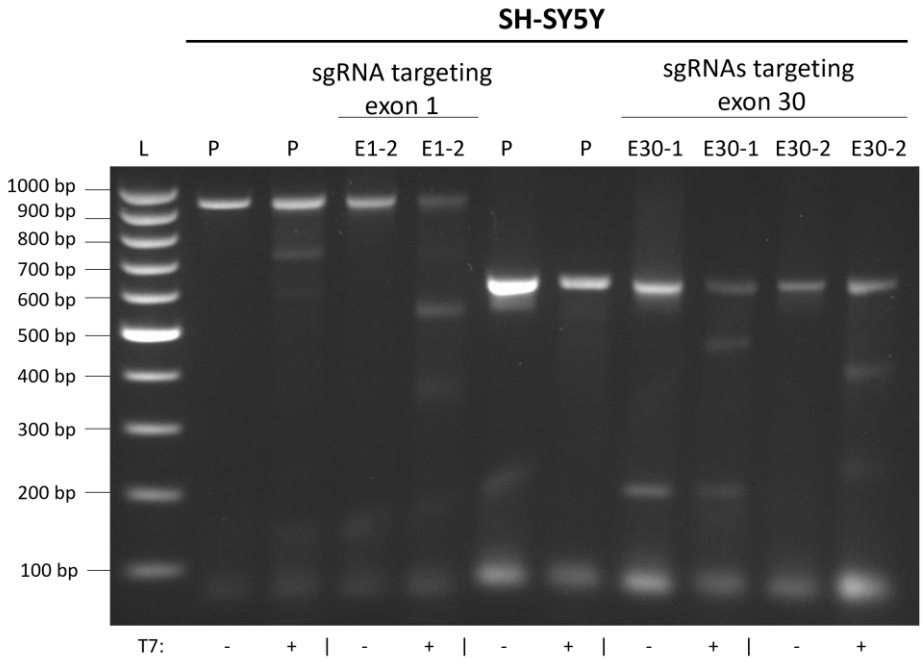

Figure 3.9: Testing of SH-SY5Y bulk populations for INDELS using T7 endonuclease. DNA of bulk populations transfected with a sgRNA containing plasmids targeting *NF1* in exon 1 or exon 30 were digested with T7 endonuclease to detect mismatched DNA, which indicates INDELS. Samples were loaded on an agarose gel for analysis. In comparison to the undigested as well as the parental sample (P) all bulk populations showed additional DNA bands. GeneRuler 100 bp was used as a DNA ladder (L). Digestion of the samples is indicated below the image with a +.

Single cell clones SH-SY5Y E1-2 #1 as well as SH-SY5Y E30-2 #2 showed additional DNA bands in T7 digested samples in comparison to the respective undigested sample and the parental sample, indicating INDELS. Therefore, these single cell clones were used for further analysis.

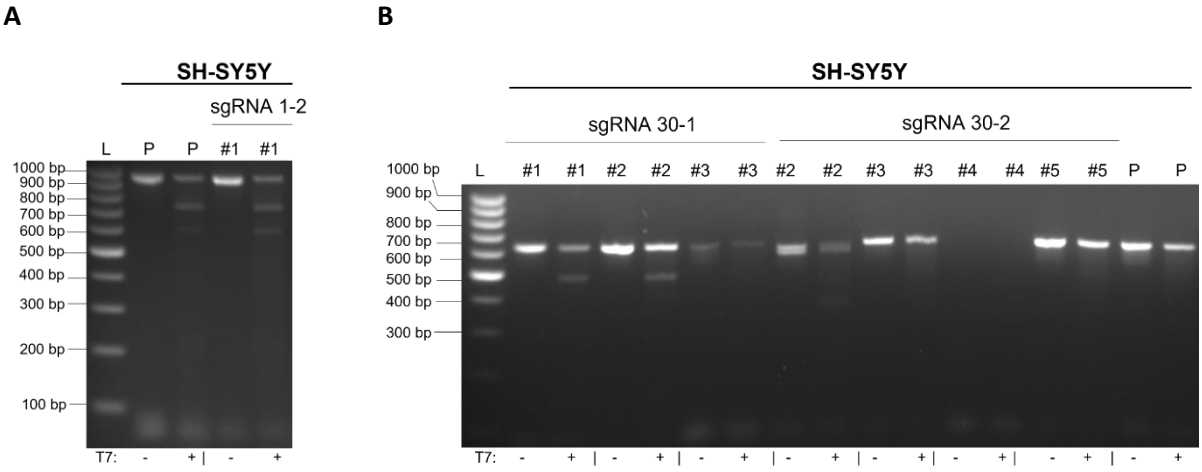

Figure 3.10 Testing of SH-SY5Y isolated single cell clones for INDELS using T7 endonuclease. DNA of isolated single cell clones of INDEL positive bulk populations were digested with T7 endonuclease to detect mismatched DNA, which indicates INDELS. Samples were loaded on an agarose gel for analysis. In comparison to the undigested as well as the parental sample (P) single cell clones with additional DNA bands were used for further analysis. GeneRuler 100 bp was used as a DNA ladder (L). Digestion of the samples is indicated below the images with a +.

Sequences of INDELS for respective isogenic cell lines were determined by subcloning of PCR products, subsequent Sanger sequencing and comparison to the parental sequence (Figure 3.11). Determined INDEL sequences are listed in Table 3-1. For SH-SY5Y E1-2 #1 a 16 bp deletion was observed 6 bp upstream of the PAM sequence GGG.

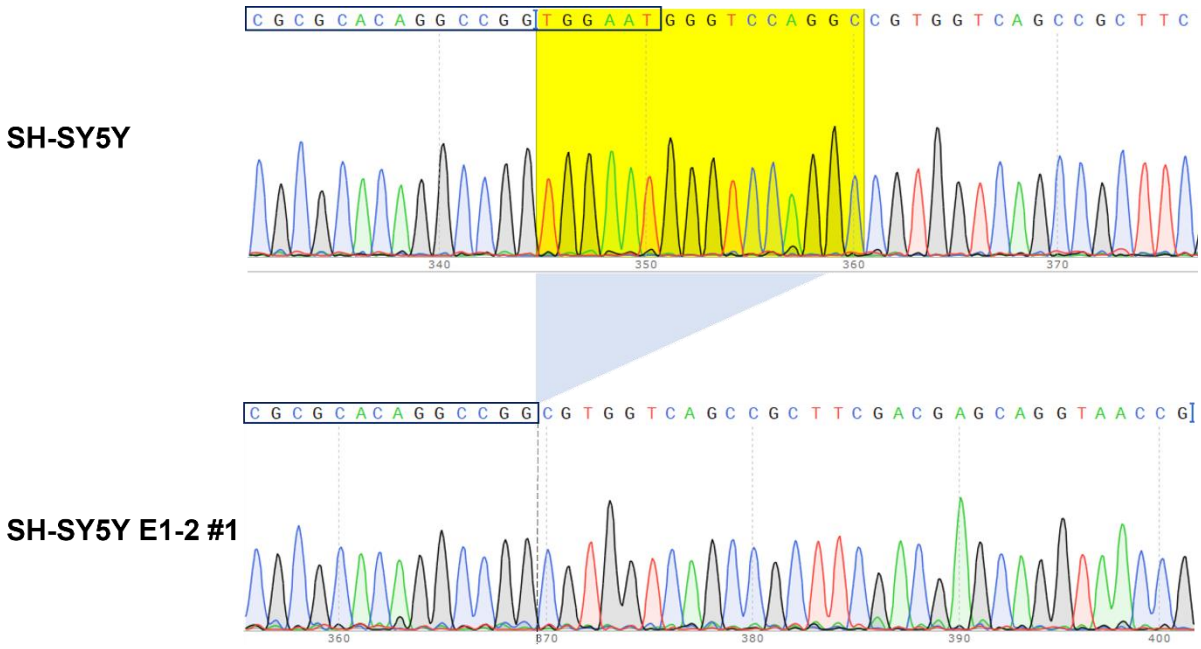

Figure 3.11 Comparison of sequencing chromatograms of Sanger sequencing. The top panel shows the sequence of the parental cell line SH-SY5Y. The sgRNA sequence is framed in black and followed by the PAM sequence GGG. The sequence deleted in the isolated single cell clone SH-SY5Y E1-2 #1 is shown in yellow in the top panel. The bottom panel shows the sequencing chromatogram of SH-SY5Y E1-2 #1.

Table 3-1: INDEL sequences of isogenic cell lines in the *NF1* gene.

Isogenic cell line	INDEL
SH-SY5Y E1-2 #1	16 bp deletion
	TGGAATGGGTCCAGGC
SH-SY5Y E30-2 #2	15 bp deletion
	CCCCCCTCAACTTCG
	40 bp deletion
	CTTCGAAGTGTGTGCCACTGTTTATACCAGGTATGCTTACAG
LAN-5 *NF1* KO #1	181 bp insertion
	GCAGCGGACCTTCGACAACGGCAGCATCCCCCACCAGATCCACCTGGGAGAGCTGCA
	CGCCATTCTGCGGCGGCAGGAAGATTTTTACCCATTCCTGAAGGACAACCGGGAAAA

	GATCGAGAAGATCCTGACCTTCCGCATCCCCTACTACGTGGGCCCTCTGGCCAGGGG
	AAACAGCAGA
LAN-5 *NF1* KO #2	195 bp insertion
	CCGACGTGCTTCGCGCGCAACTTTGCCCGCGCTTCTTCGTCCATATTATGTAGCGGTT
	GTCCCACCAGACTCACTTCGCCACTGCTGCCGTCATCAAGCCCGGCGAGGATCGCCA
	GCAAGGCTGACTTACCCGATCCCGACTCGCCCACCAGTGCGATGGTCTCGCCACGTTT
	GACAACCAGCTCAACTCCGGT
	1 bp deletion
	G

The identified INDELS either led to premature stop codons or modified amino acid sequences, which might not allow proper protein folding. Western blot experiments confirmed the *NF1* knockout on a protein level indicated by absence of a protein band (Figure 3.12). SH-SY5Y E1-2 #1 and SH-SY5Y E30-2 #2 are hereafter named SH-SY5Y *NF1* KO #1 and SH-SY5Y *NF1* KO #2 respectively.

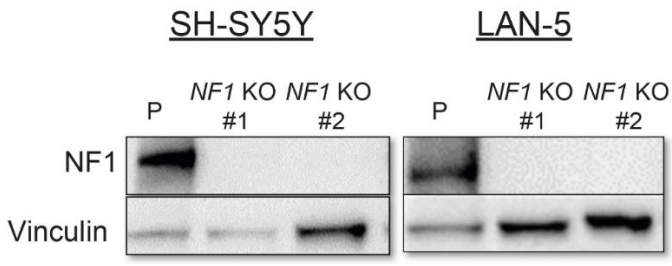

Figure 3.12 NF1 protein levels were investigated in isogenic *NF1* knockout cell lines using western blot. SH-SY5Y as well as LAN-5 *NF1* knockout cell lines showed an absence of NF1 protein in comparison to the respective parental line (P). Staining of Vinculin was used as a loading control. Previously published in Berlak *et al*.[1].

In addition to NF1 protein levels ERK1/2 as well as phosphorylated ERK1/2 protein levels were investigated in *NF1* knockout clones and increased levels of phosphorylated ERK1/2 observed in comparison to the parental cell lines (Figure 3.13), indicating increased RAS/MAPK signalling as expected from the literature due to the role of NF1 as a negative regulator of RAS signalling [128, 129].

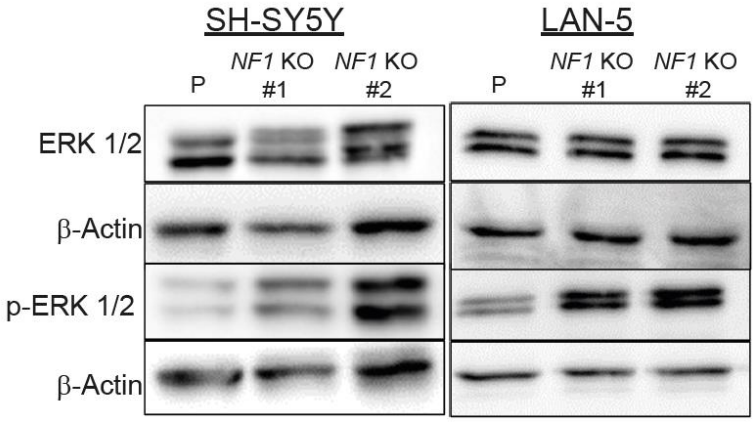

Figure 3.13 Western blot analysis of total and phosphorylated ERK 1/2 indicates increased RAS/MAPK signalling in *NF1* knockout single cell clones in comparison to the parental line (P). Beta Actin staining was used as a loading control. Previously published in Berlak *et al*.[1].

In summary, isogenic *ALK*-driven neuroblastoma cell lines harbouring an *NF1* knockout were generated and validated on a DNA as well as protein level and were characterized by increased RAS/MAPK signalling.

3.3 Functional analysis of *NF1* knockout cell lines

3.3.1 Investigation of ALK inhibitor sensitivity of *NF1* knockout cell lines

To investigate whether a knockout of *NF1* can lead to an ALK inhibitor resistance phenotype in *ALK*-driven neuroblastoma cell lines, as indicated by the genome-wide CRISPR/Cas9 knockout screen, isogenic *NF1* knockout cell lines were exposed to different ALK inhibitor concentrations and cell viability assessed. In order to use the ATP quantification assay CellTiter-Glo® quenching effects of inhibitors and media compositions were investigated upfront (Figure 8.1 and Figure 8.2). Based on the definition of resistance by McDermott *et al*., three of the four isogenic *NF1* knockout cell line models were resistant to ceritinib treatment (Figure 3.14 and Figure 3.15, Table 3-2 and Table 3-4) [194]. Based on the resistance definition LAN-5 *NF1* KO #2 was not resistant to ceritinib.

A

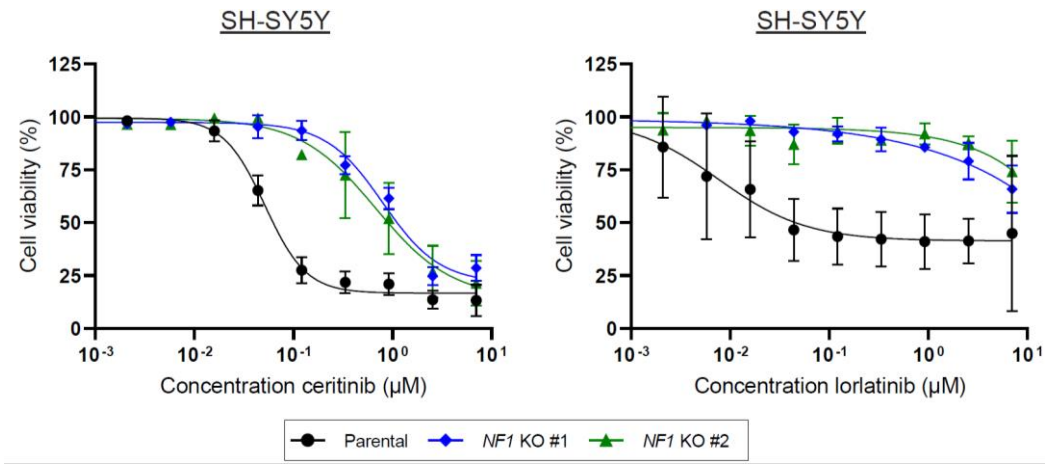

B

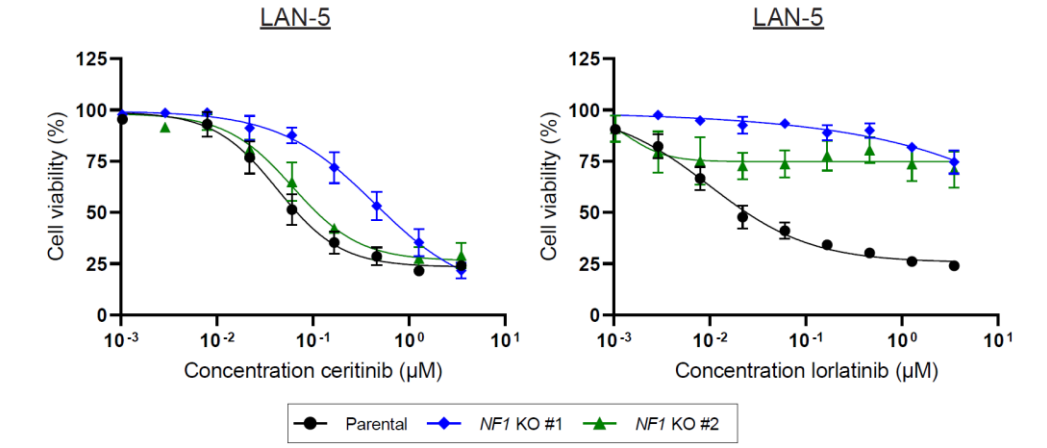

Figure 3.14 Cell viability of *NF1* knockout clones and the parental cell line was assessed during ALK inhibitor exposure with ceritinib or lorlatinib for 72 h using the live-cell imaging system Incucyte. *NF1* knockout cell lines showed a decreased sensitivity towards ALK inhibitors. The 4-parameter logistic model was fitted to the concentration-response datasets using the least square method; values represent cell viability mean ± SD, n=3. Previously published in Berlak *et al.*[1]

Table 3-2: Best-fit parameter and 95% confidence intervals derived of nonlinear regression models to describe live-cell imaging analysis derived concentration-response data for ceritinib.

Cell line	relative IC_{50} in nM	95% CI IC_{50} in nM	Fold resistance	*m*	95% CI *m*	E_{max} in %
SH-SY5Y	50.7	44.2 to 58.8	na	-2.17	-3.12 to -1.64	84.1
SH-SY5Y *NF1* KO #1	750	562 to 1000	14.8	-1.40	-1.95 to -1.00	79.4
SH-SY5Y *NF1* KO #2	619	387 to 1200	12.2	-1.45	-2.42 to -0.840	83.0
LAN-5	42.7	34.2 to 53.8	na	-1.31	-1.73 to -1.01	75.7
LAN-5 *NF1* KO #1	440	286 to 1000	10.3	-0.871	-1.19 to -0.62	90.4
LAN-5 *NF1* KO #2	61.7	47.2 to 80.3	1.44	-1.25	-1.69 to -0.94	72.0

All four isogenic *NF1* knockout cell lines were less sensitive to lorlatinib exposure in comparison to the respective parental line (Table 3-3 and Figure 3.14).

Table 3-3: Absolute IC_{50} values and E_{max} derived of live-cell imaging analysis-based concentration-response data for lorlatinib.

	SH-SY5Y	SH-SY5Y *NF1* KO #1	SH-SY5Y *NF1* KO #2	LAN-5	LAN-5 *NF1* KO #1	LAN-5 *NF1* KO #2
lorlatinib						
absolute IC_{50}	42.7 nM	na	na	21.9 nM	na	na
E_{max}	58.0%	35%	26%	75.0%	30.0%	25.1%

Attempts to fit the 4PL as well as the 3PL using the least square method did not result in a good description of the concentration-response data of lorlatinib. For the investigated concentration range of lorlatinib only the E_{max} values could be compared. The less sensitive phenotype of *NF1* knockout clones for lorlatinib in comparison to the respective parental lines was observed by decreased E_{max} values.

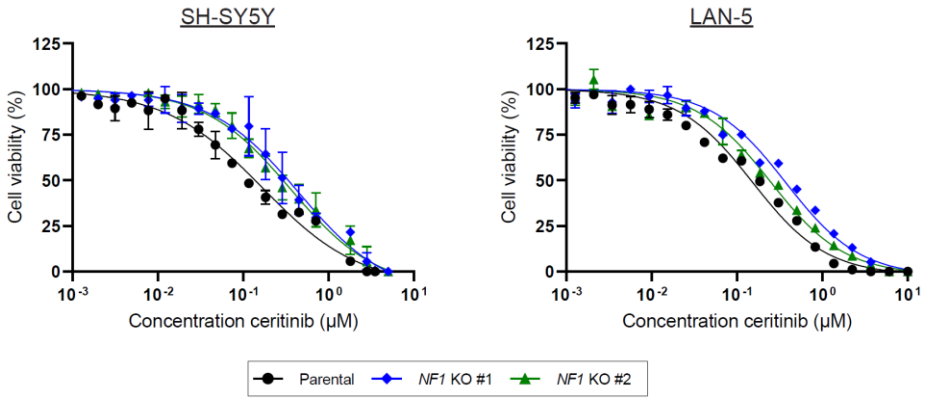

Figure 3.15 Cell viability of *NF1* knockout clones and the parental cell line was assessed after 72 h of ALK inhibitor exposure with ceritinib using an ATP quantification assay. The 4-parameter logistic model for SH-SY5Y with a Top constraint at 100% or the 3-parameter logistics model for LAN-5 with a Top constraint at 100% were fitted to the concentration-response data using the least square method. *NF1* knockout cell lines showed a decreased sensitivity towards ALK inhibitors; values represent cell viability mean ± SD, n=3. For LAN-5 n=1.

Table 3-4 Best-fit parameter and 95% confidence intervals derived of nonlinear regression models to describe CellTiter-Glo® derived concentration-response data for ceritinib.

Cell line	relative IC_{50} in nM	95% CI IC_{50} in nM	Fold resistance	*m*	95% CI *m*	E_{max} in %
SH-SY5Y	168	129 to 236	na	-0.760	-0.882 to -0.652	100
SH-SY5Y *NF1* KO #1	445	305 to 896	2.65	-0.835	-1.08 to -0.643	100
SH-SY5Y *NF1* KO #2	358	274 to 517	2.13	-0.860	-1.01 to -0.733	100
LAN-5	152	133 to 174	na	-	-	100
LAN-5 *NF1* KO #1	374	325 to 430	2.46	-	-	100
LAN-5 *NF1* KO #2	249	223 to 277	1.64	-	-	100

Taken together, a knockout of *NF1* leads to an ALK inhibitor resistant phenotype in *ALK*-driven neuroblastoma cell lines. This further confirmed the results of the genome-wide CRISPR/Cas9 knockout screen.

3.3.2 Differential gene expression in *NF1* knockout cell lines

To further investigate the ALK inhibitor resistant phenotype of *ALK*-driven neuroblastoma *NF1* knockout cell lines, differential gene expression during ALK inhibitor exposure was investigated for two different time points.

Analysis of mRNA sequencing data was kindly provided by Dr. Joern Toedling. By investigation of mRNA sequencing reads the detected INDELS in the *NF1* gene were further confirmed in *NF1* knockout cell lines (Figure 8.3) and *NF1* expression still observed in these isogenic lines (Figure 3.16). This was expected, as it was reported that mRNA transcripts of CRISPR/Cas9 knocked out genes are still generated but no functional protein synthesized due to NMD [279]. Predicted sgRNA off-target genes like *NINL*, *ELK3*, *CTNNA3* and *EPHB1* were also investigated for the occurrence of INDELS but predicted off-target sequences showed an absent or very low sequencing read coverage. These off-target sequences should be further investigated using targeted sequencing approaches to preclude off-target editing. Furthermore, sequencing reads were used to check for the presence of *ALK* mutations, which were confirmed (Figure 8.4) and a decreased *ALK* expression observed in *NF1* knockout cell lines in comparison to the parental line (Figure 3.16). Other studies reporting on ALK inhibitor resistant neuroblastoma cell lines described reduced *ALK* expression in resistant cells as well [181]. The reduced *ALK* expression in *NF1* knockout cells might be explained by a reduced *PHOX2B* expression (Figure 3.17),

a transcription factor, that was described to bind to the *ALK* promoter and regulates its expression [280].

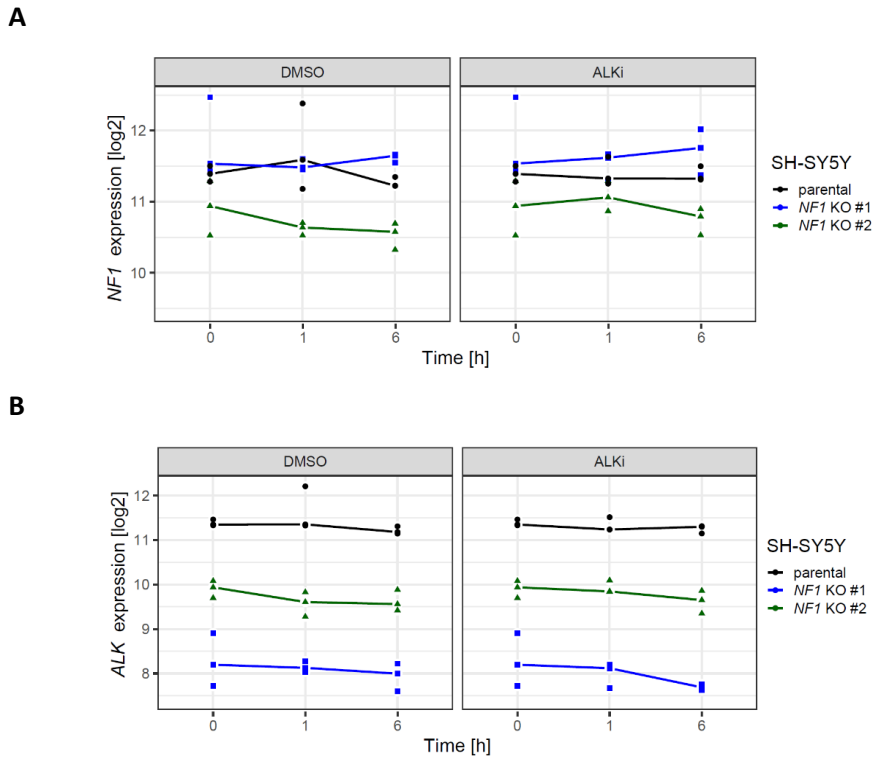

Figure 3.16 SH-SY5Y and generated isogenic *NF1* knockout lines were exposed to DMSO (vehicle control) or ceritinib (ALKi) for 1 h and 6 h. Isolated mRNA of the different samples was submitted for mRNA sequencing. **(A)** shows the expression of *NF1* for different timepoints and treatments on a log2 scale and **(B)** the expression of *ALK*.

Furthermore, the mRNA-sequencing data was used to investigate the expression of genes of the RAS pathway signature as an additional indirect measurement of RAS-activity [114]. *ETV4*, *ETV5*, *DUSP4*, *DUSP6* and *SPRY4* showed decreased expression in the parental cell line during ALK inhibitor exposure but were stable or only little affected in *NF1* knockout clones indicating increased RAS-activity (Figure 3.18).

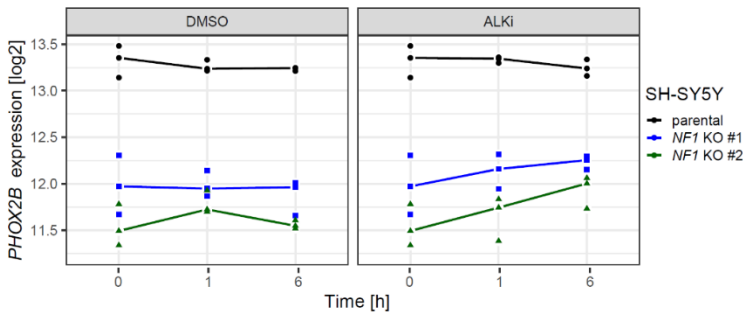

Figure 3.17 SH-SY5Y and generated isogenic *NF1* knockout lines were exposed to DMSO (vehicle control) or ceritinib (ALKi) for 1 h and 6 h. Isolated mRNA of the different samples was submitted for mRNA sequencing. Expression of *PHOX2B* is shown on a log2 scale.

IRS2 expression, encoding a signalling adaptor protein, that was described to be activated by the ALK kinase and is ALK inhibitor sensitive was stable during ceritinib exposure in *NF1* knockout clones (Figure 3.19) further indicating an ALK inhibitor resistant phenotype of these cell lines. [79].

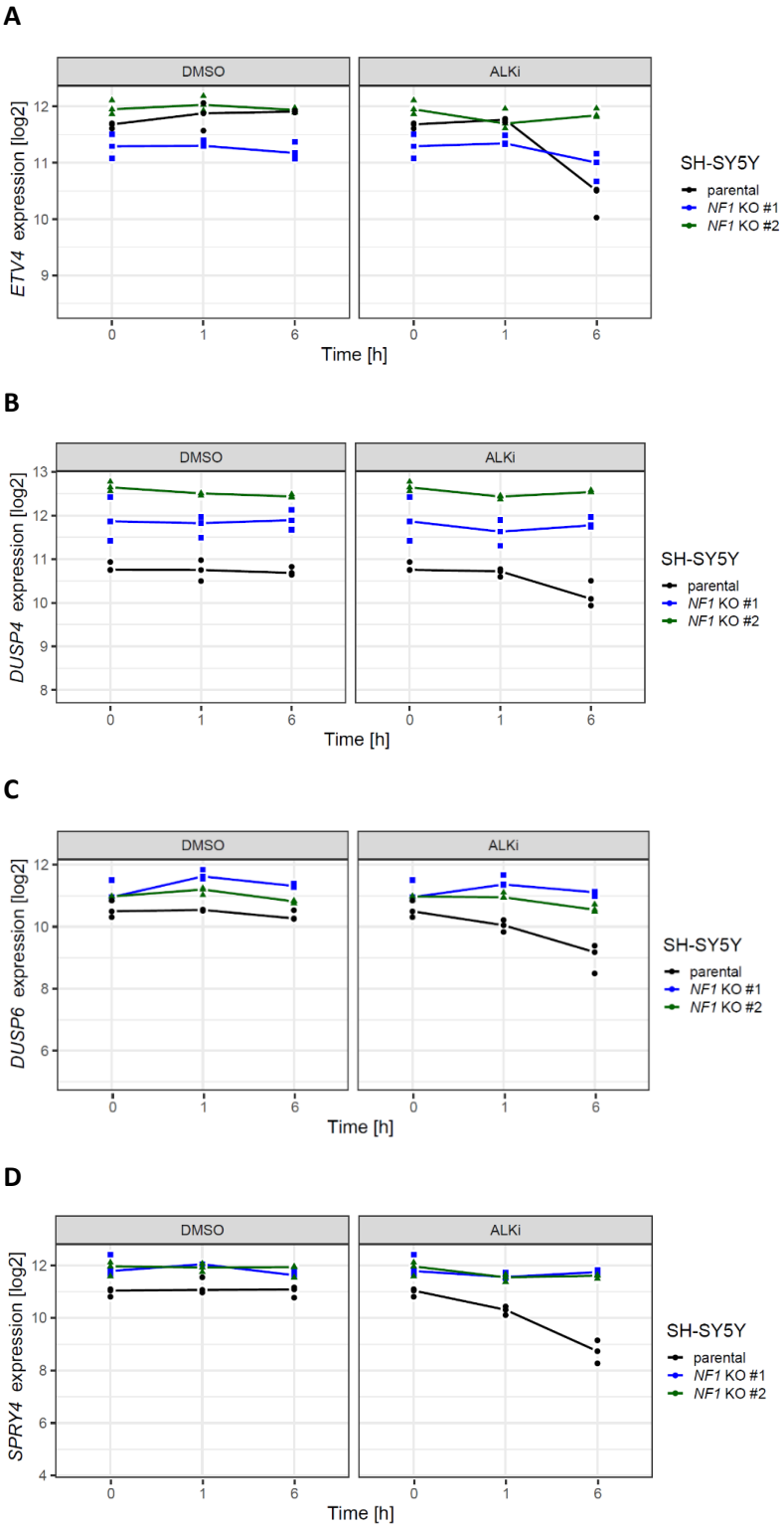

Figure 3.18 SH-SY5Y and generated isogenic *NF1* knockout lines were exposed to DMSO (vehicle control) or ceritinib (ALKi) for 1 h and 6 h. Isolated mRNA of the different samples was submitted for mRNA sequencing. Expression of several genes of the RAS pathway signature is shown on a log2 scale

To identify genes differentially expressed in *NF1* knockout cell lines in comparison to the parental cell line the mRNA-sequencing data was analysed using a linear regression model taking into account different factors influencing gene expression, like the drug exposure duration, the specific drug and the cell line type.

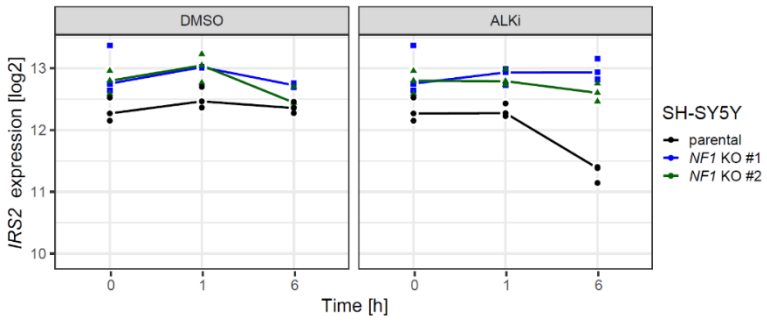

Figure 3.19 SH-SY5Y and generated isogenic *NF1* knockout lines were exposed to DMSO (vehicle control) or ceritinib (ALKi) for 1 h and 6 h. Isolated mRNA of the different samples was submitted for mRNA sequencing. Expression of *IRS2* during DMSO (control) or ceritinib (ALKi) exposure over time for SH-SY5Y or respective *NF1* KO cell lines is shown on a log2 scale.

TMEM229A, *SGK1*, *CHST11*, *SPRY4*, *ETV5*, *ADAM29*, *AC118758.1* and *SHISA3* were genes with significant differential expression during 6 h of ALK inhibitor exposure in both *NF1* knockout clones. One of them was *ETV5* is a gene of the RAS pathway signature (Figure 3.20) [115]. *ETV5* expression was stable during ALK inhibitor exposure in *NF1* knockout cell lines but not in the parental cell lines as expected, due to the increased RAS activity in these cells. Furthermore, the expression of the receptor kinase RET was increased in *NF1* knockout cell lines in comparison to the parental line (Figure 3.20), but also affected during ceritinib exposure.

It has been described, that *ETV5* expression is regulated by ALK-RAS-ERK activity in neuroblastoma and that ETV5 binds to the RET promoter regulating its gene expression [116, 290, 291]. *RET* is a proto-oncogene encoding a receptor tyrosine kinase and its activation can mediate activation of *e.g.*, RAS/MAPK, JAK/STAT and PI3K/AKT signalling [281, 282]. Therefore, it might be that a ETV5-RET loop is a bypass mechanism leading to ALK inhibitor resistance in addition to the increased RAS activity. This should be further investigated using qPCR and western blot.

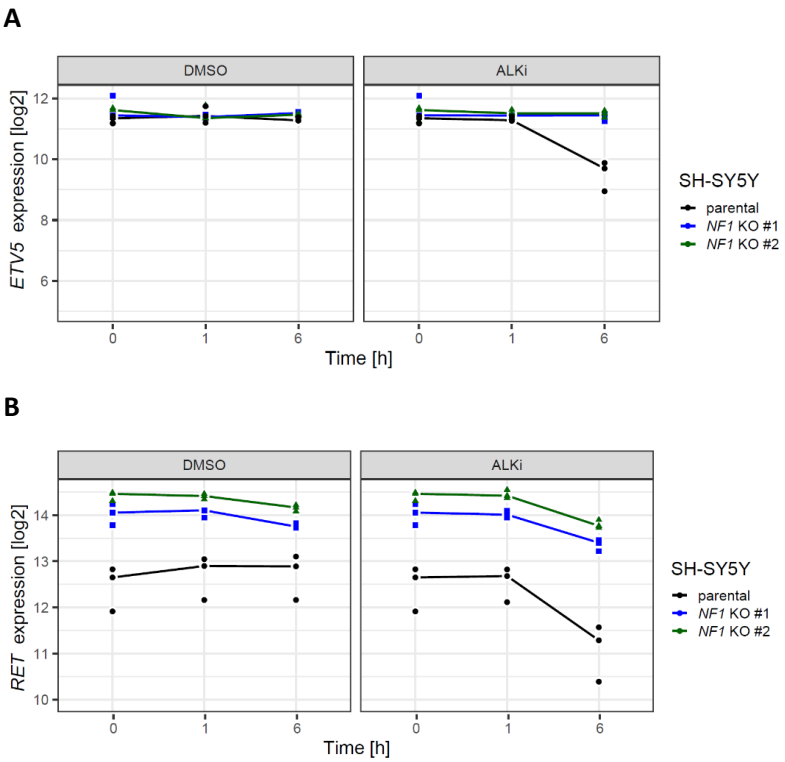

Figure 3.20 SH-SY5Y and generated isogenic *NF1* knockout lines were exposed to DMSO (vehicle control) or ceritinib (ALKi) for 1 h and 6 h. Isolated mRNA of the different samples was submitted for mRNA sequencing. Expression of *ETV5* and *RET* during DMSO (control) or ceritinib (ALKi) exposure over time for SH-SY5Y or respective *NF1* KO cell lines is shown on a log2 scale.

In summary, the presence of *ALK* mutations and *NF1* INDELS was confirmed by mRNA sequencing reads as well as their gene expression. Furthermore, increased RAS signalling could be confirmed by increased expression of genes of the RAS pathway signature. Additionally, it could be hypothesised that a possible bypass mechanism, consisting of an ETV5-RET loop, might mediate ALK inhibitor resistance.

3.3.3 Investigating collateral sensitivities of *NF1* knockout cell lines

To understand how a loss of NF1 protein alters ALK signalling pathways and to identify collateral sensitivities pointing towards new treatment options for patients with *ALK*-driven neuroblastoma resistant to ALK inhibitors, perturbation experiments and subsequent computational modelling of signalling networks using steady-state analysis of signalling networks (STASNet) were performed [259].

3.3.3.1 Computational modelling of signalling networks using STASNet

The quantification of phosphorylation of signalling components downstream of ALK associated an NF1 protein loss with increased RAS/MAPK signalling (Figure 3.21), in line with the role of NF1 as a negative regulator of RAS/MAPK signalling [129]. Furthermore, increased phosphorylated MEK, ERK and AKT level were measured in *NF1* knockout cell lines with and without subsequent stimulation with growth factors after inhibitor exposure. The same response on a protein level was observed for LAN-5 *NF1* knockout cell lines exposed to either lorlatinib or ceritinib (Figure 3.21 C). The perturbation-response data together with a prior knowledge network of the signalling topology served as input for the

STASNet signalling network modelling pipeline. The output of the modelling procedure were quantified signalling interactions and differences due to the loss of NF1 protein. STASNet adjusted model parameters representing the strength of signalling interactions in the signalling network and inhibitor efficacy until the model simulations fitted the data optimally. This analysis and sample processing upfront were kindly provided by Dr. Mathurin Dorel. Using this modelling approach, a weakened negative feedback from ERK to RAF in isogenic *NF1* knockout clones in comparison to the respective parental cell line was observed (Figure 3.22). This negative feedback from ERK to RAF restricts MAPK signalling in parental cells in agreement with the observation, that EGF stimulation only activated MEK during MEK inhibitor exposure. In *NF1* knockout cells EGF activated MAPK signalling efficiently regardless of MEK inhibition.

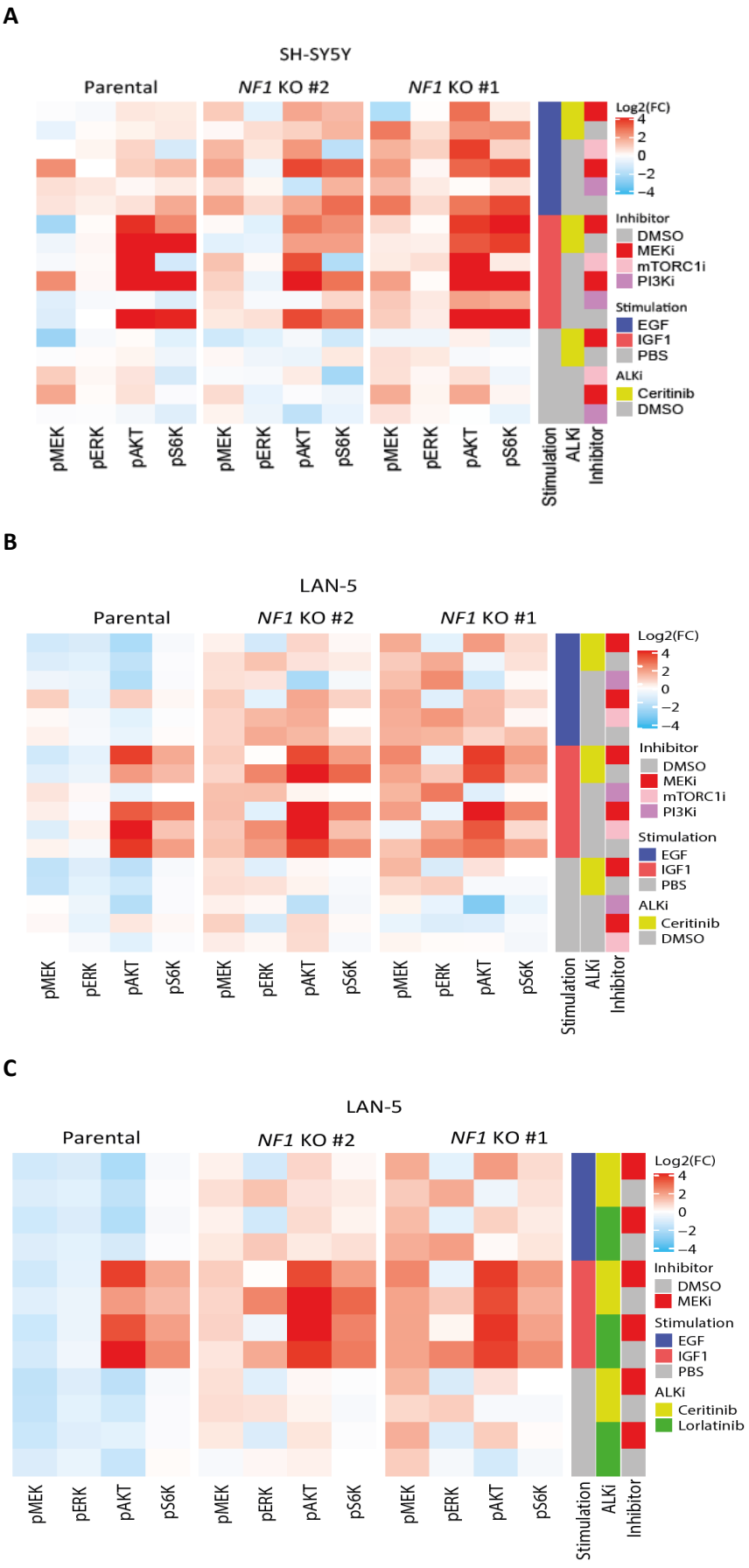

Figure 3.21 *NF1* knockout cell line models show increased RAS/MAPK signalling. (**A** and **B**) Measurement and quantification of 4 phosphoproteins after perturbation with ceritinib (ALKi), trametinib (MEKi), rapamycin (mTORi), pictilisib (PI3Ki) or DMSO and subsequent stimulation with EGF, IGF or PBS (carrier) of *NF1* knockout models and respective parental lines. Values are shown as log2(fold change) to PBS+DMSO control. *NF1* knockout cell lines show increased RAS/MAPK signalling in comparison to the respective parental cell line. (**C**) LAN-5 *NF1* knockout models show a similar response to different ALK inhibitors. Previously published in Berlak *et al*. [1].

A strong negative ERK to RAF feedback as detected in the parental neuroblastoma cell lines, is a known resistance mechanism against MEK inhibitors as it results in an accumulation of phosphorylated MEK leading to reactivation of downstream targets [168, 170].

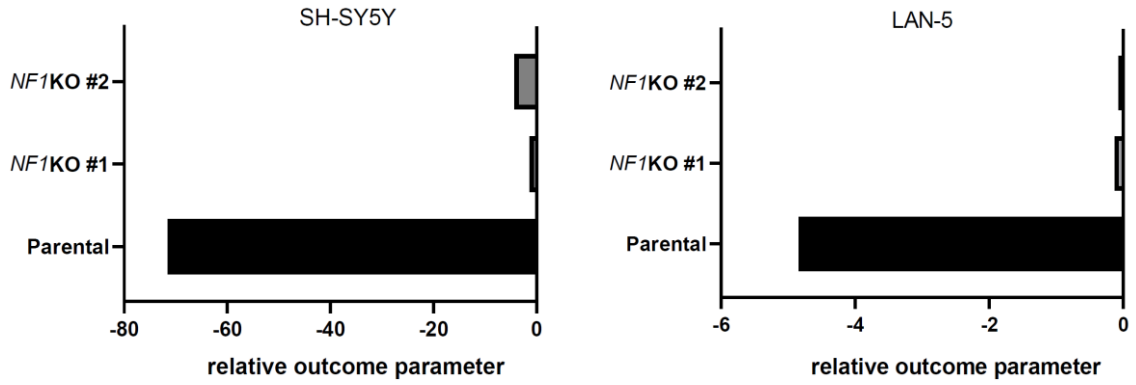

Figure 3.22 Outcome parameters for the ERK to RAF inhibitory feedback are shown as bar chart with separate scaling for LAN-5 and SH-SY5Y cell lines. *NF1* knockout models show a weaker ERK to RAF inhibitory feedback in comparison to the respective parental cell line. Negative feedback is indicated by a negative relative outcome parameter and interaction strength by decreased negative values.

Taken together these results suggested that a knockout of *NF1* in *ALK*-driven neuroblastoma cell lines is associated with loss of a negative ERK to RAF feedback. This weakened or absent negative feedback might lead to an increased MEK inhibitor sensitivity of *NF1* knockout cells.

3.3.3.2 Investigating collateral sensitivities: MEK and RAF inhibitor sensitivity

Based on the results of computational modelling of signalling networks in *ALK*-driven *NF1* knockout neuroblastoma cell lines using STASNet, their MEK inhibitor sensitivity was investigated. The 4PL was fitted to the concentration-response data derived from a CellTiter-Glo® assay after 72 h of MEK inhibitor exposure of the cell lines using the least square method. The decreased absolute IC_{50} and increased E_{max} values indicated an increased MEK inhibitor sensitivity of *NF1* knockout clones in comparison to the respective parental cell lines (Figure 3.23 and Table 3-5). This was not observed for SH-SY5Y *NF1* KO#2.

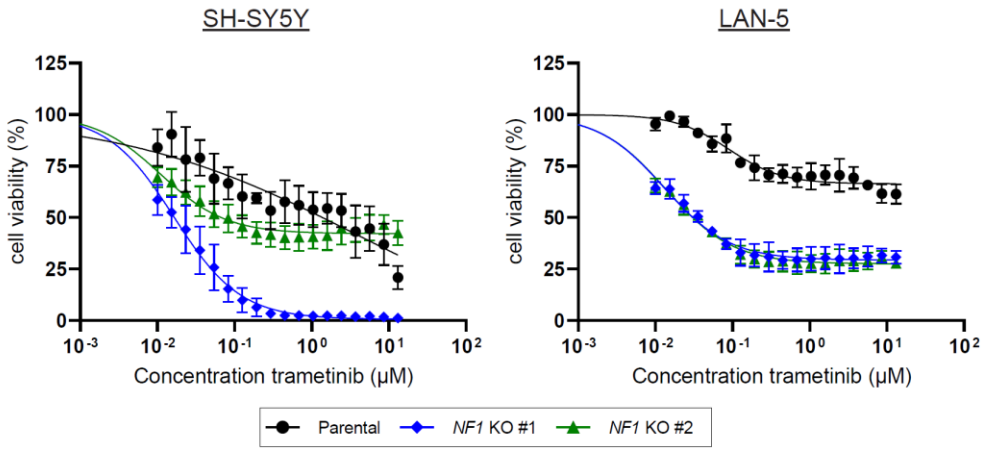

Figure 3.23 Cell viability of *NF1* knockout clones and the parental cell line was assessed after 72 h of MEK inhibitor exposure with trametinib using the ATP quantification assay CellTiter-Glo®. The 4-parameter logistic model with a Top constraint at 100% was fitted to the concentration-response data using the least square method. *NF1* knockout cell lines showed an increased sensitivity towards MEK inhibitors; values represent cell viability mean ± SD, n=3. Previously published in Berlak *et al.* [1].

Table 3-5 Absolute IC_{50} values and E_{max} derived of CellTiter-Glo® concentration-response data for trametinib.

	SH-SY5Y	SH-SY5Y *NF1* KO #1	SH-SY5Y *NF1* KO #2	LAN-5	LAN-5 *NF1* KO #1	LAN-5 *NF1* KO #2
absolute IC_{50}	1.29 µM	0.0164 µM	0.068 µM	na	0,0300 µM	0,0300 µM
E_{max}	80%	100%	58%	33.6%	70.6%	72.5%

Furthermore, *NF1* knockout clones showed increased sensitivity towards exposure with the pan-RAF inhibitor LY3009120 in comparison to the parental cell line, again with the exception of SH-SY5Y *NF1* KO #2 (Table 3-6 and Figure 3.24). A similar sensitivity to RAF inhibitors was described by Whittaker *et al.* for melanoma and colorectal cancer cell lines that were characterized by an increased RAS/MAPK signalling due to deactivating NF1 mutations [281].

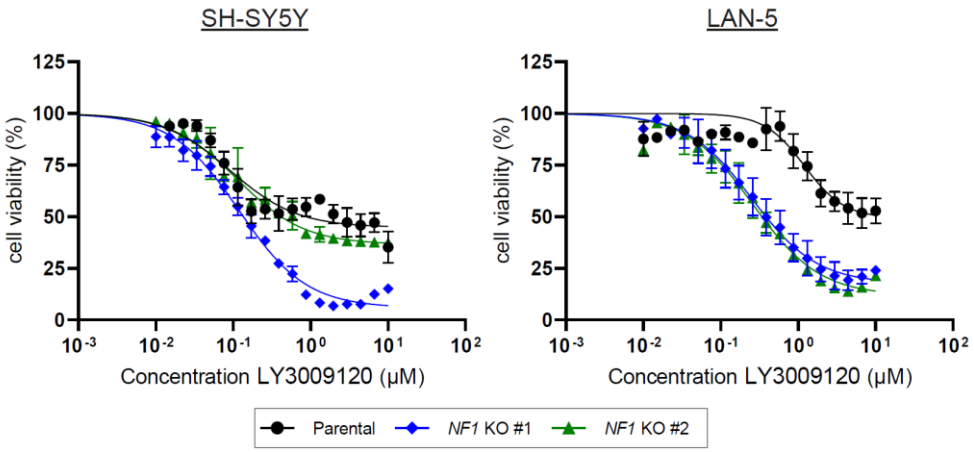

Figure 3.24 Cell viability of *NF1* knockout clones and the parental cell line was assessed after 72 h of pan-RAF inhibitor exposure with LY3009120 using the ATP quantification assay CellTiter-Glo®. The 4-parameter logistic model with a Top constraint at 100% was fitted to the concentration-response data of LAN-5 using the least square method. The 3-parameter logistic model with a Top constraint at 100% was fitted to the concentration-response data of SH-SY5Y using the least square method. *NF1* knockout cell lines showed an increased sensitivity towards this pan-RAF inhibitor; values represent cell viability mean ± SD, n=3.

Table 3-6 Absolute IC_{50} values and E_{max} derived of CellTiter-Glo® concentration-response data for LY3009120.

	SH-SY5Y	SH-SY5Y *NF1* KO #1	SH-SY5Y *NF1* KO #2	LAN-5	LAN-5 *NF1* KO #1	LAN-5 *NF1* KO #2
absolute IC_{50}	0.383 µM	0.134 µM	0.348 µM	10,06 µM	0.393 µM	0.335 µM
E_{max}	55.2%	94.2%	63.5%	50.7%	82.4%	88.2%

Taken together this data suggests MEK inhibition as a new collateral sensitivity in *ALK*-driven *NF1* knockout neuroblastoma cell lines, which confirms observations made using computational modelling. In addition, *NF1* knockout models showed an increased RAF inhibitor sensitivity.

3.3.3.3 Validation of ALK downstream signalling with Western Blots

To further investigate and confirm observations made by quantification of phosphorylated protein levels using a bead-based ELISA assay as well as computational modelling and ATP quantification derived concentration-response data, cell responses during inhibitor exposure were investigated using western blot. Increased activity of ALK downstream signalling in *NF1* knockout clones was further confirmed by elevated pMEK, pERK and pAKT protein levels (Figure 3.25). An ALK inhibitor resistant phenotype was further confirmed by increased pMEK, pERK and pAKT protein levels during ALK

inhibitor exposure. Furthermore, low levels of MEK phosphorylation (Ser217/221) and an absence of ERK phosphorylation in *NF1* knockout clones was observed during trametinib treatment. These results were consistent with computational modelling data, which indicated a weak or missing ERK to RAF feedback.

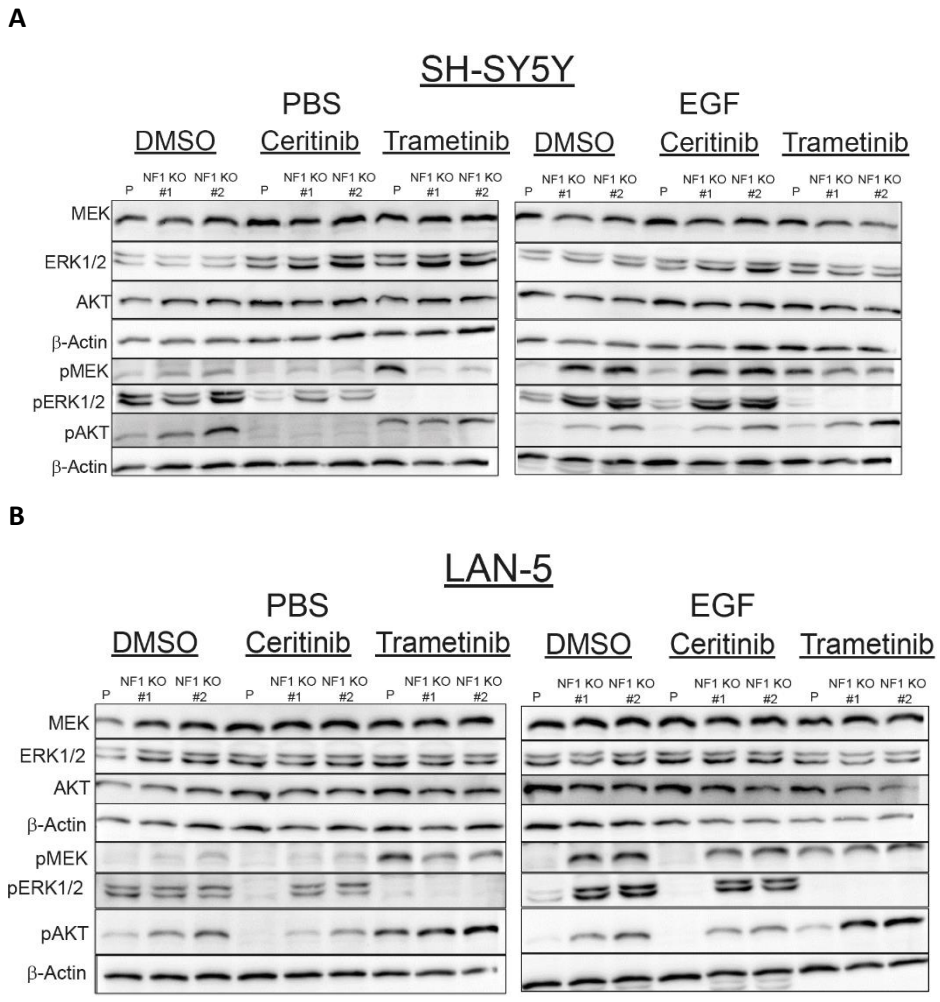

Figure 3.25 Western blot analysis of 24 h-serum-starved *NF1* knockout and respective parental cell lines exposed to DMSO, ceritinib, lorlatinib or trametinib for 1 h with subsequent stimulation for 30 min with EGF or PBS (carrier). Total as well as phosphorylated protein levels of MEK, ERK and AKT were investigated. Staining of β-Actin was used as a loading control. Previously published in Berlak *et al*. [1].

In conclusion, a NF1 protein loss leads to increased ALK downstream pathway signalling and an ALK inhibitor resistant phenotype in *ALK*-driven neuroblastoma cell lines. Furthermore, a knockout of *NF1* might lead to loss of the ERK to RAF inhibitory feedback (Figure 3.26), which results in a new collateral sensitivity towards MEK inhibitor exposure of *NF1* knockout clones.

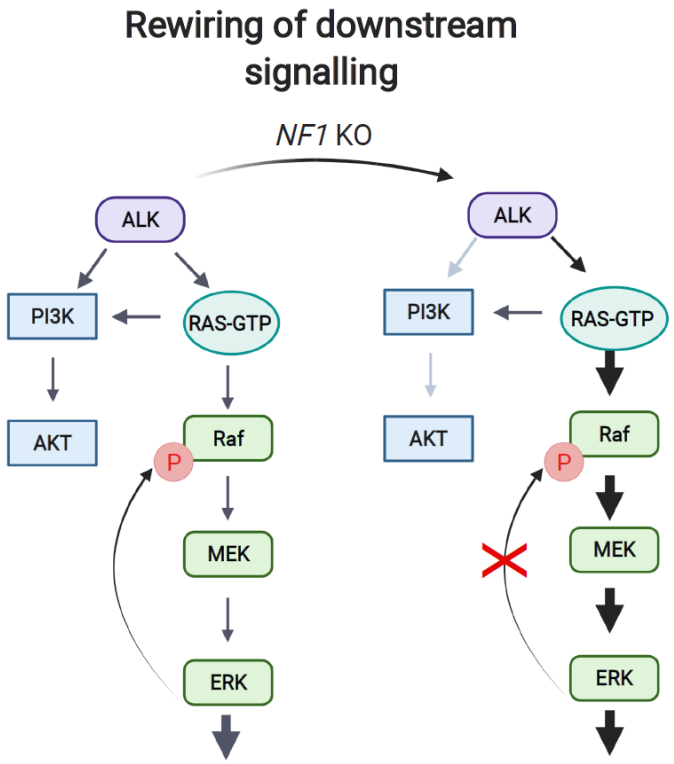

Figure 3.26 Schematic representation of ALK downstream signalling pathways in ALK-driven neuroblastoma cell lines without and with NF1 knockout. NF1 knockout (KO) clones shift their dependency towards the RAS/MAPK axis and have a weakened negative ERK to RAF feedback. Colour intensity from grey to black as well as arrow thickness from thin to fat describe pathway activity. ALK= anaplastic lymphoma kinase, RAS-GTP= GTP-bound RAS, Raf= RAF proto-oncogene serine/threonine-protein kinase, MEK= dual specificity mitogen-activated protein kinase kinase, ERK= mitogen-activated protein kinase, PI3K= Phosphatidylinositol 3-kinase, AKT= protein kinase B (PKB), red P= inhibitory phosphorylation.

4 Discussion

Refractory high-risk neuroblastoma is a devastating malignancy with limited treatment options that may benefit from a more profound understanding of targeted, ALKi treatment strategies and associated resistance mechanisms. This thesis successfully identified genes associated with an ALK inhibitor resistant phenotype and unveiled genomic alterations conferring ALKi resistance. Further, it was elucidated how these genomic alterations alter transduction signalling cascades. The following chapters will focus on the discussion of *in vitro* methods to identify genes associated with drug resistance and methods for functional validation as well as elaborate on the role of identified genes in signalling transduction cascades and accompanying collateral sensitivities with respect to clinical applications.

4.1 RAS/MAPK pathway signalling alterations render NB models ALKi resistant

4.1.1 Forward genetic screens

CRISPR-based genetic forward screening approaches have successfully been used to elucidate cell response to targeted therapies and to identify response-associated genes putatively responsible for resistance development to different inhibitors in a variety of malignancies [277, 282, 283]. Such screens can be performed using various CRISPR systems, which either mediate gene knockouts or knockdowns (CRISPR interference) as well as CRISPR systems that enhance gene expression (CRISPR activation) [284]. Each of these systems is compatible with one or more sgRNA libraries, and this library diversity can be used to address a variety of scientific questions, *i.e.*, some enable a genome-wide screen, while others are focused on a certain class of genes, biological functions, or signalling pathways [209, 285]. Screens can be divided into negative as well as positive selection screens. The type to be used depends on the scientific question or hypothesis to be investigated. During negative selection screens, sgRNAs that affect a certain gene and thereby lead to selection disadvantages will be depleted or absent at the endpoint of the screen [286]. In a positive selection screen cells of interest, containing a certain sgRNA which alters the target gene and thereby confers selection advantages, will be enriched over time under a selective pressure [286]. Major challenges of CRISPR screens include identifying genes associated with the investigated phenotype among the derived gene 'hit list' and evaluating specificity and robustness of the results.

In this study, positive selection CRISPR/Cas9 knockout screens, during which cells of interest are enriched over time, were performed to identify genes associated with ALKi resistance in the *ALK*-mutated neuroblastoma cell line SH-SY5Y. After exposure to lorlatinib and ceritinib, the sgRNAs targeting the tumour suppressor gene *NF1* [287] were found to be highly enriched in the ALK inhibitor treated samples in comparison to the spectrum of sgRNAs in the baseline (t_0) and vehicle control (DMSO) samples. Both technical replicates for lorlatinib and ceritinib showed an enrichment of all four

sgRNAs for *NF1,* further supporting *NF1* as a robust hit. A loss of *NF1* had already been described to be associated with resistance towards targeted therapies in other malignancies, *e.g*., BRAF-inhibition in melanoma, BCR-ABL-inhibition in chronic myeloid leukaemia and endocrine therapies in advanced breast cancer [275-278]. De Bruin *et al*. reported reduced *NF1* expression in lung cancer in association with resistance to the EGFR-inhibitor (EGFRi) erlotinib [275]. In this study, a genome-wide RNA interference screen was performed in an EGFRi-sensitive human lung adenocarcinoma cell line in the presence and absence of erlotinib [275]. De Bruin *et al.* observed that a knockdown of *NF1* expression resulted in enhanced cell survival during erlotinib exposure and confirmed this in a murine model [275]. They further confirmed the clinical relevance of their findings by analysing human EGFR-mutant lung adenocarcinoma samples before and after acquired resistance to erlotinib [275]. Interestingly, in contrast to the results of the present thesis, De Bruin *et al.* reported, that cells with reduced *NF1* expression were resistant to erlotinib and the MEKi AZD-6244 (selumetinib), but sensitive to a combination treatment [275]. Both MEKi, trametinib and selumetinib, are allosteric MEKi and bind to a pocket in the inactive conformation of MEK 1/2 [288].

There are currently multiple tools available to analyse CRISPR screens, but MAGeCK emerged as a standard tool for this task [234]. MAGeCK determines β-scores (similar to fold change values) and a gene 'hit list' is derived based on calculated *P*-values (determined by performance of a permutation test) [234]. Genes and respective β-scores were subjected to a GSEA [217, 218]. Using specific significance cut-offs (FDR<0.25, NES>1.5 and FWER<0.1) this analysis revealed enriched gene sets associated with translation, NMD and the respiratory electron transport. The identification of enriched gene sets associated with translation was in accordance with the literature as it has been described, that a knockout of ribosomal genes results in a strong negative selection phenotype [289, 290] ,showing an enrichment of respective gRNAs, which is therefore used as quality control [234]. The subsequently performed leading-edge analysis indicated an overlap of leading-edge genes between subsets representing genes of the respiratory chain. As an overlap was observed only within this group of respiratory chain gene sets this indicated a result specific to this biological process. Leading-edge genes associated with the respective gene sets should be further investigated regarding their association with a ALKi resistant phenotype by generating respective NB knockout cell line models or performance of RNA interference experiments or CRISPR interference to downregulate the expression of the respective genes. Subsequently, cell signalling should be investigated during exposure to ALK inhibitors.

With regard to the analysis of CRISPR screens it is important to keep in mind, that MAGeCK-derived β-scores and hits should be in line with the extent of enrichment of sgRNAs per gene. Furthermore, potential hits retrieved from CRISRP/Cas9 knockout library screens should be validated as each sgRNA

has a certain number of off-targets with a predicted off-target activity [286]. In particular, hits called with only one enriched sgRNA should be interpreted with caution as single sgRNAs targeting a gene might be enriched in samples treated with inhibitors, but the observed effect could result from an off-target effect. It should also be kept in mind that some sgRNA containing constructs are lost in the long screening process either at the stage of plasmid library amplification, the state of virus production or at the timepoint of infection. Especially a comparison of sequencing data derived of the plasmid pool itself as well as of the cell pool after infection with lentiviral particles containing these plasmids (t_0, baseline sample) provide information about which sgRNA containing plasmids are lost (*e.g.*, due to technical issues) and which gene knockouts can be lethal in the investigated model system. A comparison derived gene list could be further compared to already published data of reports from three research groups that investigated essential genes [291-293]. Hart *et al*. as well as Wang *et al*. investigated essential genes in human cancer cell lines performing CRISPR/Cas9 knockout screens, but also pointed to differences in core fitness genes dependent on cancer type, oncogenic drivers, developmental origin and further additional factors [292, 293].

The chosen duration and concentration to perform the screen may affect the selection of resilient and resistant cell clones. Kinetic experiments of CRISPR/Cas9 knockout positive selection screens revealed, that a quarter of cells infected with virus containing sgRNAs targeting essential genes are depleted at day 7 and the rest within the next 18 days [294]. In contrast the study by Cross *et al*. detected the deletion of those cells between 3 and 7 days [295]. In a positive selection screen with an applied selection pressure as *e.g.*, a compound, the screen durations should be dependent on the drug's mechanism of action as well. In addition, some CRISPR-mediated gene alterations may lead to a resilient phenotype but not to a resistant phenotype. This resilient phenotype may arise during the screen due to cell plasticity allowing cells a phenotypic switch to adapt to environmental conditions *e.g.*, to drug exposure, without the need for *de novo* mutations [296, 297].

So far only one research group has previously reported the performance of a CRISPR screen in *ALK*-mutated neuroblastoma cell lines to investigate ALKi resistance. Trigg *et al*. performed a CRISPR activation screen using the CRISPR-synergistic activation mediator (SAM)-system in a 3-vector format [284], which induced overexpression of targeted genes, in SH-SY5Y and CHLA-20 cells [204]. Cells were exposed to respective IC_{50} and IC_{75} concentrations of ceritinib and brigatinib for 14 days [204]. They identified overexpression of *PIM1*, a gene encoding the PIM1 kinase, to be associated with ALKi resistance [204] in contrast to the knockout screen described in this thesis, that identified the tumour suppressor gene *NF1*. Meanwhile, other CRISPR knockout or knockdown systems have been described, like Cas9 nickase variants that introduce knockouts, CasRX-mediated knockdown systems (and other CRISPRi systems) or base editor systems, that are reported to be superior to the classic CRISPR/Cas9

knockout system, due to less frequent off-targets, increased target specificity and increased efficiency [298-301].

An alternative approach to identify resistance-conferring genes is the continuous exposure of cell lines of interest to increasing concentrations of investigated drugs. This approach was also utilized in the study Berlak *et al.* to render the *ALK*-mutated NB cell line NBLW-R resistant to ceritinib and lorlatinib. It was postulated that cell line models generated by a constant drug exposure represent clinically irrelevant resistance models [194], which was not confirmed by Berlak *et al*.[1]. For all technical replicates of ceritinib or lorlatinib treatments the well-described oncogenic $NRAS^{Q61K}$ mutation, that leads to increased RAS/MAPK pathway signalling, was detected using panel sequencing [101]. Cells were exposed to ALK inhibitors for a period of 3 months, which is a comparatively short duration, in contrast to 8-12 months used in previous studies to render cells resistant [181, 203]. In the study by Debruyne *et al*., acquired genomic alterations of resistant cell lines had been investigated by PCR amplification of the ALK kinase domain sequence and subsequent amplicon sequencing [181]. Only increased activity of other RTKs was considered to lead to an ALKi-resistant phenotype, which was investigated using a phospho-RTK array [181]. As this type of experimental approach to identify new resistance mechanisms requires extensive passaging and long cultivation times of cell lines *in vitro*, cell models should be thoroughly sequenced on a whole-genome-scale for multiple genomic alterations and compared to a control, which was not exposed to the compound of interest. It has been reported, that an extensive passaging of cell lines causes a genetic drift and a higher frequency of mutations [302]. Taking this into account, it would not be possible to distinguish whether a certain mutation was acquired due to specific inhibitor treatment or due to a genetic drift derived from long passaging. Therefore, single cell clones of resistant cell populations should be isolated to generate isogenic cell lines. In case of multiple mutations appropriate perturbed models need to be generated.

In the study by Berlak *et al*., even though ALKi-resistant NBLW-R cell populations were sequenced using a rather broad approach in comparison to preceding studies, it is highly likely that some mutations were not detected due to the design of the targeted sequencing panel [303]. Additional methods to further investigate genomic alterations in the NBLW-R cell populations would be whole-genome sequencing or whole-exome sequencing. Isolated single cell clones should be sequenced with the above-mentioned methods and detected genomic alterations further investigated to distinguish between driver and passenger mutations [190].

Despite differences in discussed approaches, both methods utilised in this thesis and in Berlak *et al*. identified genes of the RAS/MAPK pathway to mediate ALKi resistance.

4.1.2 Assays to assess drug response

To further elucidate the relevance of the identified mutations, it was indispensable to investigate the functional effect of observed genomic alterations separately. ATP quantification assays, colony formation assays as well as live-cell imaging experiments are often used to investigate the response towards targeted therapies of genetically perturbed *in vitro* model systems [194, 195].

In the present thesis, based on results of unbiased screening approaches, validated SH-SY5Y and LAN-5 *NF1* knockout clones were generated and used to assess ALK inhibitor response *in vitro*. Cell viability was assayed using an ATP-quantification assay and total cell numbers were assessed using a live-cell imaging system (Incucyte). A resistant phenotype was defined based on McDermott *et al*. [194]. Accordingly, clinically relevant resistance models show a fold resistance (IC_{50} resistant cell line / IC_{50} parental cell line) of 2-5-fold and high-level laboratory models, which are assumed to be clinically irrelevant by McDermott *et al*., a fold resistances ≥ 12 [194]. The clinical relevance of models with fold resistances ≥ 12 might have been questioned as these are often highly adapted models, but the definition should be used with caution [194]. McDermott *et al*. derived this definition for *in vitro* resistance based on comparison of patient derived cancer cells before and after acquisition of clinical resistance to chemotherapy [194]. In this thesis, both assays indicated an ALK inhibitor resistant phenotype, but assay-dependent either a clinically relevant or a clinically irrelevant high-level laboratory model, according to proposed resistance definitions based on FR [194]. Ideally, the algorithms implemented in the live-cell imaging system would allow a stringent discrimination between viable cells and apoptotic cells, but this was only achieved to a certain extent using brightfield microscopy. Hence, a clear discrimination whether these cells are already apoptotic or not is only possible by use of membrane penetrating dyes, which bind apoptotic markers. The ATP quantification assay on the other hand, neglects the possibility of a metabolic change of the cell upon cell perturbation (*e.g*., CRISPR-mediated knockout).

Furthermore, 'loss of cell viability' detected by this assay cannot be attributed specifically to effects caused by either (1) reduced cell numbers due to cell death or reduced proliferation, or (2) reduced intracellular ATP levels inherent in apoptotic, senescence or differentiated cells. Additionally, it has been reported that apoptotic cells might increase ATP levels and contribute to a false positive readout, as increased cytosolic ATP levels have been detected after sub-cellular as well as plasma membrane dissociation [304].

Unexpectedly, the LAN-5 *NF1* KO clone #2 (Figure 3.14 and Figure 3.15) was found to be not resistant to ceritinib exposure (FR 1.64 and 1.44) as assessed by the CellTiter-Glo® assay as well as live-cell imaging and according to the proposed resistance definition (FR ≥ 2), whereas SH-SY5Y and respective *NF1* KO cell lines as well as LAN-5 and LAN-5 *NF1* KO clone #1 had a FR of 2.13 to 2.65 derived from

CellTiter-Glo® and FR of 10.3 to 14.8 derived from live-cell imaging experiments. This observation made in LAN-5 *NF1* KO clone #2 could be explained by a shifted dependency towards ceritinib off-targets (ROS1, IGF-1R and INSR) [155, 156] in comparison to the LAN-5 parental line or an increased expression of these. However, this cell line was resistant in other assays like ELISA assays and western blot experiments as indicated by elevated pMEK and pERK levels during exposure to ceritinib. In general, resistance was more pronounced against lorlatinib than ceritinib. The ALK specificity and affinity of these two inhibitors may cause these differences, with lorlatinib being more specific for mutant ALK, while ceritinib is known to be less specific with more off-target cytotoxic effects [305].

For a better understanding of clinically relevant resistance models, pairs of patient-derived cell lines before and after acquisition of resistance to therapeutics should be established. These would enable a more robust or malignancy-specific definition for resistance of *in vitro* systems and might help to further discriminate between clinically relevant and clinically irrelevant high-level laboratory models. Patient-derived cell lines could be established as 2D or 3D cell culture models. Those may represent a higher genetic likeliness and are a closer representation of the native tumours in comparison to cell lines that have been established over 30 years ago [214, 215], which over time have possibly acquired additional mutations and are now well-adapted to artificial cell culture conditions. Furthermore, the use of patient derived xenograft (PDX) models should be implemented to a bigger extent.

In this work, an unbiased screening approach identified genomic alterations associated with resistance to different ALK inhibitors. One particular genomic alteration was further investigated generating appropriate models and was validated to lead to an ALKi-resistant phenotype using different techniques to investigate cell viability.

4.2 Acquisition of mutations conferring ALKi resistance is observed in NB patient samples

Tumour biopsies of NB patients enrolled in ALKi clinical trials were analysed using diagnostic panel sequencing, before and after acquisition of ALKi resistance [1]. Interestingly, *de novo NF1* mutations were detected in tumours of two patients treated with ceritinib [1].

This observation further supports the relevance of results seen in cell line models using CRISPR/Cas9 knockout screens as well as *NF1* knockout models. This is the first study until now investigating ALKi resistance in NB cell line models that substantiates genes and mechanisms identified *in vitro* with alterations detected in relevant patient samples. Furthermore, *NF1* is the first reported tumour suppressor gene to be associated with an ALK inhibitor resistant phenotype in neuroblastoma. Up to now, RAS/MAPK pathway mutations have mainly been reported in relapsed neuroblastoma after chemotherapy treatment and once for a relapsed neuroblastoma treated with lorlatinib [33, 34, 306]. Reported *in vitro* systems used to investigate ALKi resistance in NB so far, associated increased

activation of alternative kinases like PIM1 [204] and AXL [181] as well as upregulation of the transcription factor *BORIS* [203] with an ALK inhibitor resistant phenotype.

In order to thoroughly address tumour evolution and temporal as well as spatial ITH and to identify an optimal time point for effective use of alternative therapies opening by collateral sensitivities implementation of dynamic sampling is required [207, 307]. However, dynamic sampling of tumour tissue might be problematic in the field of paediatric oncology and could rather be addressed by a minimally invasive methodology, *e.g*. the use of liquid biopsy, which would allow genomic diagnostics based on free circulating tumour DNA (ctDNA) in the blood [308]. This approach would on the other hand not allow to investigate spatial heterogeneity, and it was shown that only 88% of clonal single nucleotide variants (SNVs) detected in tumour tissue are also detected using liquid biopsy [308]. On the other hand, if dynamic sampling would be based on tumour tissue, clinicians would be challenged by the choice of lesions to take for sequencing and to define optimal sampling timepoints during treatment with targeted therapies. In both cases it would be necessary to classify detected mutations into driver mutations, leading to a selective advantage and increased proliferation and potentially conferring a resistant phenotype, and passenger mutations, not influencing selection but potentially rendering tumour cells resilient or resistant at a later timepoint [309]. This distinction will be of great importance for profound treatment decisions, *e.g*., using targeted therapies. Furthermore, the detected genomic alterations should be investigated for known collateral sensitivities. Together with the possibility of spatial ITH, a profound treatment decision might be challenging, even though dynamic sampling was implemented.

In summary, this thesis provided evidence that mutations associated with an ALKi resistant phenotype *in vitro* are useful to understand genomic alterations in patient samples and resistance mechanisms.

4.3 Analysis of signal transduction cascades in perturbed *in vitro* systems

It was shown that a loss of *NF1* leads to increased downstream signalling along the RAS/MAPK signalling axis [129]. Hence, in the thesis presented here, ALK downstream signalling was investigated in *NF1* KO clones models using western blot, computational modelling, and inhibitor screens.

Simulated network response analysis based on experimental perturbation data using the STASNet systems biology tool [259] indicated a shift of downstream signalling towards the RAS/MAPK axis, which was also observed using western blot for *NF1* KO cell lines. These experiments were based on detection of phosphorylated (activated) RAS effectors like MEK and ERK [123, 124]. As these RAS effectors are not directly downstream of RAS, this approach is an indirect measurement of RAS activity. Furthermore, it was postulated by several groups that RAF, which is directly downstream of RAS and

directly upstream of MEK, could also be activated RAS independently [310-312]. Therefore, performing a RAS activity assay using a direct measurement via RAF would allow the exclusion of RAS-independent RAF activity in *NF1* KO cell lines.

Using computational modelling a weakened or absent inhibitory ERK to RAF feedback was identified, which in turn gives rise to a new collateral sensitivity. It was shown that *BRAF V600E*-mutated cell lines, that have a disrupted inhibitory ERK to RAF feedback, harbour elevated baseline phosphorylated MEK levels and are dependent on MAPK signalling for cell proliferation and MEK inhibitor (MEKi) sensitive [170]. On the contrary, intact inhibitory feedback has been reported for a MEKi-resistant phenotype, where MEK inhibition with different MEK inhibitors caused increased level of phosphorylated MEK and a possible reactivation of the pathway [168, 170]. In addition, it has been reported that *ALK*-mutated neuroblastoma cell lines are MEKi-resistant, which would further support the hypothesis that MEK inhibitor sensitivity of *NF1* KO models is a result of a weakened or absent ERK to RAF feedback [171, 313]. The observed trametinib (MEKi) and LY3009120 (pan-RAFi) sensitivity of *NF1* KO clones, assessed by an inhibitor screen, further substantiated this hypothesis. Even though the increased sensitivity was not observed for SH-SY5Y *NF1* KO#2 in concentration-response data, all *NF1* KO clones showed an absence of pMEK in contrast to elevated pMEK level observed in parental cell lines during trametinib treatment. This finding is in line with results for the *ALK*-mutated neuroblastoma cell line CLB-GA. In that study by Redaelli *et al*. [314], cells which had been rendered resistant to lorlatinib by continuous exposure, acquired truncating *NF1* mutations as well as activating *EGFR* and *Erb4* mutations and became sensitive to trametinib (MEKi) treatment [314]. Furthermore, this observation is consistent with a report that postulated a correlation of binimetinib (MEKi) sensitivity of NB cell lines and low *NF1* expression [315]. The observed collateral sensitivities for *NF1* knockout cells indicate the opportunity for an effective combination treatment using MEKi and RAFi , that has been reported to improve overall survival and progression-free survival in *BRAF V600E/K*-mutant metastatic melanoma, that also harbour a disrupted inhibitory ERK to RAF feedback [165]. There is, however, a conflicting report from 2013, describing a loss of *NF1* to lead to RAFi and MEKi resistance in $BRAF^{V600E}$-mutant malignancies [276].

A better understanding of the proposed weakened or absent inhibitory ERK to RAF feedback could help to confirm this hypothesis. The feedback should be investigated using western blot analysis during ALKi and MEKi treatment using antibodies detecting inhibitory phosphorylation sites of RAF with available antibodies detecting p-c-RAF Ser43, p-c-RAF Ser642 and p-c-RAF Ser289, Ser296, Ser301 [316]. In addition, RAF inhibitory phosphorylation patterns or cluster could be investigated in *NF1* knockout cells performing a RAF pull down using antibodies binding inhibitory phosphorylation sites on RAF coupled with mass spectrometry (MS) experiments. Alternatively, the inhibitory feedback could be

investigated using radioactive labelling of phosphorylation sites with ^{32}Pi (orthophosphate), RAF pull down and subsequent SDS-PAGE and *e.g.*, phosphoimaging. *NF1* knockout cell lines should also be subjected to exposure with selective RAFi and the RAF isoform involved in the absent inhibitory ERK feedback identified.

To date, a regulatory function of NF1 protein for ERK or RAF signalling has not been reported. Several interaction partners of NF1 have been described, but neither direct interactions with RAF nor any interactions that would diminish inhibitory RAF phosphorylation have been reported so far. Based on literature NF1 and RAF could get into proximity via 14-3-3 proteins. RAF, 14-3-3 protein as well as MEK 1/2 and ERK 1/2 are all bound by the scaffold protein KSR1 [122]. NF1 on the other hand can be bound by 14-3-3 protein upon protein kinase A-mediated phosphorylation, which inhibits its GAP activity [148]. The interaction of NF1 with RAF and 14-3-3 protein, both bound by KSR1, might cause a steric hindrance, that prevents ERK phosphorylation of RAF. This possible protein-protein interaction has to be investigated further using western blot detecting relevant phosphorylation sites on RAF or interactive studies of RAF and NF1 need to be performed, *e.g.*, using fluorescence resonance energy transfer (FRET) based systems, surface plasmon resonance (SPR) experiments, crystallography or MS coupled pull-down experiments.

In order to elucidate such mechanisms in cell line models with a single perturbation, it is indispensable to investigate additional genomic alterations before the system is perturbed. The *NF1* KO clones were generated in the *ALK*-mutated neuroblastoma cell lines SH-SY5Y and LAN-5, both free of further mutations in ALK downstream signalling pathways, using the CRISPR/Cas9 system and validated using Sanger Sequencing and western blot. The mRNA-sequencing data of the parental SH-SY5Y and *NF1* KO models were used to investigate for the occurrence for editing events in predicted sgRNA off-target genes but predicted off-target sequences showed an absent or very low read coverage. These off-target sequences should be further investigated using targeted sequencing approaches to preclude off-target editing.

To identify differential expression of genes in *NF1* KO cell lines in comparison to the parental cell line the mRNA-seq data was analysed using a linear regression model that takes the drug exposure duration, the specific drug, and the cell line type as factors influencing gene expression into account. Among the genes with significant differential expression was *ETV5*. Its expression was stable during ALKi exposure in *NF1* KO cell lines but not in the parental cell lines as expected, due to the increased RAS activity in *NF1* KO cell lines. Furthermore, the expression of the receptor kinase RET was increased in *NF1* KO cell lines in comparison to the parental line, but also affected during ceritinib exposure. It has been described, that ETV5 binds to the *RET* promoter regulating its gene expression [317]. Therefore, a

ETV5-RET loop might be a bypass mechanism leading to ALKi resistance in addition to the increased RAS activity. This should be further investigated in *NF1* knockout cell lines using qPCR and western blot.

NF1 transcripts were still detected in the mRNA-sequencing data, which is in agreement with the observation that CRISPR/Cas9-mediated knockouts are primarily detectable on a protein level as transcripts are still generated and exported from the nucleus to the cytoplasm, but no functional protein is synthesized due to NMD [279, 318]. In genomically modified cell models altered using the CRISPR/Cas9 system, it is important to exclude not only predicted off-target effects, but also to delineate additional alterations. It was reported that Cas9 nuclease expression itself leads to an upregulation of the p53 pathway and that this activation affects the sensitivity for chemical perturbations [319]. In this study of Enache *et al*. [319], the Cas9-coding sequence had been integrated into the cell genome via lentiviral infection, in contrast to the approach of transient transfection used within this thesis. However, this does not exclude the possibility to observe similar events.

In addition, it was shown that CRISPR/Cas9-introduced insertions and deletions vary strongly in length (1 bp up to 9.5 kb), which could lead to large chromosomal deletions extending beyond the targeted region [320, 321]. Therefore, it should be considered to validate CRISPR/Cas9 cell clones using whole-genome sequencing to detect all possible alterations. As this is not feasible, other approaches should be considered, *e. g*., a PCR panel with primers, flanking a wide region of the targeted genomic sequence as well as predicted off-target regions, coupled with gel electrophoresis or long-read sequencing. Furthermore, there is the option to use the GUIDE-seq approach published by Malinin *et al*. [322], where double-stranded oligonucleotide tags are integrated at the site of the Cas9-induced DNA double-stranded breaks. This allows an efficient detection of off-target and on-target editing on a genome-wide scale.

Taken together, this study showed that systems used to introduce genomic alterations for investigation of resistance-associated mutations can provide interesting findings, but still suffer from limitations that need to be addressed. Nevertheless, cell line models with loss of *NF1* were found to be sensitive to MEK inhibitor treatment, an acquired collateral sensitivity, due to a weakened or absent inhibitory ERK-RAF feedback.

4.4 Resistance mutations lead to new collateral sensitivities

In this study, new collateral sensitivities to MEK inhibition as well as RAF inhibition have been identified in ALKi resistant *ALK*-mutated NB cells with *NF1* loss. The concept of collateral sensitivities, describing cells being resistant to one inhibitor acquire new sensitivities towards an alternate agent, was described for chemotherapy-resistant malignancies [205, 206]. There are also reports of collateral sensitivities for malignancies resistant to targeted therapies. One example is the study by Acar *et al*..

The authors treated *EGFR* mutant NSCLC cell lines with trametinib over time to generate a resistant cell population [323]. They characterized the cells using whole-exome sequencing and confirmed results using digital droplet PCR (ddPCR) and single cell RNA-sequencing [323]. Trametinib-resistant NSCLC cells showed a loss of *CDKN2A,* and Acar *et al*. observed treatment with the histone deacetylase (HDAC) inhibitor quisinostat as effective, identifying a new collateral sensitivity [323]. In the study by Grolmusz *et al*. a ribociclib-resistant breast cancer cell line was generated by ribociclib exposure for five months [324]. Cells were characterized by whole-exome and RNA-sequencing and a loss of the G2/M checkpoint associated with the resistant phenotype [324]. Grolmusz *et al*. identified Wee-1 inhibitor (adavosertib) sensitivity as a collateral sensitivity.

MEKi sensitivity, as a new collateral sensitivity, has been associated multiple times with low or absent *NF1* expression in neuroblastoma, in line with the data presented in the thesis discussed here [314, 315, 325]. Therefore, it should be considered to establish *NF1* as a predictive biomarker [326] for MEKi treatment with trametinib. A predictive biomarker is defined as biomarker that allows the identification of individuals, being more likely to experience a favourable or an unfavourable effect when exposed to a medical product or an environmental agent than similar individuals without the biomarker [326]. Expression of *DUSP6* has been proposed as an alternative predictive biomarker [326] for trametinib treatment of ovarian and cervical cancer cell lines as a lack of *DUSP6* expression correlated with a MEKi-resistant phenotype [327]. This is not reflected by observations made for *NF1* KO models and the respective parental line, as the parental line was not trametinib-sensitive but a *DUSP6* expression of 2^{10} observed (Figure 3.18 C). RAF inhibition was also observed as a new collateral sensitivity in *NF1* knockout cells. A similar sensitivity to RAF inhibitors was described by Whittaker *et al.* for melanoma and colorectal cancer cell lines that were characterized by an increased RAS/MAPK signalling due to deactivating *NF1* mutations [262]. Furthermore, they described a synergy in these cell lines of MEKi and a pan-RAF inhibitor, but not between MEKi and the selective BRAF inhibitors PLX4720 or dabrafenib [281]. Therefore, the role of the three RAF isoforms should be investigated to further confirm and refine an effective therapeutic strategy for *ALK*-driven ALKi resistant neuroblastoma with *NF1* loss. The combination of the MEKi Trametinib and the selective BRAF inhibitor dabrafenib was FDA approved for *BRAF V600E*-mutated metastatic NSCLC in 2013 [164, 165]. As *BRAF V600E*-mutated cell lines were described to have a disrupted inhibitory ERK to RAF feedback like *NF1* knockout clones, a combination treatment of MEKi and RAFi should be investigated for *ALK*-driven ALKi resistant neuroblastoma with *NF1* loss [170].

In this study, it could not be determined whether the loss of *NF1* and the accompanying MEK inhibitor sensitivity were due to tumour evolution, meaning that cells with *NF1* loss were present in the primary tumour already, or if this was a *de novo* mutation acquired and selected for during inhibitor exposure.

Clonal evolution driven by Darwinian selection can favour cells harbouring mutations that increase cell fitness and render these cells the dominant population [296, 328]. The acquired mutations can be classified into driver mutations, leading to a selective advantage and increased proliferation, passenger mutations, not influencing selection, and disadvantageous mutations [309]. This fitness advantage of driver mutant lineages is further supported by the tumour microenvironment. The most prominent populations can also arise due to cell plasticity allowing cells a phenotypic switch to adapt to environmental conditions [296]. This cell plasticity drives slow-cycling drug-tolerant, *i.e*. resilient cell populations which can become drug-resistant cells [329]. One aspect of cell plasticity has been described for neuroblastoma, that is a phenotypic switch from adrenergic to mesenchymal cells, the latter presenting as more chemoresistant *in vitro* and potentially enriched in post-treatment and relapsed tumours [57, 58]. This phenotypic switch in NB was postulated to be mediated by NOTCH signalling [330]. In case NB patient samples also indicate a phenotypic switch, a combination treatment regimen of cytotoxic drugs, targeted therapies and compounds targeting cell plasticity (*e.g*., compounds against NOTCH receptors to abrogate signalling, which are currently investigated in clinical trials), should be investigated [331]. Furthermore, a combination therapy of ceritinib or lorlatinib with trametinib could also be favourable for patients with *ALK*-driven neuroblastoma. Though it might not be effective, as it is unknown whether the observed inactivating *NF1* mutations in ALK inhibitor resistant neuroblastoma were *de novo* mutations due to ALK inhibitor treatment or if the main cell population shifted towards cells harbouring those inactivating *NF1* mutations due to the selective pressure. Taking this into consideration it might be interesting to investigate a sequential treatment of patients in question with ALKi and MEKi. This as well as a treatment regimen of cytotoxic drugs, targeted therapies and compounds targeting cell plasticity could be investigated using PDX models with primary tumour tissue to better mimic this very dynamic process including tumour microenvironment and the context of cell fitness, as currently, *in vitro* cultures do not capture *e.g*. the tumour microenvironment [332]. Organ-on-a-chip experiments might be a suitable alternative or complementary approach to PDX models. This reverse engineering of cellular systems enables the cultivation of cells in defined microfluidic compartments, but only mimics key aspects of a tissue and requires extensive knowledge of tissue interactions, *e.g*., with the extracellular matrix and compositions [333, 334]. The chip surface material can also influence cell behaviour or might interact with the drugs as known for polydimethylsiloxane (PDMS), absorbing hydrophobic molecules [333]. Experiments with established organ-on-a-chip systems are, compared to PDX models, cost effective and results can be derived quickly [333].

In summary, the here presented findings further highlight that a dynamic sampling in the clinic is inevitable to find the best treatment options at a certain time point and to identify collateral sensitivities along this dynamic process.

5 Conclusions and perspectives

The present thesis aimed to identify and understand ALK inhibitor resistance mechanisms in *ALK*-driven neuroblastoma. Genes associated with an ALK inhibitor resistant phenotype in the *ALK*-driven neuroblastoma cell line SH-SY5Y were investigated using a genome-wide CRISPR/Cas9-mediated knockout screen. Single guide RNAs targeting genes encoding proteins that interact with or that regulate ALK downstream signalling pathways were enriched in both ALK inhibitor exposed samples in comparison to the sgRNA spectrum of the t_0 and DMSO control samples. One of those genes with enriched sgRNAs was *NF1,* which encodes NF1 protein, a negative regulator of RAS. The role of *NF1* in ALK inhibitor-resistant cells was further investigated by creating *NF1* knockout cell line models. These models did not only show increased activity of RAS/MAPK and AKT signalling, which was confirmed using different methods, but also an ALKi-resistant phenotype, which was due to increased ALK downstream signalling. Furthermore, collateral sensitivities were revealed using perturbation experiments and modelling of signalling networks. *NF1* knockout cell line models showed an increased sensitivity towards the MEK inhibitor trametinib due to a weakened inhibitory ERK to RAF feedback and were also more sensitive to the pan-Raf inhibitor LY3009120 than respective parental lines.

The proposed weakened or absent inhibitory ERK to RAF feedback should be investigated by western blot during ALKi and MEKi treatment using antibodies detecting inhibitory phosphorylation sites of RAF with available antibodies detecting p-c-RAF Ser43, p-c-RAF Ser642 and p-c-RAF Ser289, Ser296, Ser301. In addition, RAF inhibitory phosphorylation patterns or cluster could be investigated in *NF1* knockout cells performing a RAF pull down using antibodies binding inhibitory phosphorylation sites on RAF coupled with mass spectrometry experiments. Alternatively, the inhibitory feedback could be investigated using radioactive labelling of phosphorylation sites with ^{32}Pi (orthophosphate), RAF pull down and subsequent SDS-PAGE and *e.g.*, phosphoimaging. *NF1* knockout cell lines should also be subjected to exposure with selective RAFi and the RAF isoform involved in the absent inhibitory ERK feedback identified.

ALK inhibitors should be studied as a monotherapy in *ALK*-driven neuroblastoma as first line treatment in high-risk neuroblastoma patients, depending on clinical trial outcomes for primary and relapsed neuroblastoma. Tumour evolution should be closely monitored for dynamic treatment decisions and to not miss the time point of collateral sensitivities. Not only the aspect of *de novo* mutations should be considered in the choice of therapy, but also accompanying or alternative tumour dynamics should be targeted. The development of resistance mechanisms should be further investigated *in vitro*, in order to obtain a standardised definition of resistance *in vitro* and to define what type of cell line

models represent clinically relevant models. Furthermore, models also mimicking the tumour microenvironment should be implemented and their influence on resistance development studied.

Overall, this work demonstrated that CRISPR screens and isogenic cell line models can be used to identify genes associated with an ALK inhibitor resistant phenotype that are clinically relevant and to provide clinically relevant mechanistic models. Furthermore, the present thesis underlines how modelling of signalling pathway can be used to reveal new collateral sensitivities and new potential therapy options, which could impact clinical practice and clinical trial design. In addition, it suggests *NF1* as a predictive biomarker for MEK inhibitor treatment, which should be included in companion diagnostics for trametinib therapy. In the future, MEK inhibition should be considered as a treatment option in the clinic for patients with *ALK*-driven neuroblastoma, characterized by inactivating *NF1* mutations, and a sequential treatment or a pre-emptive combination therapy with ALK inhibitor and MEK inhibitor exploited.

6 Bibliography

[1] M. Berlak, E. Tucker, M. Dorel, A. Winkler, A. McGearey, E. Rodriguez-Fos, B.M. da Costa, K. Barker, E. Fyle, E. Calton, S. Eising, K. Ober, D. Hughes, E. Koutroumanidou, P. Carter, R. Stankunaite, P. Proszek, N. Jain, C. Rosswog, H. Dorado-Garcia, J.J. Molenaar, M. Hubank, G. Barone, J. Anderson, P. Lang, H.E. Deubzer, A. Künkele, M. Fischer, A. Eggert, C. Kloft, A.G. Henssen, M. Boettcher, F. Hertwig, N. Blüthgen, L. Chesler, J.H. Schulte. Mutations in ALK signaling pathways conferring resistance to ALK inhibitor treatment lead to collateral vulnerabilities in neuroblastoma cells. Mol Cancer. 21: 126 (2022).

[2] D.J. Anderson, R. Axel. A bipotential neuroendocrine precursor whose choice of cell fate is determined by NGF and glucocorticoids. Cell. 47: 1079-1090 (1986).

[3] D.J. Anderson, J.F. Carnahan, A. Michelsohn, P.H. Patterson. Antibody markers identify a common progenitor to sympathetic neurons and chromaffin cells in vivo and reveal the timing of commitment to neuronal differentiation in the sympathoadrenal lineage. J Neurosci. 11: 3507-3519 (1991).

[4] J.M. Maris. Recent advances in neuroblastoma. N Engl J Med. 362: 2202-2211 (2010).

[5] F. Erdmann, P. Kaatsch, D. Grabow, C. Spix. German Childhood Cancer Registry - Annual Report 2019 (1980-2018). Institute of Medical Biostatistics, Epidemiology and Informatics (IMBEI) at the University Medical Center of the Johannes Gutenberg University Mainz. (2020).

[6] T. Simon, B. Hero, J.H. Schulte, H. Deubzer, P. Hundsdoerfer, D. von Schweinitz, J. Fuchs, M. Schmidt, V. Prasad, B. Krug, B. Timmermann, I. Leuschner, M. Fischer, T. Langer, K. Astrahantseff, F. Berthold, H. Lode, A. Eggert. 2017 GPOH Guidelines for Diagnosis and Treatment of Patients with Neuroblastic Tumors. Klin Padiatr. 229: 147-167 (2017).

[7] N.R. Pinto, M.A. Applebaum, S.L. Volchenboum, K.K. Matthay, W.B. London, P.F. Ambros, A. Nakagawara, F. Berthold, G. Schleiermacher, J.R. Park, D. Valteau-Couanet, A.D. Pearson, S.L. Cohn. Advances in Risk Classification and Treatment Strategies for Neuroblastoma. J Clin Oncol. 33: 3008-3017 (2015).

[8] S.J. Diede. Spontaneous regression of metastatic cancer: learning from neuroblastoma. Nat Rev Cancer. 14: 71-72 (2014).

[9] F. Berthold, C. Spix, P. Kaatsch, F. Lampert. Incidence, Survival, and Treatment of Localized and Metastatic Neuroblastoma in Germany 1979-2015. Paediatr Drugs. 19: 577-593 (2017).

[10] K.T. Vo, K.K. Matthay, J. Neuhaus, W.B. London, B. Hero, P.F. Ambros, A. Nakagawara, D. Miniati, K. Wheeler, A.D. Pearson, S.L. Cohn, S.G. DuBois. Clinical, biologic, and prognostic differences on the basis of primary tumor site in neuroblastoma: a report from the international neuroblastoma risk group project. J Clin Oncol. 32: 3169-3176 (2014).

[11] K.K. Matthay, J.M. Maris, G. Schleiermacher, A. Nakagawara, C.L. Mackall, L. Diller, W.A. Weiss. Neuroblastoma. Nat Rev Dis Primers. 2: 16078 (2016).

[12] V. Strenger, R. Kerbl, H.J. Dornbusch, R. Ladenstein, P.F. Ambros, I.M. Ambros, C. Urban. Diagnostic and prognostic impact of urinary catecholamines in neuroblastoma patients. Pediatr Blood Cancer. 48: 504-509 (2007).

[13] G. Cullot, J. Boutin, J. Toutain, F. Prat, P. Pennamen, C. Rooryck, M. Teichmann, E. Rousseau, I. Lamrissi-Garcia, V. Guyonnet-Duperat, A. Bibeyran, M. Lalanne, V. Prouzet-Mauléon, B. Turcq, C. Ged, J.M. Blouin, E. Richard, S. Dabernat, F. Moreau-Gaudry, A. Bedel. CRISPR-Cas9 genome editing induces megabase-scale chromosomal truncations. Nat Commun. 10: 1136 (2019).

[14] S.G. Dubois, E. Geier, V. Batra, S.W. Yee, J. Neuhaus, M. Segal, D. Martinez, B. Pawel, G. Yanik, A. Naranjo, W.B. London, S. Kreissman, D. Baker, E. Attiyeh, M.D. Hogarty, J.M. Maris, K. Giacomini, K.K. Matthay. Evaluation of Norepinephrine Transporter Expression and Metaiodobenzylguanidine Avidity in Neuroblastoma: A Report from the Children's Oncology Group. Int J Mol Imaging. 2012: 250834 (2012).

[15] H. Komuro, M.B. Valentine, S.T. Rowe, V.J. Kidd, S.-i. Makino, G.M. Brodeur, S.L. Cohn, A.T. Look. Fluorescence in situ hybridization analysis of chromosome 1p36 deletions in human MYCN amplified neuroblastoma. J Pediatr Surg. 33: 1695-1698 (1998).

[16] S.L. Cohn, A.D. Pearson, W.B. London, T. Monclair, P.F. Ambros, G.M. Brodeur, A. Faldum, B. Hero, T. Iehara, D. Machin, V. Mosseri, T. Simon, A. Garaventa, V. Castel, K.K. Matthay. The International Neuroblastoma Risk Group (INRG) classification system: an INRG Task Force report. J Clin Oncol. 27: 289-297 (2009).

[17] T. Monclair, G.M. Brodeur, P.F. Ambros, H.J. Brisse, G. Cecchetto, K. Holmes, M. Kaneko, W.B. London, K.K. Matthay, J.G. Nuchtern, D. von Schweinitz, T. Simon, S.L. Cohn, A.D. Pearson. The International Neuroblastoma Risk Group (INRG) staging system: an INRG Task Force report. J Clin Oncol. 27: 298-303 (2009).

[18] G.M. Brodeur, J. Pritchard, F. Berthold, N.L. Carlsen, V. Castel, R.P. Castelberry, B. De Bernardi, A.E. Evans, M. Favrot, F. Hedborg. Revisions of the international criteria for neuroblastoma diagnosis, staging, and response to treatment. J Clin Oncol. 11: 1466-1477 (1993).

[19] M.S. Irwin, A. Naranjo, F.F. Zhang, S.L. Cohn, W.B. London, J.M. Gastier-Foster, N.C. Ramirez, R. Pfau, S. Reshmi, E. Wagner, J. Nuchtern, S. Asgharzadeh, H. Shimada, J.M. Maris, R. Bagatell, J.R. Park, M.D. Hogarty. Revised Neuroblastoma Risk Classification System: A Report From the Children's Oncology Group. J Clin Oncol. 39: 3229-3241 (2021).

[20] S. Ackermann, M. Cartolano, B. Hero, A. Welte, Y. Kahlert, A. Roderwieser, C. Bartenhagen, E. Walter, J. Gecht, L. Kerschke, R. Volland, R. Menon, J.M. Heuckmann, M. Gartlgruber, S. Hartlieb, K.O. Henrich, K. Okonechnikov, J. Altmuller, P. Nurnberg, S. Lefever, B. de Wilde, F.

Sand, F. Ikram, C. Rosswog, J. Fischer, J. Theissen, F. Hertwig, A.D. Singhi, T. Simon, W. Vogel, S. Perner, B. Krug, M. Schmidt, S. Rahmann, V. Achter, U. Lang, C. Vokuhl, M. Ortmann, R. Buttner, A. Eggert, F. Speleman, R.J. O'Sullivan, R.K. Thomas, F. Berthold, J. Vandesompele, A. Schramm, F. Westermann, J.H. Schulte, M. Peifer, M. Fischer. A mechanistic classification of clinical phenotypes in neuroblastoma. Science. 362: 1165-1170 (2018).

[21] W.H. Liang, S.M. Federico, W.B. London, A. Naranjo, M.S. Irwin, S.L. Volchenboum, S.L. Cohn. Tailoring Therapy for Children With Neuroblastoma on the Basis of Risk Group Classification: Past, Present, and Future. JCO Clin Cancer. 895-905 (2020).

[22] F. Berthold, J. Boos, S. Burdach, R. Erttmann, G. Henze, J. Hermann, T. Klingebiel, B. Kremens, F.H. Schilling, M. Schrappe, T. Simon, B. Hero. Myeloablative megatherapy with autologous stem-cell rescue versus oral maintenance chemotherapy as consolidation treatment in patients with high-risk neuroblastoma: a randomised controlled trial. Lancet Oncol. 6: 649-658 (2005).

[23] F. Berthold, A. Ernst, B. Hero, T. Klingebiel, B. Kremens, F.H. Schilling, T. Simon. Long-term outcomes of the GPOH NB97 trial for children with high-risk neuroblastoma comparing high-dose chemotherapy with autologous stem cell transplantation and oral chemotherapy as consolidation. Br J Cancer. 119: 282-290 (2018).

[24] J. Pritchard, S.J. Cotterill, S.M. Germond, J. Imeson, J. de Kraker, D.R. Jones. High dose melphalan in the treatment of advanced neuroblastoma: results of a randomised trial (ENSG-1) by the European Neuroblastoma Study Group. Pediatr Blood Cancer. 44: 348-357 (2005).

[25] K.K. Matthay, C.P. Reynolds, R.C. Seeger, H. Shimada, E.S. Adkins, D. Haas-Kogan, R.B. Gerbing, W.B. London, J.G. Villablanca. Long-term results for children with high-risk neuroblastoma treated on a randomized trial of myeloablative therapy followed by 13-cis-retinoic acid: a children's oncology group study. J Clin Oncol. 27: 1007-1013 (2009).

[26] F. Giammarile, A. Chiti, M. Lassmann, B. Brans, G. Flux. EANM procedure guidelines for 131I-meta-iodobenzylguanidine (131I-mIBG) therapy. Eur J Nucl Med Mol Imaging. 35: 1039-1047 (2008).

[27] M. Schmidt, T. Simon, B. Hero, W. Eschner, M. Dietlein, F. Sudbrock, R. Bongartz, F. Berthold, H. Schicha. Is there a benefit of 131 I-MIBG therapy in the treatment of children with stage 4 neuroblastoma? A retrospective evaluation of The German Neuroblastoma Trial NB97 and implications for The German Neuroblastoma Trial NB2004. Nuklearmedizin. 45: 145-151 (2006).

[28] M. Schmidt, B. Hero, T. Simon. I-131-mIBG therapy in neuroblastoma: established role and prospective applications. Clin Transl Imaging. 4: 87-101 (2016).

[29] T. Simon, B. Hero, A. Eggert, H. Lode, M. Fischer, B. Timmermann, R. Schwarz, J. Fuchs, D. Von Schweinitz, C. Vokuhl, M. Schmidt, F. Körber, J. Schäfer. S1-Leitlinie 025-008 Neuroblastom. (2019).

[30] I. Mueller, K. Ehlert, S. Endres, L. Pill, N. Siebert, S. Kietz, P. Brock, A. Garaventa, D. Valteau-Couanet, E. Janzek, N. Hosten, A. Zinke, W. Barthlen, E. Varol, H. Loibner, R. Ladenstein, H.N. Lode. Tolerability, response and outcome of high-risk neuroblastoma patients treated with long-term infusion of anti-GD(2) antibody ch14.18/CHO. MAbs. 10: 55-61 (2018).

[31] A.L. Yu, A.L. Gilman, M.F. Ozkaynak, W.B. London, S.G. Kreissman, H.X. Chen, M. Smith, B. Anderson, J.G. Villablanca, K.K. Matthay, H. Shimada, S.A. Grupp, R. Seeger, C.P. Reynolds, A. Buxton, R.A. Reisfeld, S.D. Gillies, S.L. Cohn, J.M. Maris, P.M. Sondel. Anti-GD2 antibody with GM-CSF, interleukin-2, and isotretinoin for neuroblastoma. N Engl J Med. 363: 1324-1334 (2010).

[32] T. Simon, F. Berthold, A. Borkhardt, B. Kremens, B. De Carolis, B. Hero. Treatment and outcomes of patients with relapsed, high-risk neuroblastoma: results of German trials. Pediatr Blood Cancer. 56: 578-583 (2011).

[33] T.F. Eleveld, D.A. Oldridge, V. Bernard, J. Koster, L. Colmet Daage, S.J. Diskin, L. Schild, N.B. Bentahar, A. Bellini, M. Chicard, E. Lapouble, V. Combaret, P. Legoix-Ne, J. Michon, T.J. Pugh, L.S. Hart, J. Rader, E.F. Attiyeh, J.S. Wei, S. Zhang, A. Naranjo, J.M. Gastier-Foster, M.D. Hogarty, S. Asgharzadeh, M.A. Smith, J.M. Guidry Auvil, T.B. Watkins, D.A. Zwijnenburg, M.E. Ebus, P. van Sluis, A. Hakkert, E. van Wezel, C.E. van der Schoot, E.M. Westerhout, J.H. Schulte, G.A. Tytgat, M.E. Dolman, I. Janoueix-Lerosey, D.S. Gerhard, H.N. Caron, O. Delattre, J. Khan, R. Versteeg, G. Schleiermacher, J.J. Molenaar, J.M. Maris. Relapsed neuroblastomas show frequent RAS-MAPK pathway mutations. Nat Genet. 47: 864-871 (2015).

[34] A. Schramm, J. Köster, Y. Assenov, K. Althoff, M. Peifer, E. Mahlow, A. Odersky, D. Beisser, C. Ernst, A.G. Henssen, H. Stephan, C. Schröder, L. Heukamp, A. Engesser, Y. Kahlert, J. Theissen, B. Hero, F. Roels, J. Altmüller, P. Nürnberg, K. Astrahantseff, C. Gloeckner, K. De Preter, C. Plass, S. Lee, H.N. Lode, K.O. Henrich, M. Gartlgruber, F. Speleman, P. Schmezer, F. Westermann, S. Rahmann, M. Fischer, A. Eggert, J.H. Schulte. Mutational dynamics between primary and relapse neuroblastomas. Nat Genet. 47: 872-877 (2015).

[35] R.C. Seeger, G.M. Brodeur, H. Sather, A. Dalton, S.E. Siegel, K.Y. Wong, D. Hammond. Association of multiple copies of the N-myc oncogene with rapid progression of neuroblastomas. N Engl J Med. 313: 1111-1116 (1985).

[36] M. Huang, W.A. Weiss. Neuroblastoma and MYCN. Cold Spring Harb Perspect Med. 3: a014415 (2013).

[37] N. Tanaka, M. Fukuzawa. MYCN downregulates integrin alpha1 to promote invasion of human neuroblastoma cells. Int J Oncol. 33: 815-821 (2008).

[38] C.M. van Golen, M.E. Soules, A.R. Grauman, E.L. Feldman. N-Myc overexpression leads to decreased β1 integrin expression and increased apoptosis in human neuroblastoma cells. Oncogene. 22: 2664-2673 (2003).

[39] N.K. Cheung, J. Zhang, C. Lu, M. Parker, A. Bahrami, S.K. Tickoo, A. Heguy, A.S. Pappo, S. Federico, J. Dalton, I.Y. Cheung, L. Ding, R. Fulton, J. Wang, X. Chen, J. Becksfort, J. Wu, C.A. Billups, D. Ellison, E.R. Mardis, R.K. Wilson, J.R. Downing, M.A. Dyer. Association of age at diagnosis and genetic mutations in patients with neuroblastoma. Jama. 307: 1062-1071 (2012).

[40] J.J. Molenaar, J. Koster, D.A. Zwijnenburg, P. van Sluis, L.J. Valentijn, I. van der Ploeg, M. Hamdi, J. van Nes, B.A. Westerman, J. van Arkel, M.E. Ebus, F. Haneveld, A. Lakeman, L. Schild, P. Molenaar, P. Stroeken, M.M. van Noesel, I. Øra, E.E. Santo, H.N. Caron, E.M. Westerhout, R. Versteeg. Sequencing of neuroblastoma identifies chromothripsis and defects in neuritogenesis genes. Nature. 483: 589-593 (2012).

[41] M. Peifer, F. Hertwig, F. Roels, D. Dreidax, M. Gartlgruber, R. Menon, A. Krämer, J.L. Roncaioli, F. Sand, J.M. Heuckmann, F. Ikram, R. Schmidt, S. Ackermann, A. Engesser, Y. Kahlert, W. Vogel, J. Altmüller, P. Nürnberg, J. Thierry-Mieg, D. Thierry-Mieg, A. Mariappan, S. Heynck, E. Mariotti, K.O. Henrich, C. Gloeckner, G. Bosco, I. Leuschner, M.R. Schweiger, L. Savelyeva, S.C. Watkins, C. Shao, E. Bell, T. Höfer, V. Achter, U. Lang, J. Theissen, R. Volland, M. Saadati, A. Eggert, B. de Wilde, F. Berthold, Z. Peng, C. Zhao, L. Shi, M. Ortmann, R. Büttner, S. Perner, B. Hero, A. Schramm, J.H. Schulte, C. Herrmann, R.J. O'Sullivan, F. Westermann, R.K. Thomas, M. Fischer. Telomerase activation by genomic rearrangements in high-risk neuroblastoma. Nature. 526: 700-704 (2015).

[42] T.J. Pugh, O. Morozova, E.F. Attiyeh, S. Asgharzadeh, J.S. Wei, D. Auclair, S.L. Carter, K. Cibulskis, M. Hanna, A. Kiezun, J. Kim, M.S. Lawrence, L. Lichenstein, A. McKenna, C.S. Pedamallu, A.H. Ramos, E. Shefler, A. Sivachenko, C. Sougnez, C. Stewart, A. Ally, I. Birol, R. Chiu, R.D. Corbett, M. Hirst, S.D. Jackman, B. Kamoh, A.H. Khodabakshi, M. Krzywinski, A. Lo, R.A. Moore, K.L. Mungall, J. Qian, A. Tam, N. Thiessen, Y. Zhao, K.A. Cole, M. Diamond, S.J. Diskin, Y.P. Mosse, A.C. Wood, L. Ji, R. Sposto, T. Badgett, W.B. London, Y. Moyer, J.M. Gastier-Foster, M.A. Smith, J.M. Guidry Auvil, D.S. Gerhard, M.D. Hogarty, S.J. Jones, E.S. Lander, S.B. Gabriel, G. Getz, R.C. Seeger, J. Khan, M.A. Marra, M. Meyerson, J.M. Maris. The genetic landscape of high-risk neuroblastoma. Nat Genet. 45: 279-284 (2013).

[43] L.J. Valentijn, J. Koster, D.A. Zwijnenburg, N.E. Hasselt, P. van Sluis, R. Volckmann, M.M. van Noesel, R.E. George, G.A. Tytgat, J.J. Molenaar, R. Versteeg. TERT rearrangements are frequent in neuroblastoma and identify aggressive tumors. Nat Genet. 47: 1411-1414 (2015).

[44] Y.P. Mosse, M. Laudenslager, L. Longo, K.A. Cole, A. Wood, E.F. Attiyeh, M.J. Laquaglia, R. Sennett, J.E. Lynch, P. Perri, G. Laureys, F. Speleman, C. Kim, C. Hou, H. Hakonarson, A. Torkamani, N.J. Schork, G.M. Brodeur, G.P. Tonini, E. Rappaport, M. Devoto, J.M. Maris. Identification of ALK as a major familial neuroblastoma predisposition gene. Nature. 455: 930-935 (2008).

[45] R.E. George, T. Sanda, M. Hanna, S. Fröhling, W. Luther, 2nd, J. Zhang, Y. Ahn, W. Zhou, W.B. London, P. McGrady, L. Xue, S. Zozulya, V.E. Gregor, T.R. Webb, N.S. Gray, D.G. Gilliland, L. Diller, H. Greulich, S.W. Morris, M. Meyerson, A.T. Look. Activating mutations in ALK provide a therapeutic target in neuroblastoma. Nature. 455: 975-978 (2008).

[46] Y. Chen, J. Takita, Y.L. Choi, M. Kato, M. Ohira, M. Sanada, L. Wang, M. Soda, A. Kikuchi, T. Igarashi, A. Nakagawara, Y. Hayashi, H. Mano, S. Ogawa. Oncogenic mutations of ALK kinase in neuroblastoma. Nature. 455: 971-974 (2008).

[47] I. Janoueix-Lerosey, D. Lequin, L. Brugières, A. Ribeiro, L. de Pontual, V. Combaret, V. Raynal, A. Puisieux, G. Schleiermacher, G. Pierron, D. Valteau-Couanet, T. Frebourg, J. Michon, S. Lyonnet, J. Amiel, O. Delattre. Somatic and germline activating mutations of the ALK kinase receptor in neuroblastoma. Nature. 455: 967-970 (2008).

[48] L.C. Heukamp, T. Thor, A. Schramm, K. De Preter, C. Kumps, B. De Wilde, A. Odersky, M. Peifer, S. Lindner, A. Spruessel, F. Pattyn, P. Mestdagh, B. Menten, S. Kuhfittig-Kulle, A. Künkele, K. König, L. Meder, S. Chatterjee, R.T. Ullrich, S. Schulte, J. Vandesompele, F. Speleman, R. Büttner, A. Eggert, J.H. Schulte. Targeted expression of mutated ALK induces neuroblastoma in transgenic mice. Sci Transl Med. 4: 141ra191 (2012).

[49] H. Carén, F. Abel, P. Kogner, T. Martinsson. High incidence of DNA mutations and gene amplifications of the ALK gene in advanced sporadic neuroblastoma tumours. Biochem J. 416: 153-159 (2008).

[50] S. De Brouwer, K. De Preter, C. Kumps, P. Zabrocki, M. Porcu, E.M. Westerhout, A. Lakeman, J. Vandesompele, J. Hoebeeck, T. Van Maerken, A. De Paepe, G. Laureys, J.H. Schulte, A. Schramm, C. Van Den Broecke, J. Vermeulen, N. Van Roy, K. Beiske, M. Renard, R. Noguera, O. Delattre, I. Janoueix-Lerosey, P. Kogner, T. Martinsson, A. Nakagawara, M. Ohira, H. Caron, A. Eggert, J. Cools, R. Versteeg, F. Speleman. Meta-analysis of neuroblastomas reveals a skewed ALK mutation spectrum in tumors with MYCN amplification. Clin Cancer Res. 16: 4353-4362 (2010).

[51] J.H. Schulte, S. Lindner, A. Bohrer, J. Maurer, K. De Preter, S. Lefever, L. Heukamp, S. Schulte, J. Molenaar, R. Versteeg, T. Thor, A. Künkele, J. Vandesompele, F. Speleman, H. Schorle, A. Eggert, A. Schramm. MYCN and ALKF1174L are sufficient to drive neuroblastoma development from neural crest progenitor cells. Oncogene. 32: 1059-1065 (2013).

[52] G. Schleiermacher, N. Javanmardi, V. Bernard, Q. Leroy, J. Cappo, T. Rio Frio, G. Pierron, E. Lapouble, V. Combaret, F. Speleman, B. de Wilde, A. Djos, I. Ora, F. Hedborg, C. Träger, B.M. Holmqvist, J. Abrahamsson, M. Peuchmaur, J. Michon, I. Janoueix-Lerosey, P. Kogner, O. Delattre, T. Martinsson. Emergence of new ALK mutations at relapse of neuroblastoma. J Clin Oncol. 32: 2727-2734 (2014).

[53] N. Bown, S. Cotterill, M. Łastowska, S. O'Neill, A.D.J. Pearson, D. Plantaz, M. Meddeb, G. Danglot, C. Brinkschmidt, H. Christiansen, G. Laureys, J. Nicholson, A. Bernheim, D.R. Betts, J. Vandesompele, N. Van Roy, F. Speleman. Gain of Chromosome Arm 17q and Adverse Outcome in Patients with Neuroblastoma. N Engl J. 340: 1954-1961 (1999).

[54] E.F. Attiyeh, W.B. London, Y.P. Mossé, Q. Wang, C. Winter, D. Khazi, P.W. McGrady, R.C. Seeger, A.T. Look, H. Shimada, G.M. Brodeur, S.L. Cohn, K.K. Matthay, J.M. Maris. Chromosome 1p and 11q deletions and outcome in neuroblastoma. N Engl J Med. 353: 2243-2253 (2005).

[55] J. Karlsson, A. Valind, L. Holmquist Mengelbier, S. Bredin, L. Cornmark, C. Jansson, A. Wali, J. Staaf, B. Viklund, I. Øra, A. Börjesson, T. Backman, N. Braekeveldt, B. Sandstedt, N. Pal, A. Isaksson, B.G. Lackner, T. Jonson, D. Bexell, D. Gisselsson. Four evolutionary trajectories underlie genetic intratumoral variation in childhood cancer. Nat Genet. 50: 944-950 (2018).

[56] L.H. Mengelbier, J. Karlsson, D. Lindgren, A. Valind, H. Lilljebjörn, C. Jansson, D. Bexell, N. Braekeveldt, A. Ameur, T. Jonson, H.G. Kultima, A. Isaksson, J. Asmundsson, R. Versteeg, M. Rissler, T. Fioretos, B. Sandstedt, A. Börjesson, T. Backman, N. Pal, I. Øra, M. Mayrhofer, D. Gisselsson. Intratumoral genome diversity parallels progression and predicts outcome in pediatric cancer. Nat Commun. 6: 6125 (2015).

[57] V. Boeva, C. Louis-Brennetot, A. Peltier, S. Durand, C. Pierre-Eugène, V. Raynal, H.C. Etchevers, S. Thomas, A. Lermine, E. Daudigeos-Dubus, B. Geoerger, M.F. Orth, T.G.P. Grünewald, E. Diaz, B. Ducos, D. Surdez, A.M. Carcaboso, I. Medvedeva, T. Deller, V. Combaret, E. Lapouble, G. Pierron, S. Grossetête-Lalami, S. Baulande, G. Schleiermacher, E. Barillot, H. Rohrer, O. Delattre, I. Janoueix-Lerosey. Heterogeneity of neuroblastoma cell identity defined by transcriptional circuitries. Nat Genet. 49: 1408-1413 (2017).

[58] T. van Groningen, J. Koster, L.J. Valentijn, D.A. Zwijnenburg, N. Akogul, N.E. Hasselt, M. Broekmans, F. Haneveld, N.E. Nowakowska, J. Bras, C.J.M. van Noesel, A. Jongejan, A.H. van Kampen, L. Koster, F. Baas, L. van Dijk-Kerkhoven, M. Huizer-Smit, M.C. Lecca, A. Chan, A. Lakeman, P. Molenaar, R. Volckmann, E.M. Westerhout, M. Hamdi, P.G. van Sluis, M.E. Ebus, J.J. Molenaar, G.A. Tytgat, B.A. Westerman, J. van Nes, R. Versteeg. Neuroblastoma is composed of two super-enhancer-associated differentiation states. Nat Genet. 49: 1261-1266 (2017).

[59] T. Iwahara, J. Fujimoto, D. Wen, R. Cupples, N. Bucay, T. Arakawa, S. Mori, B. Ratzkin, T. Yamamoto. Molecular characterization of ALK, a receptor tyrosine kinase expressed specifically in the nervous system. Oncogene. 14: 439-449 (1997).

[60] Y. Yarden, A. Ullrich. Growth factor receptor tyrosine kinases. Annu Rev Biochem. 57: 443-478 (1988).

[61] C.C. Lee, Y. Jia, N. Li, X. Sun, K. Ng, E. Ambing, M.Y. Gao, S. Hua, C. Chen, S. Kim, P.Y. Michellys, S.A. Lesley, J.L. Harris, G. Spraggon. Crystal structure of the ALK (anaplastic lymphoma kinase) catalytic domain. Biochem J. 430: 425-437 (2010).

[62] S.W. Morris, C. Naeve, P. Mathew, P.L. James, M.N. Kirstein, X. Cui, D.P. Witte. ALK, the chromosome 2 gene locus altered by the t(2;5) in non-Hodgkin's lymphoma, encodes a novel neural receptor tyrosine kinase that is highly related to leukocyte tyrosine kinase (LTK). Oncogene. 14: 2175-2188 (1997).

[63] R.T. Bossi, M.B. Saccardo, E. Ardini, M. Menichincheri, L. Rusconi, P. Magnaghi, P. Orsini, N. Avanzi, A.L. Borgia, M. Nesi, T. Bandiera, G. Fogliatto, J.A. Bertrand. Crystal Structures of Anaplastic Lymphoma Kinase in Complex with ATP Competitive Inhibitors. Biochemistry. 49: 6813-6825 (2010).

[64] S. Favelyukis, J.H. Till, S.R. Hubbard, W.T. Miller. Structure and autoregulation of the insulin-like growth factor 1 receptor kinase. Nat Struct Biol. 8: 1058-1063 (2001).

[65] J. Zheng, D.R. Knighton, N.H. Xuong, S.S. Taylor, J.M. Sowadski, L.F. Ten Eyck. Crystal structures of the myristylated catalytic subunit of cAMP-dependent protein kinase reveal open and closed conformations. Protein Sci. 2: 1559-1573 (1993).

[66] S.K. Hanks, T. Hunter. Protein kinases 6. The eukaryotic protein kinase superfamily: kinase (catalytic) domain structure and classification. Faseb j. 9: 576-596 (1995).

[67] S.C. Bresler, D.A. Weiser, P.J. Huwe, J.H. Park, K. Krytska, H. Ryles, M. Laudenslager, E.F. Rappaport, A.C. Wood, P.W. McGrady, M.D. Hogarty, W.B. London, R. Radhakrishnan, M.A. Lemmon, Y.P. Mossé. ALK mutations confer differential oncogenic activation and sensitivity to ALK inhibition therapy in neuroblastoma. Cancer Cell. 26: 682-694 (2014).

[68] A.V. Reshetnyak, J. Mohanty, F. Tomé, D.E. Puleo, A.N. Plotnikov, M. Ahmed, N. Kaur, A. Poliakov, A.M. Cinnaiyan, I. Lax, J. Schlessinger. Identification of a biologically active fragment of ALK and LTK-Ligand 2 (augmentor-α). Proc Natl Acad Sci U S A. 115: 8340-8345 (2018).

[69] J. Guan, G. Umapathy, Y. Yamazaki, G. Wolfstetter, P. Mendoza, K. Pfeifer, A. Mohammed, F. Hugosson, H. Zhang, A.W. Hsu, R. Halenbeck, B. Hallberg, R.H. Palmer. FAM150A and FAM150B are activating ligands for anaplastic lymphoma kinase. Elife. 4: e09811 (2015).

[70] G.E. Stoica, A. Kuo, A. Aigner, I. Sunitha, B. Souttou, C. Malerczyk, D.J. Caughey, D. Wen, A. Karavanov, A.T. Riegel, A. Wellstein. Identification of anaplastic lymphoma kinase as a receptor for the growth factor pleiotrophin. J Biol Chem. 276: 16772-16779 (2001).

[71] G.E. Stoica, A. Kuo, C. Powers, E.T. Bowden, E.B. Sale, A.T. Riegel, A. Wellstein. Midkine binds to anaplastic lymphoma kinase (ALK) and acts as a growth factor for different cell types. J Biol Chem. 277: 35990-35998 (2002).

[72] N. Maeda, T. Nishiwaki, T. Shintani, H. Hamanaka, M. Noda. 6B4 proteoglycan/phosphacan, an extracellular variant of receptor-like protein-tyrosine phosphatase zeta/RPTPbeta, binds pleiotrophin/heparin-binding growth-associated molecule (HB-GAM). J Biol Chem. 271: 21446-21452 (1996).

[73] K. Meng, A. Rodríguez-Peña, T. Dimitrov, W. Chen, M. Yamin, M. Noda, T.F. Deuel. Pleiotrophin signals increased tyrosine phosphorylation of beta-catenin through inactivation of the intrinsic catalytic activity of the receptor-type protein tyrosine phosphatase beta/zeta. Proc Natl Acad Sci U S A. 97: 2603-2608 (2000).

[74] H. Muramatsu, K. Zou, N. Sakaguchi, S. Ikematsu, S. Sakuma, T. Muramatsu. LDL receptor-related protein as a component of the midkine receptor. Biochem Biophys Res Commun. 270: 936-941 (2000).

[75] H. Muramatsu, P. Zou, H. Suzuki, Y. Oda, G.Y. Chen, N. Sakaguchi, S. Sakuma, N. Maeda, M. Noda, Y. Takada, T. Muramatsu. alpha4beta1- and alpha6beta1-integrins are functional receptors for midkine, a heparin-binding growth factor. J Cell Sci. 117: 5405-5415 (2004).

[76] T. Nakanishi, K. Kadomatsu, T. Okamoto, K. Ichihara-Tanaka, T. Kojima, H. Saito, Y. Tomoda, T. Muramatsu. Expression of syndecan-1 and -3 during embryogenesis of the central nervous system in relation to binding with midkine. J Biochem. 121: 197-205 (1997).

[77] K. Pulford, L. Lamant, S.W. Morris, L.H. Butler, K.M. Wood, D. Stroud, G. Delsol, D.Y. Mason. Detection of anaplastic lymphoma kinase (ALK) and nucleolar protein nucleophosmin (NPM)-ALK proteins in normal and neoplastic cells with the monoclonal antibody ALK1. Blood. 89: 1394-1404 (1997).

[78] S.W. Morris, M.N. Kirstein, M.B. Valentine, K.G. Dittmer, D.N. Shapiro, D.L. Saltman, A.T. Look. Fusion of a kinase gene, ALK, to a nucleolar protein gene, NPM, in non-Hodgkin's lymphoma. Science. 263: 1281-1284 (1994).

[79] M. Shiota, J. Fujimoto, T. Semba, H. Satoh, T. Yamamoto, S. Mori. Hyperphosphorylation of a novel 80 kDa protein-tyrosine kinase similar to Ltk in a human Ki-1 lymphoma cell line, AMS3. Oncogene. 9: 1567-1574 (1994).

[80] M. Soda, Y.L. Choi, M. Enomoto, S. Takada, Y. Yamashita, S. Ishikawa, S. Fujiwara, H. Watanabe, K. Kurashina, H. Hatanaka, M. Bando, S. Ohno, Y. Ishikawa, H. Aburatani, T. Niki, Y. Sohara, Y.

Sugiyama, H. Mano. Identification of the transforming EML4-ALK fusion gene in non-small-cell lung cancer. Nature. 448: 561-566 (2007).

[81] C.A. Griffin, A.L. Hawkins, C. Dvorak, C. Henkle, T. Ellingham, E.J. Perlman. Recurrent involvement of 2p23 in inflammatory myofibroblastic tumors. Cancer Res. 59: 2776-2780 (1999).

[82] E. Lin, L. Li, Y. Guan, R. Soriano, C.S. Rivers, S. Mohan, A. Pandita, J. Tang, Z. Modrusan. Exon array profiling detects EML4-ALK fusion in breast, colorectal, and non-small cell lung cancers. Mol Cancer Res. 7: 1466-1476 (2009).

[83] B. Hallberg, R.H. Palmer. Mechanistic insight into ALK receptor tyrosine kinase in human cancer biology. Nat Rev Cancer. 13: 685-700 (2013).

[84] P. Mazot, A. Cazes, M.C. Boutterin, A. Figueiredo, V. Raynal, V. Combaret, B. Hallberg, R.H. Palmer, O. Delattre, I. Janoueix-Lerosey, M. Vigny. The constitutive activity of the ALK mutated at positions F1174 or R1275 impairs receptor trafficking. Oncogene. 30: 2017-2025 (2011).

[85] W.J. Fantl, D.E. Johnson, L.T. Williams. Signalling by receptor tyrosine kinases. Annu Rev Biochem. 62: 453-481 (1993).

[86] B. Souttou, N.B. Carvalho, D. Raulais, M. Vigny. Activation of anaplastic lymphoma kinase receptor tyrosine kinase induces neuronal differentiation through the mitogen-activated protein kinase pathway. J Biol Chem. 276: 9526-9531 (2001).

[87] M. Kasprzycka, M. Marzec, X. Liu, Q. Zhang, M.A. Wasik. Nucleophosmin/anaplastic lymphoma kinase (NPM/ALK) oncoprotein induces the T regulatory cell phenotype by activating STAT3. Proc Natl Acad Sci U S A. 103: 9964 (2006).

[88] R. Chiarle, W.J. Simmons, H. Cai, G. Dhall, A. Zamo, R. Raz, J.G. Karras, D.E. Levy, G. Inghirami. Stat3 is required for ALK-mediated lymphomagenesis and provides a possible therapeutic target. Nat Med. 11: 623-629 (2005).

[89] R.Y. Bai, T. Ouyang, C. Miething, S.W. Morris, C. Peschel, J. Duyster. Nucleophosmin-anaplastic lymphoma kinase associated with anaplastic large-cell lymphoma activates the phosphatidylinositol 3-kinase/Akt antiapoptotic signaling pathway. Blood. 96: 4319-4327 (2000).

[90] K.B. Emdal, A.K. Pedersen, D.B. Bekker-Jensen, A. Lundby, S. Claeys, K. De Preter, F. Speleman, C. Francavilla, J.V. Olsen. Integrated proximal proteomics reveals IRS2 as a determinant of cell survival in ALK-driven neuroblastoma. Sci Signal. 11: (2018).

[91] M. Barbacid. ras GENES. Annual Review of Biochemistry. 56: 779-827 (1987).

[92] K. Koera, K. Nakamura, K. Nakao, J. Miyoshi, K. Toyoshima, T. Hatta, H. Otani, A. Aiba, M. Katsuki. K-Ras is essential for the development of the mouse embryo. Oncogene. 15: 1151-1159 (1997).

[93] L.M. Esteban, C. Vicario-Abejón, P. Fernández-Salguero, A. Fernández-Medarde, N. Swaminathan, K. Yienger, E. Lopez, M. Malumbres, R. McKay, J.M. Ward, A. Pellicer, E. Santos. Targeted genomic disruption of H-ras and N-ras, individually or in combination, reveals the dispensability of both loci for mouse growth and development. Mol Cell Biol. 21: 1444-1452 (2001).

[94] K.M. Haigis, K.R. Kendall, Y. Wang, A. Cheung, M.C. Haigis, J.N. Glickman, M. Niwa-Kawakita, A. Sweet-Cordero, J. Sebolt-Leopold, K.M. Shannon, J. Settleman, M. Giovannini, T. Jacks. Differential effects of oncogenic K-Ras and N-Ras on proliferation, differentiation and tumor progression in the colon. Nat Genet. 40: 600-608 (2008).

[95] D. Bar-Sagi. A Ras by Any Other Name. Mol Cell Biol. 21: 1441-1443 (2001).

[96] G.L. Temeles, J.B. Gibbs, J.S. D'Alonzo, I.S. Sigal, E.M. Scolnick. Yeast and mammalian ras proteins have conserved biochemical properties. Nature. 313: 700-703 (1985).

[97] J.B. Gibbs, I.S. Sigal, M. Poe, E.M. Scolnick. Intrinsic GTPase activity distinguishes normal and oncogenic ras p21 molecules. Proc Natl Acad Sci U S A. 81: 5704-5708 (1984).

[98] J.P. McGrath, D.J. Capon, D.V. Goeddel, A.D. Levinson. Comparative biochemical properties of normal and activated human ras p21 protein. Nature. 310: 644-649 (1984).

[99] R.W. Sweet, S. Yokoyama, T. Kamata, J.R. Feramisco, M. Rosenberg, M. Gross. The product of ras is a GTPase and the T24 oncogenic mutant is deficient in this activity. Nature. 311: 273-275 (1984).

[100] P.A. Boriack-Sjodin, S.M. Margarit, D. Bar-Sagi, J. Kuriyan. The structural basis of the activation of Ras by Sos. Nature. 394: 337-343 (1998).

[101] D.K. Simanshu, D.V. Nissley, F. McCormick. RAS Proteins and Their Regulators in Human Disease. Cell. 170: 17-33 (2017).

[102] K. Scheffzek, M.R. Ahmadian, W. Kabsch, L. Wiesmüller, A. Lautwein, F. Schmitz, A. Wittinghofer. The Ras-RasGAP complex: structural basis for GTPase activation and its loss in oncogenic Ras mutants. Science. 277: 333-338 (1997).

[103] M.R. Ahmadian, P. Stege, K. Scheffzek, A. Wittinghofer. Confirmation of the arginine-finger hypothesis for the GAP-stimulated GTP-hydrolysis reaction of Ras. Nature Structural Biology. 4: 686-689 (1997).

[104] S.A. Moodie, B.M. Willumsen, M.J. Weber, A. Wolfman. Complexes of Ras.GTP with Raf-1 and mitogen-activated protein kinase kinase. Science. 260: 1658-1661 (1993).

[105] P.H. Warne, P.R. Viciana, J. Downward. Direct interaction of Ras and the amino-terminal region of Raf-1 in vitro. Nature. 364: 352-355 (1993).

[106] X.-F. Zhang, J. Settleman, J. Kyriakis, E. Takeuchi-Suzuki, S.J. Elledge, M.S. Marshall, J.T. Bruder, U.R. Rapp, J. Avruch. Normal and oncogenic p21ras proteins bind to the amino-terminal regulatory domain of c-Raf-1. Nature. 364: 308-313 (1993).

[107] A.B. Vojtek, S.M. Hollenberg, J.A. Cooper. Mammalian Ras interacts directly with the serine/threonine kinase raf. Cell. 74: 205-214 (1993).

[108] P. Rodriguez-Viciana, P.H. Warne, R. Dhand, B. Vanhaesebroeck, I. Gout, M.J. Fry, M.D. Waterfield, J. Downward. Phosphatidylinositol-3-OH kinase as a direct target of Ras. Nature. 370: 527-532 (1994).

[109] Y. Pylayeva-Gupta, E. Grabocka, D. Bar-Sagi. RAS oncogenes: weaving a tumorigenic web. Nature reviews. Cancer. 11: 761-774 (2011).

[110] K.S. Ravichandran. Signaling via Shc family adapter proteins. Oncogene. 20: 6322-6330 (2001).

[111] S.F. Walk, M.E. March, K.S. Ravichandran. Roles of Lck, Syk and ZAP-70 tyrosine kinases in TCR-mediated phosphorylation of the adapter protein Shc. Eur J Immunol. 28: 2265-2275 (1998).

[112] J. McGlade, A. Cheng, G. Pelicci, P.G. Pelicci, T. Pawson. Shc proteins are phosphorylated and regulated by the v-Src and v-Fps protein-tyrosine kinases. Proc Natl Acad Sci U S A. 89: 8869-8873 (1992).

[113] A. Faisal, S. Kleiner, Y. Nagamine. Non-redundant role of Shc in Erk activation by cytoskeletal reorganization. J Biol Chem. 279: 3202-3211 (2004).

[114] S.E. Egan, B.W. Giddings, M.W. Brooks, L. Buday, A.M. Sizeland, R.A. Weinberg. Association of Sos Ras exchange protein with Grb2 is implicated in tyrosine kinase signal transduction and transformation. Nature. 363: 45-51 (1993).

[115] N. Li, A. Batzer, R. Daly, V. Yajnik, E. Skolnik, P. Chardin, D. Bar-Sagi, B. Margolis, J. Schlessinger. Guanine-nucleotide-releasing factor hSos1 binds to Grb2 and links receptor tyrosine kinases to Ras signalling. Nature. 363: 85-88 (1993).

[116] M. Rozakis-Adcock, R. Fernley, J. Wade, T. Pawson, D. Bowtell. The SH2 and SH3 domains of mammalian Grb2 couple the EGF receptor to the Ras activator mSos1. Nature. 363: 83-85 (1993).

[117] M. Rozakis-Adcock, J. McGlade, G. Mbamalu, G. Pelicci, R. Daly, W. Li, A. Batzer, S. Thomas, J. Brugge, P.G. Pelicci, J. Schlessinger, T. Pawson, et al. Association of the Shc and Grb2/Sem5 SH2-containing proteins is implicated in activation of the Ras pathway by tyrosine kinases. Nature. 360: 689-692 (1992).

[118] A. Aronheim, D. Engelberg, N. Li, N. al-Alawi, J. Schlessinger, M. Karin. Membrane targeting of the nucleotide exchange factor Sos is sufficient for activating the Ras signaling pathway. Cell. 78: 949-961 (1994).

[119] D. Bar-Sagi. The Sos (Son of sevenless) protein. Trends Endocrinol Metab. 5: 165-169 (1994).

[120] K. Hibino, T. Shibata, T. Yanagida, Y. Sako. Activation kinetics of RAF protein in the ternary complex of RAF, RAS-GTP, and kinase on the plasma membrane of living cells: single-molecule imaging analysis. J Biol Chem. 286: 36460-36468 (2011).

[121] P. Dent, W. Haser, T.A. Haystead, L.A. Vincent, T.M. Roberts, T.W. Sturgill. Activation of mitogen-activated protein kinase kinase by v-Raf in NIH 3T3 cells and in vitro. Science. 257: 1404-1407 (1992).

[122] D.K. Morrison. KSR: a MAPK scaffold of the Ras pathway? J Cell Sci. 114: 1609-1612 (2001).

[123] C.M. Crews, A. Alessandrini, R.L. Erikson. The primary structure of MEK, a protein kinase that phosphorylates the ERK gene product. Science. 258: 478-480 (1992).

[124] N. Dhanasekaran, E. Premkumar Reddy. Signaling by dual specificity kinases. Oncogene. 17: 1447-1455 (1998).

[125] A. Loboda, M. Nebozhyn, R. Klinghoffer, J. Frazier, M. Chastain, W. Arthur, B. Roberts, T. Zhang, M. Chenard, B. Haines, J. Andersen, K. Nagashima, C. Paweletz, B. Lynch, I. Feldman, H. Dai, P. Huang, J. Watters. A gene expression signature of RAS pathway dependence predicts response to PI3K and RAS pathway inhibitors and expands the population of RAS pathway activated tumors. BMC Med Genomics. 3: 26 (2010).

[126] J. Van den Eynden, G. Umapathy, A. Ashouri, D. Cervantes-Madrid, J. Szydzik, K. Ruuth, J. Koster, E. Larsson, J. Guan, R.H. Palmer, B. Hallberg. Phosphoproteome and gene expression profiling of ALK inhibition in neuroblastoma cell lines reveals conserved oncogenic pathways. Sci Signal. 11: eaar5680 (2018).

[127] L.M. Mus, I. Lambertz, S. Claeys, C. Kumps, W. Van Loocke, C. Van Neste, G. Umapathy, M. Vaapil, C. Bartenhagen, G. Laureys, O. De Wever, D. Bexell, M. Fischer, B. Hallberg, J. Schulte, B. De Wilde, K. Durinck, G. Denecker, K. De Preter, F. Speleman. The ETS transcription factor ETV5 is a target of activated ALK in neuroblastoma contributing to increased tumour aggressiveness. Sci Rep. 10: 218 (2020).

[128] T.F. Eleveld, L. Schild, J. Koster, D.A. Zwijnenburg, L.K. Alles, M.E. Ebus, R. Volckmann, G.A. Tijtgat, P. van Sluis, R. Versteeg, J.J. Molenaar. RAS-MAPK Pathway-Driven Tumor Progression Is Associated with Loss of CIC and Other Genomic Aberrations in Neuroblastoma. Cancer Res. 78: 6297-6307 (2018).

[129] G. Bollag, D. Clapp, S. Shih, F. Adler, Y. Zhang, P. Thompson, B. Lange, M. Freedman, F. McCormick, T. Jacks, K. Shannon. Loss of NF1 results in activation of the Ras signaling pathway and leads to aberrant growth in haematopoietic cells. Nat Genet. 12: 144-148 (1996).

[130] R. Kalra, D.C. Paderanga, K. Olson, K.M. Shannon. Genetic analysis is consistent with the hypothesis that NF1 limits myeloid cell growth through p21ras. Blood. 84: 3435-3439 (1994).

[131] H.R. Bourne, D.A. Sanders, F. McCormick. The GTPase superfamily: a conserved switch for diverse cell functions. Nature. 348: 125-132 (1990).

[132] G.F. Xu, P. O'Connell, D. Viskochil, R. Cawthon, M. Robertson, M. Culver, D. Dunn, J. Stevens, R. Gesteland, R. White, et al. The neurofibromatosis type 1 gene encodes a protein related to GAP. Cell. 62: 599-608 (1990).

[133] F. Bonneau, E.D. Lenherr, V. Pena, D.J. Hart, K. Scheffzek. Solubility survey of fragments of the neurofibromatosis type 1 protein neurofibromin. Protein Expr Purif. 65: 30-37 (2009).

[134] I. D'Angelo, S. Welti, F. Bonneau, K. Scheffzek. A novel bipartite phospholipid-binding module in the neurofibromatosis type 1 protein. EMBO Rep. 7: 174-179 (2006).

[135] K. Scheffzek, M.R. Ahmadian, L. Wiesmüller, W. Kabsch, P. Stege, F. Schmitz, A. Wittinghofer. Structural analysis of the GAP-related domain from neurofibromin and its implications. Embo j. 17: 4313-4327 (1998).

[136] X. Koliou, C. Fedonidis, T. Kalpachidou, D. Mangoura. Nuclear import mechanism of neurofibromin for localization on the spindle and function in chromosome congression. J Neurochem. 136: 78-91 (2016).

[137] P.E. Gregory, D.H. Gutmann, A. Mitchell, S. Park, M. Boguski, T. Jacks, D.L. Wood, R. Jove, F.S. Collins. Neurofibromatosis type 1 gene product (neurofibromin) associates with microtubules. Somat Cell Mol Genet. 19: 265-274 (1993).

[138] G. Bollag, F. McCormick, R. Clark. Characterization of full-length neurofibromin: tubulin inhibits Ras GAP activity. Embo j. 12: 1923-1927 (1993).

[139] L. Aravind, A.F. Neuwald, C.P. Ponting. Sec14p-like domains in NF1 and Dbl-like proteins indicate lipid regulation of Ras and Rho signaling. Curr Biol. 9: R195-R197 (1999).

[140] M. Golubić, K. Tanaka, S. Dobrowolski, D. Wood, M.H. Tsai, M. Marshall, F. Tamanoi, D.W. Stacey. The GTPase stimulatory activities of the neurofibromatosis type 1 and the yeast IRA2 proteins are inhibited by arachidonic acid. Embo j. 10: 2897-2903 (1991).

[141] G. Bollag, F. McCormick. Differential regulation of rasGAP and neurofibromatosis gene product activities. Nature. 351: 576-579 (1991).

[142] S. Welti, S. Fraterman, I. D'Angelo, M. Wilm, K. Scheffzek. The sec14 homology module of neurofibromin binds cellular glycerophospholipids: mass spectrometry and structure of a lipid complex. J Mol Biol. 366: 551-562 (2007).

[143] I.B. Stowe, E.L. Mercado, T.R. Stowe, E.L. Bell, J.A. Oses-Prieto, H. Hernández, A.L. Burlingame, F. McCormick. A shared molecular mechanism underlies the human rasopathies Legius syndrome and Neurofibromatosis-1. Genes Dev. 26: 1421-1426 (2012).

[144] T. Dunzendorfer-Matt, E.L. Mercado, K. Maly, F. McCormick, K. Scheffzek. The neurofibromin recruitment factor Spred1 binds to the GAP related domain without affecting Ras inactivation. Proc Natl Acad Sci U S A. 113: 7497-7502 (2016).

[145] W. Yan, E. Markegard, S. Dharmaiah, A. Urisman, M. Drew, D. Esposito, K. Scheffzek, D.V. Nissley, F. McCormick, D.K. Simanshu. Structural Insights into the SPRED1-Neurofibromin-KRAS Complex and Disruption of SPRED1-Neurofibromin Interaction by Oncogenic EGFR. Cell Rep. 32: 107909 (2020).

[146] D. Mangoura, Y. Sun, C. Li, D. Singh, D.H. Gutmann, A. Flores, M. Ahmed, G. Vallianatos. Phosphorylation of neurofibromin by PKC is a possible molecular switch in EGF receptor signaling in neural cells. Oncogene. 25: 735-745 (2006).

[147] I. Izawa, N. Tamaki, H. Saya. Phosphorylation of neurofibromatosis type 1 gene product (neurofibromin) by cAMP-dependent protein kinase. FEBS Lett. 382: 53-59 (1996).

[148] L. Feng, S. Yunoue, H. Tokuo, T. Ozawa, D. Zhang, S. Patrakitkomjorn, T. Ichimura, H. Saya, N. Araki. PKA phosphorylation and 14-3-3 interaction regulate the function of neurofibromatosis type I tumor suppressor, neurofibromin. FEBS Letters. 557: 275-282 (2004).

[149] T.V. Bagnyukova, I.G. Serebriiskii, Y. Zhou, E.A. Hopper-Borge, E.A. Golemis, I. Astsaturov. Chemotherapy and signaling: How can targeted therapies supercharge cytotoxic agents? Cancer Biol Ther. 10: 839-853 (2010).

[150] P.L. Bedard, D.M. Hyman, M.S. Davids, L.L. Siu. Small molecules, big impact: 20 years of targeted therapy in oncology. Lancet. 395: 1078-1088 (2020).

[151] J.J. Cui, M. Tran-Dubé, H. Shen, M. Nambu, P.-P. Kung, M. Pairish, L. Jia, J. Meng, L. Funk, I. Botrous, M. McTigue, N. Grodsky, K. Ryan, E. Padrique, G. Alton, S. Timofeevski, S. Yamazaki, Q. Li, H. Zou, J. Christensen, B. Mroczkowski, S. Bender, R.S. Kania, M.P. Edwards. Structure Based Drug Design of Crizotinib (PF-02341066), a Potent and Selective Dual Inhibitor of Mesenchymal–Epithelial Transition Factor (c-MET) Kinase and Anaplastic Lymphoma Kinase (ALK). J Med Chem. 54: 6342-6363 (2011).

[152] L. Friboulet, N. Li, R. Katayama, C.C. Lee, J.F. Gainor, A.S. Crystal, P.-Y. Michellys, M.M. Awad, N. Yanagitani, S. Kim, A.C. Pferdekamper, J. Li, S. Kasibhatla, F. Sun, X. Sun, S. Hua, P. McNamara, S. Mahmood, E.L. Lockerman, N. Fujita, M. Nishio, J.L. Harris, A.T. Shaw, J.A. Engelman. The ALK Inhibitor Ceritinib Overcomes Crizotinib Resistance in Non–Small Cell Lung Cancer. Cancer Discov. 4: 662 (2014).

[153] W.-S. Huang, S. Liu, D. Zou, M. Thomas, Y. Wang, T. Zhou, J. Romero, A. Kohlmann, F. Li, J. Qi, L. Cai, T.A. Dwight, Y. Xu, R. Xu, R. Dodd, A. Toms, L. Parillon, X. Lu, R. Anjum, S. Zhang, F. Wang, J. Keats, S.D. Wardwell, Y. Ning, Q. Xu, L.E. Moran, Q.K. Mohemmad, H.G. Jang, T. Clackson, N.I. Narasimhan, V.M. Rivera, X. Zhu, D. Dalgarno, W.C. Shakespeare. Discovery of Brigatinib

(AP26113), a Phosphine Oxide-Containing, Potent, Orally Active Inhibitor of Anaplastic Lymphoma Kinase. J Med Chem. 59: 4948-4964 (2016).

[154] H. Sakamoto, T. Tsukaguchi, S. Hiroshima, T. Kodama, T. Kobayashi, T.A. Fukami, N. Oikawa, T. Tsukuda, N. Ishii, Y. Aoki. CH5424802, a selective ALK inhibitor capable of blocking the resistant gatekeeper mutant. Cancer Cell. 19: 679-690 (2011).

[155] T.W. Johnson, P.F. Richardson, S. Bailey, A. Brooun, B.J. Burke, M.R. Collins, J.J. Cui, J.G. Deal, Y.-L. Deng, D. Dinh, L.D. Engstrom, M. He, J. Hoffman, R.L. Hoffman, Q. Huang, R.S. Kania, J.C. Kath, H. Lam, J.L. Lam, P.T. Le, L. Lingardo, W. Liu, M. McTigue, C.L. Palmer, N.W. Sach, T. Smeal, G.L. Smith, A.E. Stewart, S. Timofeevski, H. Zhu, J. Zhu, H.Y. Zou, M.P. Edwards. Discovery of (10R)-7-Amino-12-fluoro-2,10,16-trimethyl-15-oxo-10,15,16,17-tetrahydro-2H-8,4-(metheno)pyrazolo[4,3-h][2,5,11]-benzoxadiazacyclotetradecine-3-carbonitrile (PF-06463922), a Macrocyclic Inhibitor of Anaplastic Lymphoma Kinase (ALK) and c-ros Oncogene 1 (ROS1) with Preclinical Brain Exposure and Broad-Spectrum Potency against ALK-Resistant Mutations. J Med Chem. 57: 4720-4744 (2014).

[156] R. Roskoski, Jr. Anaplastic lymphoma kinase (ALK) inhibitors in the treatment of ALK-driven lung cancers. Pharmacol Res. 117: 343-356 (2017).

[157] S.C. Bresler, A.C. Wood, E.A. Haglund, J. Courtright, L.T. Belcastro, J.S. Plegaria, K. Cole, Y. Toporovskaya, H. Zhao, E.L. Carpenter, J.G. Christensen, J.M. Maris, M.A. Lemmon, Y.P. Mossé. Differential inhibitor sensitivity of anaplastic lymphoma kinase variants found in neuroblastoma. Sci Transl Med. 3: 108ra114 (2011).

[158] T. Sasaki, K. Okuda, W. Zheng, J. Butrynski, M. Capelletti, L. Wang, N.S. Gray, K. Wilner, J.G. Christensen, G. Demetri, G.I. Shapiro, S.J. Rodig, M.J. Eck, P.A. Jänne. The neuroblastoma-associated F1174L ALK mutation causes resistance to an ALK kinase inhibitor in ALK-translocated cancers. Cancer Res. 70: 10038-10043 (2010).

[159] J.H. Foster, S.D. Voss, D.C. Hall, C.G. Minard, F.M. Balis, K. Wilner, S.L. Berg, E. Fox, P.C. Adamson, S.M. Blaney, B.J. Weigel, Y.P. Mossé. Activity of Crizotinib in Patients with ALK-Aberrant Relapsed/Refractory Neuroblastoma: A Children's Oncology Group Study (ADVL0912). Clin Cancer Res. 27: 3543-3548 (2021).

[160] Y.P. Mossé, M.S. Lim, S.D. Voss, K. Wilner, K. Ruffner, J. Laliberte, D. Rolland, F.M. Balis, J.M. Maris, B.J. Weigel, A.M. Ingle, C. Ahern, P.C. Adamson, S.M. Blaney. Safety and activity of crizotinib for paediatric patients with refractory solid tumours or anaplastic large-cell lymphoma: a Children's Oncology Group phase 1 consortium study. Lancet Oncol. 14: 472-480 (2013).

[161] M. Fischer, L. Moreno, D.S. Ziegler, L.V. Marshall, C.M. Zwaan, M.S. Irwin, M. Casanova, C. Sabado, B. Wulff, M. Stegert, L. Wang, F.K. Hurtado, F. Branle, B. Geoerger, J.H. Schulte.

Ceritinib in paediatric patients with anaplastic lymphoma kinase-positive malignancies: an open-label, multicentre, phase 1, dose-escalation and dose-expansion study. Lancet Oncol. 22: 1764-1776 (2021).

[162] K.C. Goldsmith, K. Kayser, S.G. Groshen, M. Chioda, H.C. Thurm, J. Chen, G. Peltz, M. Granger, J. Maris, K.K. Matthay, S. Ghazarian, J.R. Park, E. Berko, A. Marachelian, Y.P. Mosse. Phase I trial of lorlatinib in patients with ALK-driven refractory or relapsed neuroblastoma: A New Approaches to Neuroblastoma Consortium study. J Clin Oncol. 38: 10504-10504 (2020).

[163] J. Han, Y. Liu, S. Yang, X. Wu, H. Li, Q. Wang. MEK inhibitors for the treatment of non-small cell lung cancer. J Hematol Oncol. 14: 1 (2021).

[164] P. Wu, T.E. Nielsen, M.H. Clausen. FDA-approved small-molecule kinase inhibitors. Trends Pharmacol Sci. 36: 422-439 (2015).

[165] I. Lugowska, H. Koseła-Paterczyk, K. Kozak, P. Rutkowski. Trametinib: a MEK inhibitor for management of metastatic melanoma. Onco Targets Ther. 8: 2251-2259 (2015).

[166] Q. Dong, D.R. Dougan, X. Gong, P. Halkowycz, B. Jin, T. Kanouni, S.M. O'Connell, N. Scorah, L. Shi, M.B. Wallace, F. Zhou. Discovery of TAK-733, a potent and selective MEK allosteric site inhibitor for the treatment of cancer. Bioorg Med Chem Lett. 21: 1315-1319 (2011).

[167] H. Abe, S. Kikuchi, K. Hayakawa, T. Iida, N. Nagahashi, K. Maeda, J. Sakamoto, N. Matsumoto, T. Miura, K. Matsumura, N. Seki, T. Inaba, H. Kawasaki, T. Yamaguchi, R. Kakefuda, T. Nanayama, H. Kurachi, Y. Hori, T. Yoshida, J. Kakegawa, Y. Watanabe, A.G. Gilmartin, M.C. Richter, K.G. Moss, S.G. Laquerre. Discovery of a Highly Potent and Selective MEK Inhibitor: GSK1120212 (JTP-74057 DMSO Solvate). ACS Med Chem Lett. 2: 320-324 (2011).

[168] R. Fritsche-Guenther, F. Witzel, A. Sieber, R. Herr, N. Schmidt, S. Braun, T. Brummer, C. Sers, N. Blüthgen. Strong negative feedback from Erk to Raf confers robustness to MAPK signalling. Mol Syst Biol. 7: 489 (2011).

[169] R. Fritsche-Guenther, F. Witzel, S. Kempa, T. Brummer, C. Sers, N. Blüthgen. Effects of RAF inhibitors on PI3K/AKT signalling depend on mutational status of the RAS/RAF signalling axis. Oncotarget. 7: 7960-7969 (2016).

[170] B.B. Friday, C. Yu, G.K. Dy, P.D. Smith, L. Wang, S.N. Thibodeau, A.A. Adjei. BRAF V600E disrupts AZD6244-induced abrogation of negative feedback pathways between extracellular signal-regulated kinase and Raf proteins. Cancer Res. 68: 6145-6153 (2008).

[171] G. Umapathy, J. Guan, D.E. Gustafsson, N. Javanmardi, D. Cervantes-Madrid, A. Djos, T. Martinsson, R.H. Palmer, B. Hallberg. MEK inhibitor trametinib does not prevent the growth of anaplastic lymphoma kinase (ALK)-addicted neuroblastomas. Sci Signal. 10: eaam7550 (2017).

[172] R. Pisa, T.M. Kapoor. Chemical strategies to overcome resistance against targeted anticancer therapeutics. Nat Chem Biol. 16: 817-825 (2020).

[173] L.M. Ellis, D.J. Hicklin. Resistance to Targeted Therapies: Refining Anticancer Therapy in the Era of Molecular Oncology. Clin Cancer Res. 15: 7471 (2009).

[174] D.S. Neel, T.G. Bivona. Resistance is futile: overcoming resistance to targeted therapies in lung adenocarcinoma. npj Precision Onc. 1: 3 (2017).

[175] R.C. Doebele, A.B. Pilling, D.L. Aisner, T.G. Kutateladze, A.T. Le, A.J. Weickhardt, K.L. Kondo, D.J. Linderman, L.E. Heasley, W.A. Franklin, M. Varella-Garcia, D.R. Camidge. Mechanisms of resistance to crizotinib in patients with ALK gene rearranged non-small cell lung cancer. Clin Cancer Res. 18: 1472-1482 (2012).

[176] E. Pailler, V. Faugeroux, M. Oulhen, L. Mezquita, M. Laporte, A. Honoré, Y. Lecluse, P. Queffelec, M. NgoCamus, C. Nicotra, J. Remon, L. Lacroix, D. Planchard, L. Friboulet, B. Besse, F. Farace. Acquired Resistance Mutations to ALK Inhibitors Identified by Single Circulating Tumor Cell Sequencing in ALK-Rearranged Non–Small-Cell Lung Cancer. Clin Cancer Res. 25: 6671-6682 (2019).

[177] F.H. Groenendijk, R. Bernards. Drug resistance to targeted therapies: déjà vu all over again. Mol Oncol. 8: 1067-1083 (2014).

[178] M.R. Yun, S.M. Lim, S.-K. Kim, H.M. Choi, K.-H. Pyo, S.K. Kim, J.M. Lee, Y.W. Lee, J.W. Choi, H.R. Kim, M.H. Hong, K. Haam, N. Huh, J.-H. Kim, Y.S. Kim, H.S. Shim, R.A. Soo, J.-Y. Shih, J.C.-H. Yang, M. Kim, B.C. Cho. Enhancer Remodeling and MicroRNA Alterations Are Associated with Acquired Resistance to ALK Inhibitors. Cancer Res. 78: 3350-3362 (2018).

[179] R. Katayama, A.T. Shaw, T.M. Khan, M. Mino-Kenudson, B.J. Solomon, B. Halmos, N.A. Jessop, J.C. Wain, A.T. Yeo, C. Benes, L. Drew, J.C. Saeh, K. Crosby, L.V. Sequist, A.J. Iafrate, J.A. Engelman. Mechanisms of Acquired Crizotinib Resistance in ALK-Rearranged Lung Cancers. Sci Transl Med. 4: 120ra117 (2012).

[180] G. Recondo, L. Mezquita, F. Facchinetti, D. Planchard, A. Gazzah, L. Bigot, A.Z. Rizvi, R.L. Frias, J.P. Thiery, J.-Y. Scoazec, T. Sourisseau, K. Howarth, O. Deas, D. Samofalova, J. Galissant, P. Tesson, F. Braye, C. Naltet, P. Lavaud, L. Mahjoubi, A. Abou Lovergne, G. Vassal, R. Bahleda, A. Hollebecque, C. Nicotra, M. Ngo-Camus, S. Michiels, L. Lacroix, C. Richon, N. Auger, T. De Baere, L. Tselikas, E. Solary, E. Angevin, A.M. Eggermont, F. Andre, C. Massard, K.A. Olaussen, J.-C. Soria, B. Besse, L. Friboulet. Diverse Resistance Mechanisms to the Third-Generation ALK Inhibitor Lorlatinib in ALK-Rearranged Lung Cancer. Clin Cancer Res. 26: 242-255 (2020).

[181] D.N. Debruyne, N. Bhatnagar, B. Sharma, W. Luther, N.F. Moore, N.K. Cheung, N.S. Gray, R.E. George. ALK inhibitor resistance in ALK(F1174L)-driven neuroblastoma is associated with AXL activation and induction of EMT. Oncogene. 35: 3681-3691 (2016).

[182] A. Gower, W.H. Hsu, S.T. Hsu, Y. Wang, G. Giaccone. EMT is associated with, but does not drive resistance to ALK inhibitors among EML4-ALK non-small cell lung cancer. Mol Oncol. 10: 601-609 (2016).

[183] S. Lamouille, J. Xu, R. Derynck. Molecular mechanisms of epithelial-mesenchymal transition. Nat Rev Mol Cell Biol. 15: 178-196 (2014).

[184] S.M. Stefan, M. Wiese. Small-molecule inhibitors of multidrug resistance-associated protein 1 and related processes: A historic approach and recent advances. Med Res Rev. 39: 176-264 (2019).

[185] R. Straussman, T. Morikawa, K. Shee, M. Barzily-Rokni, Z.R. Qian, J. Du, A. Davis, M.M. Mongare, J. Gould, D.T. Frederick, Z.A. Cooper, P.B. Chapman, D.B. Solit, A. Ribas, R.S. Lo, K.T. Flaherty, S. Ogino, J.A. Wargo, T.R. Golub. Tumour micro-environment elicits innate resistance to RAF inhibitors through HGF secretion. Nature. 487: 500-504 (2012).

[186] C. Nowell Peter. The Clonal Evolution of Tumor Cell Populations. Science. 194: 23-28 (1976).

[187] S.W. Brady, J.A. McQuerry, Y. Qiao, S.R. Piccolo, G. Shrestha, D.F. Jenkins, R.M. Layer, B.S. Pedersen, R.H. Miller, A. Esch, S.R. Selitsky, J.S. Parker, L.A. Anderson, B.K. Dalley, R.E. Factor, C.B. Reddy, J.P. Boltax, D.Y. Li, P.J. Moos, J.W. Gray, L.M. Heiser, S.S. Buys, A.L. Cohen, W.E. Johnson, A.R. Quinlan, G. Marth, T.L. Werner, A.H. Bild. Combating subclonal evolution of resistant cancer phenotypes. Nat Commun. 8: 1231 (2017).

[188] M. Greaves, C.C. Maley. Clonal evolution in cancer. Nature. 481: 306-313 (2012).

[189] M.R. Stratton. Exploring the genomes of cancer cells: progress and promise. Science. 331: 1553-1558 (2011).

[190] I. Bozic, T. Antal, H. Ohtsuki, H. Carter, D. Kim, S. Chen, R. Karchin, K.W. Kinzler, B. Vogelstein, M.A. Nowak. Accumulation of driver and passenger mutations during tumor progression. Proc Natl Acad Sci U S A. 107: 18545-18550 (2010).

[191] J.R. Park, R. Bagatell, S.L. Cohn, A.D. Pearson, J.G. Villablanca, F. Berthold, S. Burchill, A. Boubaker, K. McHugh, J.G. Nuchtern, W.B. London, N.L. Seibel, O.W. Lindwasser, J.M. Maris, P. Brock, G. Schleiermacher, R. Ladenstein, K.K. Matthay, D. Valteau-Couanet. Revisions to the International Neuroblastoma Response Criteria: A Consensus Statement From the National Cancer Institute Clinical Trials Planning Meeting. J Clin Oncol. 35: 2580-2587 (2017).

[192] E.A. Eisenhauer, P. Therasse, J. Bogaerts, L.H. Schwartz, D. Sargent, R. Ford, J. Dancey, S. Arbuck, S. Gwyther, M. Mooney, L. Rubinstein, L. Shankar, L. Dodd, R. Kaplan, D. Lacombe, J. Verweij. New response evaluation criteria in solid tumours: revised RECIST guideline (version 1.1). Eur J Cancer. 45: 228-247 (2009).

[193] N.A. Franken, H.M. Rodermond, J. Stap, J. Haveman, C. van Bree. Clonogenic assay of cells in vitro. Nat Protoc. 1: 2315-2319 (2006).

[194] M. McDermott, A. Eustace, S. Busschots, L. Breen, M. Clynes, N. O'Donovan, B. Stordal. In vitro Development of Chemotherapy and Targeted Therapy Drug-Resistant Cancer Cell Lines: A Practical Guide with Case Studies. Front Oncol. 4: 40 (2014).

[195] E.A. Brooks, S. Galarza, M.F. Gencoglu, R.C. Cornelison, J.M. Munson, S.R. Peyton. Applicability of drug response metrics for cancer studies using biomaterials. Philos Trans R Soc Lond B Biol Sci. 374: 20180226 (2019).

[196] B. Beck, Y.-F. Chen, W. Dere, V. Devanarayan, B.J. Eastwood, M.W. Farmen, S.J. Iturria, P.W. Iversen, S.D. Kahl, Roger A. Moore, Barry D. Sawyer, J. Weidner. Assay Operations for SAR Support (2017). https://www.ncbi.nlm.nih.gov/books/NBK91994/pdf/Bookshelf_NBK91994.pdf (last access 23 Oct 2021).

[197] H. Kuroda, T. Sugimoto, K. Ueda, S. Tsuchida, Y. Horii, J. Inazawa, K. Sato, T. Sawada. Different drug sensitivity in two neuroblastoma cell lines established from the same patient before and after chemotherapy. Int J Cancer. 47: 732-737 (1991).

[198] S.-Y. Kim, J.Y. Lee, D.H. Kim, H.S. Joo, M.R. Yun, D. Jung, J. Yun, S.G. Heo, B.C. Ahn, C.W. Park, K.H. Pyo, Y.J. Chun, M.H. Hong, H.R. Kim, B.C. Cho. Patient-Derived Cells to Guide Targeted Therapy for Advanced Lung Adenocarcinoma. Sci Rep. 9: 19909 (2019).

[199] M. Fallahi-Sichani, S. Honarnejad, L.M. Heiser, J.W. Gray, P.K. Sorger. Metrics other than potency reveal systematic variation in responses to cancer drugs. Nat Chem Biol. 9: 708-714 (2013).

[200] Y. Zhao, Y. Yang, Y. Xu, S. Lu, H. Jian. AZD0530 sensitizes drug-resistant ALK-positive lung cancer cells by inhibiting SRC signaling. FEBS Open Bio. 7: 472-476 (2017).

[201] G. Hrustanovic, V. Olivas, E. Pazarentzos, A. Tulpule, S. Asthana, C.M. Blakely, R.A. Okimoto, L. Lin, D.S. Neel, A. Sabnis, J. Flanagan, E. Chan, M. Varella-Garcia, D.L. Aisner, A. Vaishnavi, S.H. Ou, E.A. Collisson, E. Ichihara, P.C. Mack, C.M. Lovly, N. Karachaliou, R. Rosell, J.W. Riess, R.C. Doebele, T.G. Bivona. RAS-MAPK dependence underlies a rational polytherapy strategy in EML4-ALK-positive lung cancer. Nat Med. 21: 1038-1047 (2015).

[202] T. Yamada, S. Takeuchi, J. Nakade, K. Kita, T. Nakagawa, S. Nanjo, T. Nakamura, K. Matsumoto, M. Soda, H. Mano, T. Uenaka, S. Yano. Paracrine receptor activation by microenvironment triggers bypass survival signals and ALK inhibitor resistance in EML4-ALK lung cancer cells. Clin Cancer Res. 18: 3592-3602 (2012).

[203] D.N. Debruyne, R. Dries, S. Sengupta, D. Seruggia, Y. Gao, B. Sharma, H. Huang, L. Moreau, M. McLane, D.S. Day, E. Marco, T. Chen, N.S. Gray, K.K. Wong, S.H. Orkin, G.C. Yuan, R.A. Young, R.E. George. BORIS promotes chromatin regulatory interactions in treatment-resistant cancer cells. Nature. 572: 676-680 (2019).

[204] R.M. Trigg, L.C. Lee, N. Prokoph, L. Jahangiri, C.P. Reynolds, G.A. Amos Burke, N.A. Probst, M. Han, J.D. Matthews, H.K. Lim, E. Manners, S. Martinez, J. Pastor, C. Blanco-Aparicio, O. Merkel, I.G. de Los Fayos Alonso, P. Kodajova, S. Tangermann, S. Hogler, J. Luo, L. Kenner, S.D. Turner. The targetable kinase PIM1 drives ALK inhibitor resistance in high-risk neuroblastoma independent of MYCN status. Nat Commun. 10: 5428 (2019).

[205] W. Szybalski, V. Bryson. Genetic studies on microbial cross resistance to toxic agents. I. Cross resistance of Escherichia coli to fifteen antibiotics. J Bacteriol. 64: 489-499 (1952).

[206] D.J. Hutchison. Cross resistance and collateral sensitivity studies in cancer chemotherapy. Adv Cancer Res. 7: 235-250 (1963).

[207] B. Zhao, J.C. Sedlak, R. Srinivas, P. Creixell, J.R. Pritchard, B. Tidor, D.A. Lauffenburger, M.T. Hemann. Exploiting Temporal Collateral Sensitivity in Tumor Clonal Evolution. Cell. 165: 234-246 (2016).

[208] J.H. Schulte, L. Moreno, D.S. Ziegler, L.V. Marshall, C.M. Zwaan, M. Irwin, M. Casanova, C. Sabado, B. Wulff, M. Stegert, L. Wang, F.K. Hurtado, F. Branle, M. Fischer, B. Geoerger. Final analysis of phase I study of ceritinib in pediatric patients with malignancies harboring activated anaplastic lymphoma kinase (ALK). J Clin Oncol. 38: 10505 (2020).

[209] J.G. Doench, N. Fusi, M. Sullender, M. Hegde, E.W. Vaimberg, K.F. Donovan, I. Smith, Z. Tothova, C. Wilen, R. Orchard, H.W. Virgin, J. Listgarten, D.E. Root. Optimized sgRNA design to maximize activity and minimize off-target effects of CRISPR-Cas9. Nat Biotechnol. 34: 184-191 (2016).

[210] S. Chen, N.E. Sanjana, K. Zheng, O. Shalem, K. Lee, X. Shi, D.A. Scott, J. Song, J.Q. Pan, R. Weissleder, H. Lee, F. Zhang, P.A. Sharp. Genome-wide CRISPR screen in a mouse model of tumor growth and metastasis. Cell. 160: 1246-1260 (2015).

[211] T. Dull, R. Zufferey, M. Kelly, R.J. Mandel, M. Nguyen, D. Trono, L. Naldini. A third-generation lentivirus vector with a conditional packaging system. J Virol. 72: 8463-8471 (1998).

[212] F.A. Ran, P.D. Hsu, J. Wright, V. Agarwala, D.A. Scott, F. Zhang. Genome engineering using the CRISPR-Cas9 system. Nat Protoc. 8: 2281-2308 (2013).

[213] P.N. Preis, H. Saya, L. Nádasdi, G. Hochhaus, V. Levin, W. Sadée. Neuronal cell differentiation of human neuroblastoma cells by retinoic acid plus herbimycin A. Cancer Res. 48: 6530-6534 (1988).

[214] R.C. Seeger, Y.L. Danon, S.A. Rayner, F. Hoover. Definition of a Thy-1 determinant on human neuroblastoma, glioma, sarcoma, and teratoma cells with a monoclonal antibody. J Immunol. 128: 983-989 (1982).

[215] J.L. Biedler, L. Helson, B.A. Spengler. Morphology and growth, tumorigenicity, and cytogenetics of human neuroblastoma cells in continuous culture. Cancer Res. 33: 2643-2652 (1973).

[216] F. Madeira, Y.M. Park, J. Lee, N. Buso, T. Gur, N. Madhusoodanan, P. Basutkar, A.R.N. Tivey, S.C. Potter, R.D. Finn, R. Lopez. The EMBL-EBI search and sequence analysis tools APIs in 2019. Nucleic Acids Res. 47: W636-W641 (2019).

[217] A. Subramanian, P. Tamayo, V.K. Mootha, S. Mukherjee, B.L. Ebert, M.A. Gillette, A. Paulovich, S.L. Pomeroy, T.R. Golub, E.S. Lander, J.P. Mesirov. Gene set enrichment analysis: A knowledge-based approach for interpreting genome-wide expression profiles. Proc Natl Acad Sci U S A. 102: 15545 (2005).

[218] V.K. Mootha, C.M. Lindgren, K.-F. Eriksson, A. Subramanian, S. Sihag, J. Lehar, P. Puigserver, E. Carlsson, M. Ridderstråle, E. Laurila, N. Houstis, M.J. Daly, N. Patterson, J.P. Mesirov, T.R. Golub, P. Tamayo, B. Spiegelman, E.S. Lander, J.N. Hirschhorn, D. Altshuler, L.C. Groop. PGC-1α-responsive genes involved in oxidative phosphorylation are coordinately downregulated in human diabetes. Nat Genet. 34: 267-273 (2003).

[219] J.T. Robinson, H. Thorvaldsdóttir, W. Winckler, M. Guttman, E.S. Lander, G. Getz, J.P. Mesirov. Integrative genomics viewer. Nat Biotechnol. 29: 24-26 (2011).

[220] H. Mi, A. Muruganujan, X. Huang, D. Ebert, C. Mills, X. Guo, P.D. Thomas. Protocol Update for large-scale genome and gene function analysis with the PANTHER classification system (v.14.0). Nat Protoc. 14: 703-721 (2019).

[221] MACHEREY-NAGEL. Endotoxin-free plasmid DNA purification- user manual. (2021).

[222] Agilent Technologies. Agilent High Sensitivity D1000 ScreenTape Assay Quick Guide for 4200 TapeStation System. (2017).

[223] Invitrogen. Qubit™ dsDNA BR Assay Kit- user guide. (2022).

[224] A. Schroeder, O. Mueller, S. Stocker, R. Salowsky, M. Leiber, M. Gassmann, S. Lightfoot, W. Menzel, M. Granzow, T. Ragg. The RIN: an RNA integrity number for assigning integrity values to RNA measurements. BMC Molecular Biology. 7: 3 (2006).

[225] Y. Nakayama, H. Yamaguchi, N. Einaga, M. Esumi. Pitfalls of DNA Quantification Using DNA-Binding Fluorescent Dyes and Suggested Solutions. PLoS One. 11: e0150528 (2016).

[226] Agilent Technologies. Performance Characteristics of the Genomic DNA ScreenTape Assay for the 4150 TapeStation System (2019). https://www.agilent.com/cs/library/technicaloverviews/public/technicaloverview-gdna-4150-tapestation-5994-0497en-agilent.pdf (last access 23 Mar 2022).

[227] T. Takaya, C. Su, K.d.L. Harpe, C.E. Crespo-Hernández, B. Kohler. UV excitation of single DNA and RNA strands produces high yields of exciplex states between two stacked bases. Proc Natl Acad Sci U S A. 105: 10285-10290 (2008).

[228] C.E. Crespo-Hernández, B. Cohen, P.M. Hare, B. Kohler. Ultrafast excited-state dynamics in nucleic acids. Chem Rev. 104: 1977-2019 (2004).

[229] B. Commoner, D. Lipkin. The Application of the Beer-Lambert Law to Optically Anisotropic Systems. Science. 110: 41-43 (1949).

[230] D.F. Swinehart. The Beer-Lambert Law. J. Chem. Educ. 39: 333 (1962).

[231] W.W. Wilfinger, K. Mackey, P. Chomczynski. Effect of pH and ionic strength on the spectrophotometric assessment of nucleic acid purity. Biotechniques. 22: 474-481 (1997).

[232] MACHEREY-NAGEL. PCR clean-up and Gel extraction- user manual. (2021).

[233] Beckman Coulter. Instructions for use Agencourt AMPure XP PCR Purification. (2016).

[234] W. Li, J. Koster, H. Xu, C.H. Chen, T. Xiao, J.S. Liu, M. Brown, X.S. Liu. Quality control, modeling, and visualization of CRISPR screens with MAGeCK-VISPR. Genome Biol. 16: 281 (2015).

[235] W. Strober. Trypan blue exclusion test of cell viability. Curr Protoc Immunol. 111: A3.B.1-A3.B.3 (1997).

[236] Clontech Laboratories. CalPhos™ Mammalian Transfection Kit User Manual. (2013).

[237] M. Feoktistova, P. Geserick, M. Leverkus. Crystal Violet Assay for Determining Viability of Cultured Cells. Cold Spring Harb Protoc. 2016: pdb.prot087379 (2016).

[238] ZYMO RESEARCH. Quick-DNA™ Midiprep Plus Kit (2021). https://files.zymoresearch.com/protocols/_d4075_quick-dna_midiprep_plus_kit.pdf (last access 21 Nov 2021).

[239] Invitrogen. Lipofectamine® LTX & PLUS™ Reagent. (2013).

[240] MACHEREY-NAGEL. Genomic DNA from tissue-NucleoSpin® Tissue. (2021).

[241] R.D. Mashal, J. Koontz, J. Sklar. Detection of mutations by cleavage of DNA heteroduplexes with bacteriophage resolvases. Nat Genet. 9: 177-183 (1995).

[242] Thermo Fisher Scientific. Pierce™ BCA Protein Assay Kit. (2020).

[243] S.P. Crouch, R. Kozlowski, K.J. Slater, J. Fletcher. The use of ATP bioluminescence as a measure of cell proliferation and cytotoxicity. J Immunol Methods. 160: 81-88 (1993).

[244] Promega Corporation. CellTiter-Glo® Luminescent Cell Viability Assay. (2015).

[245] T.C. Chou. Theoretical basis, experimental design, and computerized simulation of synergism and antagonism in drug combination studies. Pharmacol Rev. 58: 621-681 (2006).

[246] A. DeLean, P.J. Munson, D. Rodbard. Simultaneous analysis of families of sigmoidal curves: application to bioassay, radioligand assay, and physiological dose-response curves. Am J Physiol. 235: E97-E102 (1978).

[247] G.Y. Di Veroli, C. Fornari, I. Goldlust, G. Mills, S.B. Koh, J.L. Bramhall, F.M. Richards, D.I. Jodrell. An automated fitting procedure and software for dose-response curves with multiphasic features. Sci Rep. 5: 14701 (2015).

[248] J.L. Sebaugh. Guidelines for accurate EC50/IC50 estimation. Pharm Stat. 10: 128-134 (2011).

[249] H.J. Motulsky, R.E. Brown. Detecting outliers when fitting data with nonlinear regression – a new method based on robust nonlinear regression and the false discovery rate. BMC Bioinformatics. 7: 123 (2006).

[250] Invitrogen. TRIzol™ Reagent- user guide. (2020).

[251] Agilent Technologies. Agilent RNA ScreenTape Assay Quick Guide for 4200 TapeStation System. (2015).

[252] A. Dobin, C.A. Davis, F. Schlesinger, J. Drenkow, C. Zaleski, S. Jha, P. Batut, M. Chaisson, T.R. Gingeras. STAR: ultrafast universal RNA-seq aligner. Bioinformatics. 29: 15-21 (2013).

[253] Y. Liao, G.K. Smyth, W. Shi. featureCounts: an efficient general purpose program for assigning sequence reads to genomic features. Bioinformatics. 30: 923-930 (2014).

[254] M.I. Love, W. Huber, S. Anders. Moderated estimation of fold change and dispersion for RNA-seq data with DESeq2. Genome Biol. 15: 550 (2014).

[255] P. Ewels, M. Magnusson, S. Lundin, M. Käller. MultiQC: summarize analysis results for multiple tools and samples in a single report. Bioinformatics. 32: 3047-3048 (2016).

[256] H. Wickham (ed.). ggplot2: Elegant Graphics for Data Analysis. Springer, New York, 2nd ed. (2016).

[257] Bio-Rad Laboratories. Bio-Plex Pro™ Cell Signaling Assays Instruction Manual. (2013).

[258] B. Klinger, A. Sieber, R. Fritsche-Guenther, F. Witzel, L. Berry, D. Schumacher, Y. Yan, P. Durek, M. Merchant, R. Schäfer, C. Sers, N. Blüthgen. Network quantification of EGFR signaling unveils potential for targeted combination therapy. Mol Syst Biol. 9: 673-673 (2013).

[259] M. Dorel, B. Klinger, A. Sieber, A. Prahallad, T. Gross, E. Bosdriesz, L. Wessels, N. Blüthgen. Modelling signalling networks from perturbation data. Bioinformatics. 34: 4079–4086 (2018).

[260] M. Wegner, V. Diehl, V. Bittl, R. de Bruyn, S. Wiechmann, Y. Matthess, M. Hebel, M.G.B. Hayes, S. Schaubeck, C. Benner, S. Heinz, A. Bremm, I. Dikic, A. Ernst, M. Kaulich. Circular synthesized CRISPR/Cas gRNAs for functional interrogations in the coding and noncoding genome. Elife. 8: e42549 (2019).

[261] M. Wegner, K. Husnjak, M. Kaulich. Unbiased and Tailored CRISPR/Cas gRNA Libraries by SynthesizingCovalently-closed-circular (3Cs) DNA. Bio Protoc. 10: e3472 (2020).

[262] V. Diehl, M. Wegner, P. Grumati, K. Husnjak, S. Schaubeck, A. Gubas, Varun J. Shah, Ibrahim H. Polat, F. Langschied, C. Prieto-Garcia, K. Müller, A. Kalousi, I. Ebersberger, Christian H. Brandts, I. Dikic, M. Kaulich. Minimized combinatorial CRISPR screens identify genetic interactions in autophagy. Nucleic Acids Res. 49: 5684-5704 (2021).

[263] C.D. Chung, J. Liao, B. Liu, X. Rao, P. Jay, P. Berta, K. Shuai. Specific inhibition of Stat3 signal transduction by PIAS3. Science. 278: 1803-1805 (1997).

[264] Y. Ogata, T. Osaki, T. Naka, K. Iwahori, M. Furukawa, I. Nagatomo, T. Kijima, T. Kumagai, M. Yoshida, I. Tachibana, I. Kawase. Overexpression of PIAS3 suppresses cell growth and restores the drug sensitivity of human lung cancer cells in association with PI3-K/Akt inactivation. Neoplasia. 8: 817-825 (2006).

[265] U. Saini, A.A. Suarez, S. Naidu, J.J. Wallbillich, K. Bixel, R.A. Wanner, J. Bice, R.D. Kladney, J. Lester, B.Y. Karlan, P.J. Goodfellow, D.E. Cohn, K. Selvendiran. STAT3/PIAS3 Levels Serve as "Early Signature" Genes in the Development of High-Grade Serous Carcinoma from the Fallopian Tube. Cancer Res. 78: 1739-1750 (2018).

[266] T. Takeya, H. Hanafusa. Structure and sequence of the cellular gene homologous to the RSV src gene and the mechanism for generating the transforming virus. Cell. 32: 881-890 (1983).

[267] W.P. Carney, D. Petit, P. Hamer, C.J. Der, T. Finkel, G.M. Cooper, M. Lefebvre, H. Mobtaker, R. Delellis, A.S. Tischler, et al. Monoclonal antibody specific for an activated RAS protein. Proc Natl Acad Sci U S A. 83: 7485-7489 (1986).

[268] N.M. Levinson, M.A. Seeliger, P.A. Cole, J. Kuriyan. Structural basis for the recognition of c-Src by its inactivator Csk. Cell. 134: 124-134 (2008).

[269] C. Thornton, K.C. Tang, K. Phamluong, K. Luong, A. Vagts, D. Nikanjam, R. Yaka, D. Ron. Spatial and temporal regulation of RACK1 function and N-methyl-D-aspartate receptor activity through WD40 motif-mediated dimerization. J Biol Chem. 279: 31357-31364 (2004).

[270] V. Mamidipudi, B.Y. Chang, R.A. Harte, K.C. Lee, C.A. Cartwright. RACK1 inhibits the serum- and anchorage-independent growth of v-Src transformed cells. FEBS Lett. 567: 321-326 (2004).

[271] V. Mamidipudi, N.K. Dhillon, T. Parman, L.D. Miller, K.C. Lee, C.A. Cartwright. RACK1 inhibits colonic cell growth by regulating Src activity at cell cycle checkpoints. Oncogene. 26: 2914-2924 (2007).

[272] J.A. Cooper, K.L. Gould, C.A. Cartwright, T. Hunter. Tyr527 is phosphorylated in pp60c-src: implications for regulation. Science. 231: 1431-1434 (1986).

[273] L.K. Sharma, J. Lu, Y. Bai. Mitochondrial respiratory complex I: structure, function and implication in human diseases. Curr Med Chem. 16: 1266-1277 (2009).

[274] M. Holzel, S. Huang, J. Koster, I. Ora, A. Lakeman, H. Caron, W. Nijkamp, J. Xie, T. Callens, S. Asgharzadeh, R.C. Seeger, L. Messiaen, R. Versteeg, R. Bernards. NF1 is a tumor suppressor in neuroblastoma that determines retinoic acid response and disease outcome. Cell. 142: 218-229 (2010).

[275] E.C. de Bruin, C. Cowell, P.H. Warne, M. Jiang, R.E. Saunders, M.A. Melnick, S. Gettinger, Z. Walther, A. Wurtz, G.J. Heynen, D.A. Heideman, J. Gómez-Román, A. García-Castaño, Y. Gong, M. Ladanyi, H. Varmus, R. Bernards, E.F. Smit, K. Politi, J. Downward. Reduced NF1 expression confers resistance to EGFR inhibition in lung cancer. Cancer Discov. 4: 606-619 (2014).

[276] S.R. Whittaker, J.P. Theurillat, E. Van Allen, N. Wagle, J. Hsiao, G.S. Cowley, D. Schadendorf, D.E. Root, L.A. Garraway. A genome-scale RNA interference screen implicates NF1 loss in resistance to RAF inhibition. Cancer Discov. 3: 350-362 (2013).

[277] M. Boettcher, R. Tian, J.A. Blau, E. Markegard, R.T. Wagner, D. Wu, X. Mo, A. Biton, N. Zaitlen, H. Fu, F. McCormick, M. Kampmann, M.T. McManus. Dual gene activation and knockout screen reveals directional dependencies in genetic networks. Nat Biotechnol. 36: 170-178 (2018).

[278] A. Pearson, P. Proszek, J. Pascual, C. Fribbens, M.K. Shamsher, B. Kingston, B. O'Leary, M.T. Herrera-Abreu, R.J. Cutts, I. Garcia-Murillas, H. Bye, B.A. Walker, D. Gonzalez De Castro, L. Yuan, S. Jamal, M. Hubank, E. Lopez-Knowles, E.F. Schuster, M. Dowsett, P. Osin, A. Nerurkar, M. Parton, A.F.C. Okines, S.R.D. Johnston, A. Ring, N.C. Turner. Inactivating NF1 Mutations Are Enriched in Advanced Breast Cancer and Contribute to Endocrine Therapy Resistance. Clin Cancer Res. 26: 608-622 (2020).

[279] A.H. Smits, F. Ziebell, G. Joberty, N. Zinn, W.F. Mueller, S. Clauder-Münster, D. Eberhard, M. Fälth Savitski, P. Grandi, P. Jakob, A.-M. Michon, H. Sun, K. Tessmer, T. Bürckstümmer, M. Bantscheff, L.M. Steinmetz, G. Drewes, W. Huber. Biological plasticity rescues target activity in CRISPR knock outs. Nat Methods. 16: 1087-1093 (2019).

[280] T. Bachetti, D. Di Paolo, S. Di Lascio, V. Mirisola, C. Brignole, M. Bellotti, I. Caffa, C. Ferraris, M. Fiore, D. Fornasari, R. Chiarle, S. Borghini, U. Pfeffer, M. Ponzoni, I. Ceccherini, P. Perri. PHOX2B-Mediated Regulation of ALK Expression: In Vitro Identification of a Functional Relationship between Two Genes Involved in Neuroblastoma. PLoS One. 5: e13108 (2010).

[281] S.R. Whittaker, G.S. Cowley, S. Wagner, F. Luo, D.E. Root, L.A. Garraway. Combined Pan-RAF and MEK Inhibition Overcomes Multiple Resistance Mechanisms to Selective RAF Inhibitors. Mol Cancer Ther. 14: 2700-2711 (2015).

[282] P. Hou, C. Wu, Y. Wang, R. Qi, D. Bhavanasi, Z. Zuo, C. Dos Santos, S. Chen, Y. Chen, H. Zheng, H. Wang, A. Perl, D. Guo, J. Huang. A Genome-Wide CRISPR Screen Identifies Genes Critical for Resistance to FLT3 Inhibitor AC220. Cancer Res. 77: 4402-4413 (2017).

[283] K. Szlachta, C. Kuscu, T. Tufan, S.J. Adair, S. Shang, A.D. Michaels, M.G. Mullen, N.L. Fischer, J. Yang, L. Liu, P. Trivedi, E.B. Stelow, P.T. Stukenberg, J.T. Parsons, T.W. Bauer, M. Adli. CRISPR knockout screening identifies combinatorial drug targets in pancreatic cancer and models cellular drug response. Nat Commun. 9: 4275 (2018).

[284] J. Joung, S. Konermann, J.S. Gootenberg, O.O. Abudayyeh, R.J. Platt, M.D. Brigham, N.E. Sanjana, F. Zhang. Genome-scale CRISPR-Cas9 knockout and transcriptional activation screening. Nat Protoc. 12: 828-863 (2017).

[285] Y.H. Huang, O. Klingbeil, X.Y. He, X.S. Wu, G. Arun, B. Lu, T.D.D. Somerville, J.P. Milazzo, J.E. Wilkinson, O.E. Demerdash, D.L. Spector, M. Egeblad, J. Shi, C.R. Vakoc. POU2F3 is a master regulator of a tuft cell-like variant of small cell lung cancer. Genes Dev. 32: 915-928 (2018).

[286] J.G. Doench. Am I ready for CRISPR? A user's guide to genetic screens. Nat Rev Genet. 19: 67-80 (2018).

[287] K. Cichowski, T. Jacks. NF1 Tumor Suppressor Gene Function: Narrowing the GAP. Cell. 104: 593-604 (2001).

[288] G.L.G.-D. Pino, K. Li, E. Park, A.M. Schmoker, B.H. Ha, M.J. Eck. Allosteric MEK inhibitors act on BRAF/MEK complexes to block MEK activation. Proc Natl Acad Sci U S A. 118: e2107207118 (2021).

[289] T. Wang, J.J. Wei, D.M. Sabatini, E.S. Lander. Genetic Screens in Human Cells Using the CRISPR-Cas9 System. Science. 343: 80-84 (2014).

[290] O. Shalem, N.E. Sanjana, E. Hartenian, X. Shi, D.A. Scott, T. Mikkelson, D. Heckl, B.L. Ebert, D.E. Root, J.G. Doench, F. Zhang. Genome-scale CRISPR-Cas9 knockout screening in human cells. Science. 343: 84-87 (2014).

[291] V.A. Blomen, P. Májek, L.T. Jae, J.W. Bigenzahn, J. Nieuwenhuis, J. Staring, R. Sacco, F.R. van Diemen, N. Olk, A. Stukalov, C. Marceau, H. Janssen, J.E. Carette, K.L. Bennett, J. Colinge, G. Superti-Furga, T.R. Brummelkamp. Gene essentiality and synthetic lethality in haploid human cells. Science. 350: 1092-1096 (2015).

[292] T. Wang, K. Birsoy, N.W. Hughes, K.M. Krupczak, Y. Post, J.J. Wei, E.S. Lander, D.M. Sabatini. Identification and characterization of essential genes in the human genome. Science. 350: 1096-1101 (2015).

[293] T. Hart, M. Chandrashekhar, M. Aregger, Z. Steinhart, Kevin R. Brown, G. MacLeod, M. Mis, M. Zimmermann, A. Fradet-Turcotte, S. Sun, P. Mero, P. Dirks, S. Sidhu, Frederick P. Roth, Olivia S. Rissland, D. Durocher, S. Angers, J. Moffat. High-Resolution CRISPR Screens Reveal Fitness Genes and Genotype-Specific Cancer Liabilities. Cell. 163: 1515-1526 (2015).

[294] K. Tzelepis, H. Koike-Yusa, E. De Braekeleer, Y. Li, E. Metzakopian, O.M. Dovey, A. Mupo, V. Grinkevich, M. Li, M. Mazan, M. Gozdecka, S. Ohnishi, J. Cooper, M. Patel, T. McKerrell, B. Chen, A.F. Domingues, P. Gallipoli, S. Teichmann, H. Ponstingl, U. McDermott, J. Saez-Rodriguez, B.J.P. Huntly, F. Iorio, C. Pina, G.S. Vassiliou, K. Yusa. A CRISPR Dropout Screen Identifies Genetic Vulnerabilities and Therapeutic Targets in Acute Myeloid Leukemia. Cell Rep. 17: 1193-1205 (2016).

[295] B.C.S. Cross, S. Lawo, C.R. Archer, J.R. Hunt, J.L. Yarker, A. Riccombeni, A.S. Little, N.J. McCarthy, J.D. Moore. Increasing the performance of pooled CRISPR–Cas9 drop-out screening. Sci Rep. 6: 31782 (2016).

[296] J.-P. Capp, J. DeGregori, A.M. Nedelcu, A.M. Dujon, J. Boutry, P. Pujol, C. Alix-Panabières, R. Hamede, B. Roche, B. Ujvari, A. Marusyk, R. Gatenby, F. Thomas. Group phenotypic composition in cancer. Elife. 10: e63518 (2021).

[297] A.O. Pisco, S. Huang. Non-genetic cancer cell plasticity and therapy-induced stemness in tumour relapse: 'What does not kill me strengthens me'. Br J Cancer. 112: 1725-1732 (2015).

[298] S. Konermann, P. Lotfy, N.J. Brideau, J. Oki, M.N. Shokhirev, P.D. Hsu. Transcriptome Engineering with RNA-Targeting Type VI-D CRISPR Effectors. Cell. 173: 665-676.e614 (2018).

[299] M. Burmistrz, K. Krakowski, A. Krawczyk-Balska. RNA-Targeting CRISPR-Cas Systems and Their Applications. Int J Mol Sci. 21: 1122 (2020).

[300] A.V. Anzalone, P.B. Randolph, J.R. Davis, A.A. Sousa, L.W. Koblan, J.M. Levy, P.J. Chen, C. Wilson, G.A. Newby, A. Raguram, D.R. Liu. Search-and-replace genome editing without double-strand breaks or donor DNA. Nature. 576: 149-157 (2019).

[301] F.A. Ran, P.D. Hsu, C.Y. Lin, J.S. Gootenberg, S. Konermann, A.E. Trevino, D.A. Scott, A. Inoue, S. Matoba, Y. Zhang, F. Zhang. Double nicking by RNA-guided CRISPR Cas9 for enhanced genome editing specificity. Cell. 154: 1380-1389 (2013).

[302] X. Li, H.E. Francies, M. Secrier, J. Perner, A. Miremadi, N. Galeano-Dalmau, W.J. Barendt, L. Letchford, G.M. Leyden, E.K. Goffin, A. Barthorpe, H. Lightfoot, E. Chen, J. Gilbert, A. Noorani, G. Devonshire, L. Bower, A. Grantham, S. MacRae, N. Grehan, D.C. Wedge, R.C. Fitzgerald, M.J. Garnett. Organoid cultures recapitulate esophageal adenocarcinoma heterogeneity providing a model for clonality studies and precision therapeutics. Nat Commun. 9: 2983 (2018).

[303] S.L. George, E. Izquierdo, J. Campbell, E. Koutroumanidou, P. Proszek, S. Jamal, D. Hughes, L. Yuan, L.V. Marshall, F. Carceller, J.C. Chisholm, S. Vaidya, H. Mandeville, P. Angelini, A. Wasti, T. Bexelius, K. Thway, S.A. Gatz, M. Clarke, B. Al-Lazikani, G. Barone, J. Anderson, D.A. Tweddle, D. Gonzalez, B.A. Walker, J. Barton, S. Depani, J. Eze, S.W. Ahmed, L. Moreno, A. Pearson, J. Shipley, C. Jones, D. Hargrave, T.S. Jacques, M. Hubank, L. Chesler. A tailored molecular profiling programme for children with cancer to identify clinically actionable genetic alterations. Eur J Cancer. 121: 224-235 (2019).

[304] M.V. Zamaraeva, R.Z. Sabirov, E. Maeno, Y. Ando-Akatsuka, S.V. Bessonova, Y. Okada. Cells die with increased cytosolic ATP during apoptosis: a bioluminescence study with intracellular luciferase. Cell Death Differ. 12: 1390-1397 (2005).

[305] B.M. Kuenzi, L.L. Remsing Rix, P.A. Stewart, B. Fang, F. Kinose, A.T. Bryant, T.A. Boyle, J.M. Koomen, E.B. Haura, U. Rix. Polypharmacology-based ceritinib repurposing using integrated functional proteomics. Nat Chem Biol. 13: 1222-1231 (2017).

[306] T. Liu, M.D. Merguerian, S.P. Rowe, C.A. Pratilas, A.R. Chen, B.H. Ladle. Exceptional response to the ALK and ROS1 inhibitor lorlatinib and subsequent mechanism of resistance in relapsed ALK F1174L-mutated neuroblastoma. Cold Spring Harb Mol Case Stud. 7: a006064 (2021).

[307] I. Dagogo-Jack, A.T. Shaw. Tumour heterogeneity and resistance to cancer therapies. Nat Rev Clin Oncol. 15: 81-94 (2018).

[308] D.W. Cescon, S.V. Bratman, S.M. Chan, L.L. Siu. Circulating tumor DNA and liquid biopsy in oncology. Nat Cancer. 1: 276-290 (2020).

[309] I. Martincorena, K.M. Raine, M. Gerstung, K.J. Dawson, K. Haase, P. Van Loo, H. Davies, M.R. Stratton, P.J. Campbell. Universal Patterns of Selection in Cancer and Somatic Tissues. Cell. 171: 1029-1041 (2017).

[310] A.M. Cacace, M. Ueffing, A. Philipp, E.K. Han, W. Kolch, I.B. Weinstein. PKC epsilon functions as an oncogene by enhancing activation of the Raf kinase. Oncogene. 13: 2517-2526 (1996).

[311] H. Cai, U. Smola, V. Wixler, I. Eisenmann-Tappe, M.T. Diaz-Meco, J. Moscat, U. Rapp, G.M. Cooper. Role of diacylglycerol-regulated protein kinase C isotypes in growth factor activation of the Raf-1 protein kinase. Mol Cell Biol. 17: 732-741 (1997).

[312] Y. Ueda, S. Hirai, S. Osada, A. Suzuki, K. Mizuno, S. Ohno. Protein kinase C activates the MEK-ERK pathway in a manner independent of Ras and dependent on Raf. J Biol Chem. 271: 23512-23519 (1996).

[313] M. Dorel, B. Klinger, T. Mari, J. Toedling, E. Blanc, C. Messerschmidt, M. Nadler-Holly, M. Ziehm, A. Sieber, F. Hertwig, D. Beule, A. Eggert, J.H. Schulte, M. Selbach, N. Blüthgen. Neuroblastoma signalling models unveil combination therapies targeting feedback-mediated resistance. PLoS Comput Biol. 17: e1009515 (2021).

[314] S. Redaelli, M. Ceccon, M. Zappa, G.G. Sharma, C. Mastini, M. Mauri, M. Nigoghossian, L. Massimino, N. Cordani, F. Farina, R. Piazza, C. Gambacorti-Passerini, L. Mologni. Lorlatinib Treatment Elicits Multiple On- and Off-Target Mechanisms of Resistance in ALK-Driven Cancer. Cancer Res. 78: 6866-6880 (2018).

[315] S.E. Woodfield, L. Zhang, K.A. Scorsone, Y. Liu, P.E. Zage. Binimetinib inhibits MEK and is effective against neuroblastoma tumor cells with low NF1 expression. BMC Cancer. 16: 172 (2016).

[316] M.K. Dougherty, J. Müller, D.A. Ritt, M. Zhou, X.Z. Zhou, T.D. Copeland, T.P. Conrads, T.D. Veenstra, K.P. Lu, D.K. Morrison. Regulation of Raf-1 by direct feedback phosphorylation. Mol Cell. 17: 215-224 (2005).

[317] L. Lopez-Delisle, C. Pierre-Eugene, C. Louis-Brennetot, D. Surdez, V. Raynal, S. Baulande, V. Boeva, S. Grossetete-Lalami, V. Combaret, M. Peuchmaur, O. Delattre, I. Janoueix-Lerosey.

Activated ALK signals through the ERK-ETV5-RET pathway to drive neuroblastoma oncogenesis. Oncogene. 37: 1417-1429 (2018).

[318] T. Kurosaki, M.W. Popp, L.E. Maquat. Quality and quantity control of gene expression by nonsense-mediated mRNA decay. Nat Rev Mol Cell Biol. 20: 406-420 (2019).

[319] O.M. Enache, V. Rendo, M. Abdusamad, D. Lam, D. Davison, S. Pal, N. Currimjee, J. Hess, S. Pantel, A. Nag, A.R. Thorner, J.G. Doench, F. Vazquez, R. Beroukhim, T.R. Golub, U. Ben-David. Cas9 activates the p53 pathway and selects for p53-inactivating mutations. Nat Genet. 52: 662-668 (2020).

[320] H.Y. Shin, C. Wang, H.K. Lee, K.H. Yoo, X. Zeng, T. Kuhns, C.M. Yang, T. Mohr, C. Liu, L. Hennighausen. CRISPR/Cas9 targeting events cause complex deletions and insertions at 17 sites in the mouse genome. Nat Commun. 8: 15464 (2017).

[321] M. Kosicki, K. Tomberg, A. Bradley. Repair of double-strand breaks induced by CRISPR–Cas9 leads to large deletions and complex rearrangements. Nat Biotechnol. 36: 765-771 (2018).

[322] N.L. Malinin, G. Lee, C.R. Lazzarotto, Y. Li, Z. Zheng, N.T. Nguyen, M. Liebers, V.V. Topkar, A.J. Iafrate, L.P. Le, M.J. Aryee, J.K. Joung, S.Q. Tsai. Defining genome-wide CRISPR-Cas genome-editing nuclease activity with GUIDE-seq. Nat Protoc. 16: 5592-5615 (2021).

[323] A. Acar, D. Nichol, J. Fernandez-Mateos, G.D. Cresswell, I. Barozzi, S.P. Hong, N. Trahearn, I. Spiteri, M. Stubbs, R. Burke, A. Stewart, G. Caravagna, B. Werner, G. Vlachogiannis, C.C. Maley, L. Magnani, N. Valeri, U. Banerji, A. Sottoriva. Exploiting evolutionary steering to induce collateral drug sensitivity in cancer. Nat Commun. 11: 1923 (2020).

[324] V.K. Grolmusz, J. Chen, R. Emond, P.A. Cosgrove, L. Pflieger, A. Nath, P.J. Moos, A.H. Bild. Exploiting collateral sensitivity controls growth of mixed culture of sensitive and resistant cells and decreases selection for resistant cells in a cell line model. Cancer Cell Int. 20: 253 (2020).

[325] L.S. Hart, J. Rader, P. Raman, V. Batra, M.R. Russell, M. Tsang, M. Gagliardi, L. Chen, D. Martinez, Y. Li, A. Wood, S. Kim, S. Parasuraman, S. Delach, K.A. Cole, S. Krupa, M. Boehm, M. Peters, G. Caponigro, J.M. Maris. Preclinical Therapeutic Synergy of MEK1/2 and CDK4/6 Inhibition in Neuroblastoma. Clin Cancer Res. 23: 1785-1796 (2017).

[326] FDA-NIH Biomarker Working Group. Predictive Biomarker (2016). https://www.ncbi.nlm.nih.gov/books/NBK326791/ (last access 20 Oct 2021).

[327] J. Jing, J. Greshock, J.D. Holbrook, A. Gilmartin, X. Zhang, E. McNeil, T. Conway, C. Moy, S. Laquerre, K. Bachman, R. Wooster, Y. Degenhardt. Comprehensive Predictive Biomarker Analysis for MEK Inhibitor GSK1120212. Mol Cancer Ther. 11: 720-729 (2012).

[328] A.M. Dujon, A. Aktipis, C. Alix-Panabières, S.R. Amend, A.M. Boddy, J.S. Brown, J.-P. Capp, J. DeGregori, P. Ewald, R. Gatenby, M. Gerlinger, M. Giraudeau, R.K. Hamede, E. Hansen, I. Kareva, C.C. Maley, A. Marusyk, N. McGranahan, M.J. Metzger, A.M. Nedelcu, R. Noble, L.

Nunney, K.J. Pienta, K. Polyak, P. Pujol, A.F. Read, B. Roche, S. Sebens, E. Solary, K. Staňková, H. Swain Ewald, F. Thomas, B. Ujvari. Identifying key questions in the ecology and evolution of cancer. Evol Appl. 14: 877-892 (2021).

[329] S. Boumahdi, F.J. de Sauvage. The great escape: tumour cell plasticity in resistance to targeted therapy. Nat Rev Drug Discov. 19: 39-56 (2020).

[330] T. van Groningen, N. Akogul, E.M. Westerhout, A. Chan, N.E. Hasselt, D.A. Zwijnenburg, M. Broekmans, P. Stroeken, F. Haneveld, G.K.J. Hooijer, C.D. Savci-Heijink, A. Lakeman, R. Volckmann, P. van Sluis, L.J. Valentijn, J. Koster, R. Versteeg, J. van Nes. A NOTCH feed-forward loop drives reprogramming from adrenergic to mesenchymal state in neuroblastoma. Nat Commun. 10: 1530 (2019).

[331] M. Katoh, M. Katoh. Precision medicine for human cancers with Notch signaling dysregulation (Review). Int J Mol Med. 45: 279-297 (2020).

[332] R. Vander Velde, N. Yoon, V. Marusyk, A. Durmaz, A. Dhawan, D. Miroshnychenko, D. Lozano-Peral, B. Desai, O. Balynska, J. Poleszhuk, L. Kenian, M. Teng, M. Abazeed, O. Mian, A.C. Tan, E. Haura, J. Scott, A. Marusyk. Resistance to targeted therapies as a multifactorial, gradual adaptation to inhibitor specific selective pressures. Nat Commun. 11: 2393 (2020).

[333] L.A. Low, C. Mummery, B.R. Berridge, C.P. Austin, D.A. Tagle. Organs-on-chips: into the next decade. Nat Rev Drug Discov. 20: 345-361 (2021).

[334] J. Komen, S.M. van Neerven, A. van den Berg, L. Vermeulen, A.D. van der Meer. Mimicking and surpassing the xenograft model with cancer-on-chip technology. EBioMedicine. 66: 103303 (2021).

7 Publications

Original articles

M. Berlak[#], E. Tucker[#], M. Dorel, A. Winkler, A. McGearey, E. Rodriguez-Fos, B.M. da Costa, K. Barker, E. Fyle, E. Calton, S. Eising, K. Ober, D. Hughes, E. Koutroumanidou, P. Carter, R. Stankunaite, P. Proszek, N. Jain, C. Rosswog, H. Dorado-Garcia, J.J. Molenaar, M. Hubank, G. Barone, J. Anderson, P. Lang, H.E. Deubzer, A. Künkele, M. Fischer, A. Eggert, C. Kloft, A.G. Henssen, M. Boettcher, F. Hertwig, N. Blüthgen, L. Chesler, J.H. Schulte.

Mutations in ALK signaling pathways conferring resistance to ALK inhibitor treatment lead to collateral vulnerabilities in neuroblastoma cells.

Mol Cancer. 21: 126 (2022).

https://doi.org/10.1186/s12943-022-01583-z.

[#] shared first authorship; JIF: 41.4

Oral presentations

M. Berlak, J. Toedling, F. Klironomos, A. McGearey, A. Winkler, H. Dorado Garcia, A. Henssen, M. Dorel, N. Blüthgen, A. Künkele, H. Deubzer, M. Kirchner, P. Mertins, A. Eggert, F. Hertwig, C. Kloft, J. Schulte.

Activation of downstream signalling pathways is a mechanism of ALK inhibitor resistance in neuroblastoma.

Advances in Neuroblastoma Research (ANR) meeting 2021, virtual due to COVID-19 pandemic, 25-27 January 2021.

https://www.anr2022.org/resources/uploads/sites/26/2021/01/Programma-ANR2021-1.pdf, (2021).

M. Bock, K. Schönbeck, J. Toedling, F. Klironomos, S. Fuchs, P. Hundsdörfer, A. Eggert, F. Hertwig, J.H. Schulte.

Response and Resistance of ALK-mutated Neuroblastoma Cells to Ceritinib.

31. Jahrestagung der Kind-Philipp-Stiftung, Wilsede, Germany, 06-09 June 2018.

Klin Padiatr. 230: 169-169 (2018).

Conference abstracts

M. Bock, K. Schönbeck, J. Toedling, F. Klironomos, S. Fuchs, J. Rolff, A.G. Henssen, P. Hundsdörfer, A. Eggert, F. Hertwig, J.H. Schulte.

Response and Resistance of ALK-mutated Neuroblastoma Cells to Ceritinib.

"From Lab to Life" Childhood Cancer Research Initiatives (CCRI 2018), Vienna, Austria, 19-20 October 2018.

Abstractbook, No. 2018-A-67-CCRI, (2018).

M. Bock, K. Schönbeck, J. Toedling, F. Klironomos, S. Fuchs, J. Rolff, A.G. Henssen, P. Hundsdörfer, A. Eggert, F. Hertwig, J.H. Schulte.

Response and Resistance of ALK-mutated Neuroblastoma Cells to Ceritinib.

Advances in Neuroblastoma Research (ANR) meeting 2018, San Francisco, USA, 09-12 May 2018.

https://www.anrmeeting.org/dl/ANR2018/ANR_Abstract_Book_5-3-18.pdf, (2018).

8 Appendix

8.1 Supplementary figures

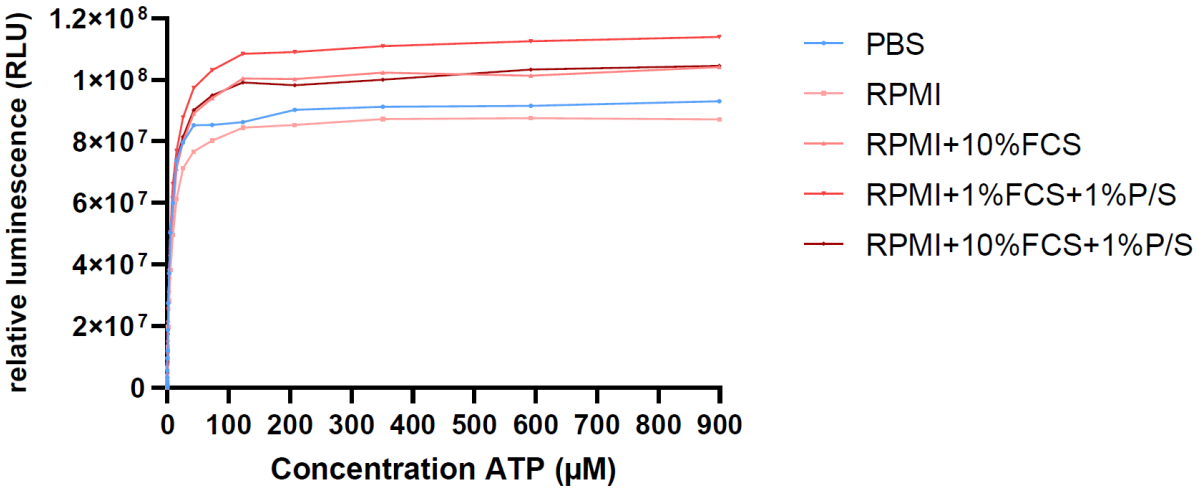

Figure 8.1 Quenching of relative luminescence resulting from a performed CellTiter-Glo® assay due to medium compositions was investigated. A range of adenosine triphosphate (ATP) concentrations was added to different medium of different compositions without or with penicillin/streptomycin (P/S) or foetal calf serum (FCS) and different concentrations of FCS. Phosphate-buffered saline (PBS) was used as a reference. The use of Roswell Park Memorial Institute (RPMI) medium or the addition of FCS or P/S did not quench relative luminescence, values represent mean ± SD, n=1.

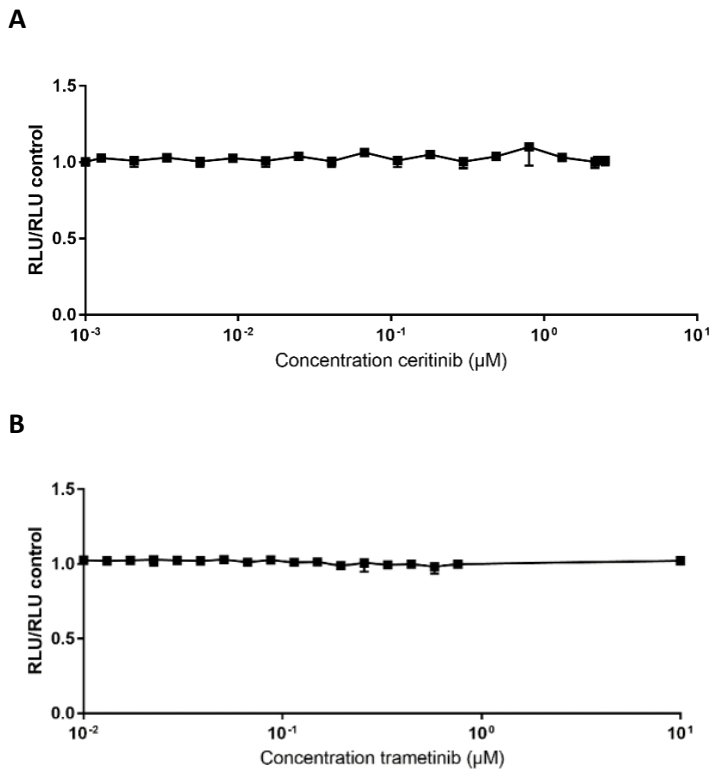

Figure 8.2 Quenching of relative luminescence resulting from a performed CellTiter-Glo® assay due compound addition was investigated. A range or ceritinib or trametinib concentrations was added to complete medium of the investigated cell line and relative luminescence measured. The signal was normalized to the reference which contained the complete medium without compound. Both investigated inhibitors, ceritinib and trametinib, did not quench the luminescence signal, values represent mean ± SD, n=1.

A

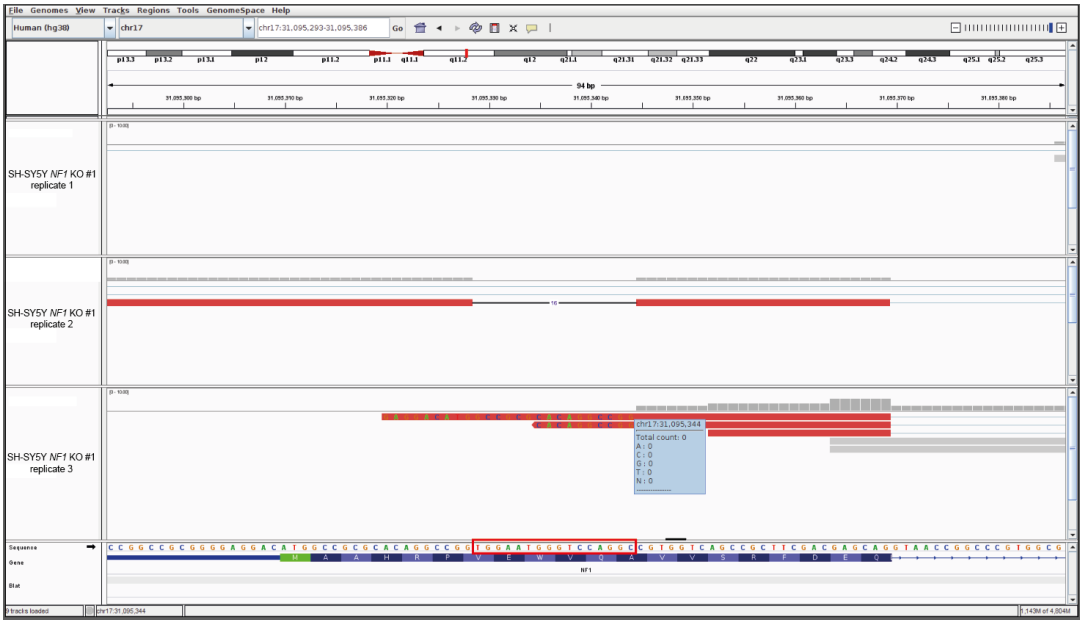

B

Figure 8.3 Detection of insertions or deletions (INDELS) in the *NF1* gene of isogenic *NF1* knockout cells due to Cas9 nuclease mediated double-strand breaks and non-homologous end joining (NHEJ). Sequencing reads of respective cell lines were investigated in exon 1 or 30 for expected INDELS, which were detected beforehand by sanger sequencing, using the integrative genomics viewer (IGV_2.8.2). **A** shows the sequencing reads of three biological replicates for the isogenic *NF1* knockout cell line SH-SY5Y *NF1* KO #1 in the chromosomal region indicated on the top (chromosome 17: 31,095,293 to 31,095,386). The reference sequence derived of the human reference genome, human genome build 38 (hg38), is shown below the three sequencing read panels and the mutated sequence of SH-SY5Y *NF1* KO #1 highlighted with a red box. **B** shows the sequencing reads of three biological replicates for the isogenic cell line SH-SY5Y *NF1* KO #2 in the chromosomal region chromosome 17: 31,249,065 to 31,249,119. As a reference sequence hg38 was used. Below the three sequencing read panels is the region of the mutated sequence highlighted with two red boxes, due to two different INDELS on each allele.

A

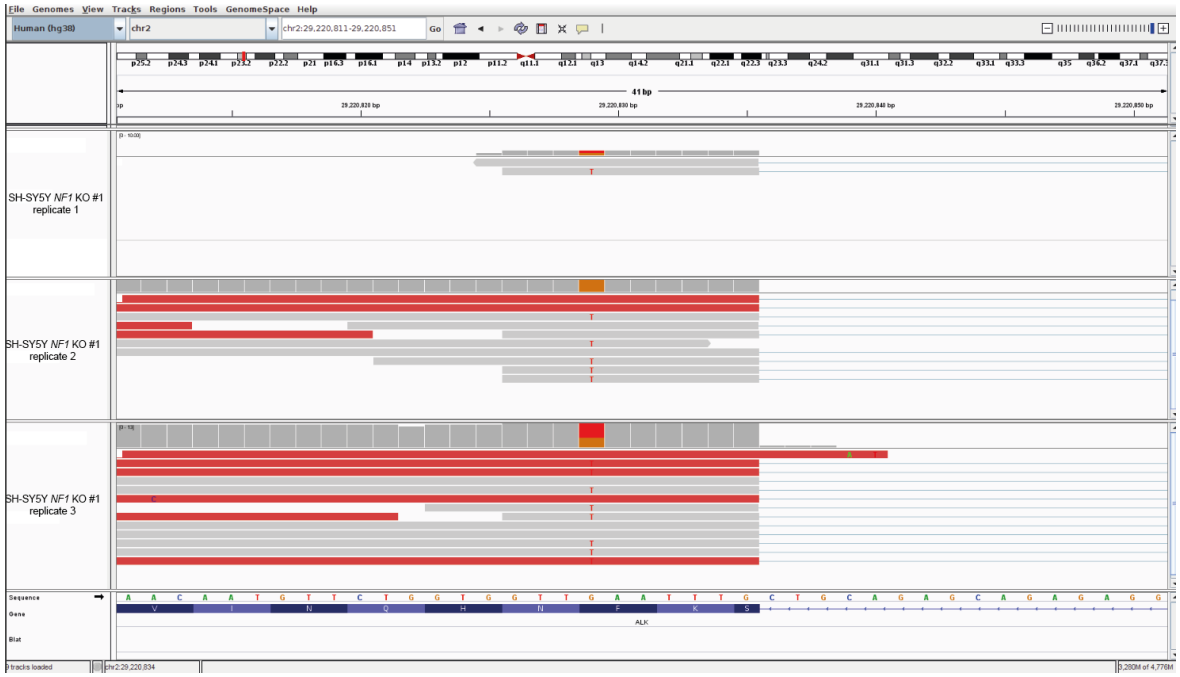

B

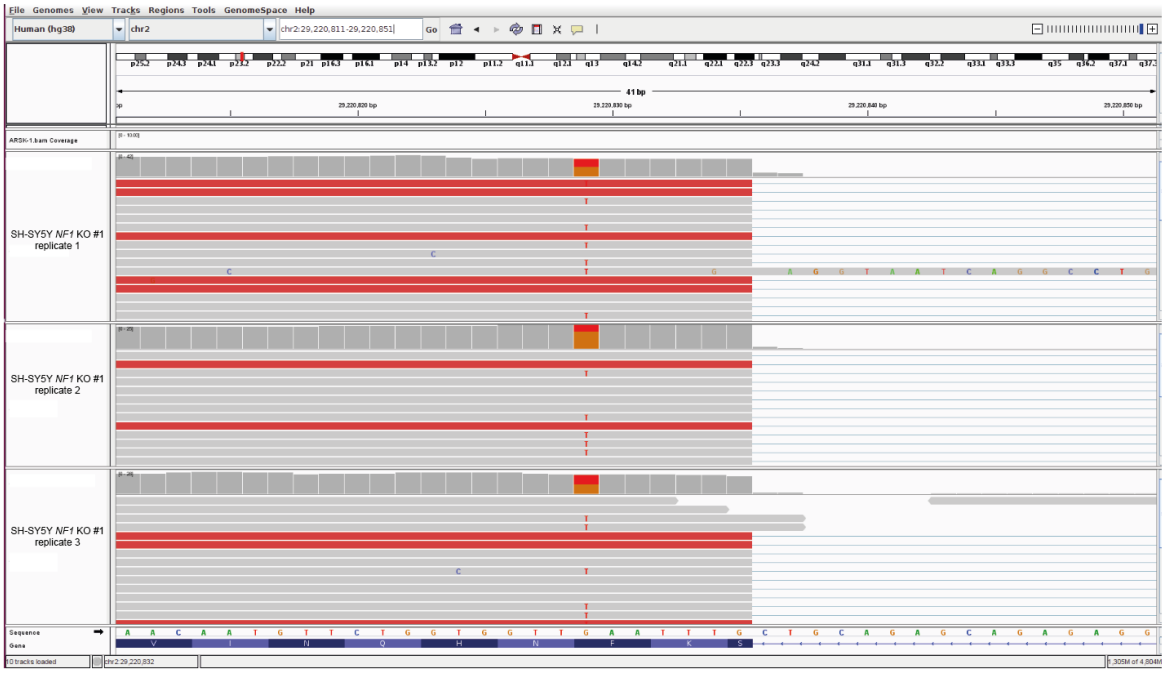

Figure 8.4 Investigation of ribonucleic acid (RNA) sequencing reads of SH-SY5Y *NF1* KO #1 and SH-SY5Y *NF1* KO #2 for anaplastic lymphoma kinase (ALK) mutated transcripts using the integrative genomics viewer (IGV_2.8.2). **A** shows the sequencing reads of three biological replicates for ALK transcripts of SH-SY5Y *NF1* KO #1 in the chromosomal region indicated on the top (chromosome 2: 29,220,811 to 29,220,851). The reference sequence derived of the human reference genome, human genome build 38 (hg38), is shown below the three sequencing read panels. Expected was the detection of a heterozygous *ALK* mutation where 3522 cytosine is mutated to adenine. Here the opposing strand is shown and therefore guanine is mutated to thymine. This mutation in *ALK* leads to an exchange of the amino acid phenylalanine 1174 to leucine. **B** shows the same as **A** just for SH-SY5Y *NF1* KO #2.

8.2 Tables

Table 8.1: Common genes with enriched sgRNAs in samples treated with different ALKis and corresponding β-scores (*P*-values cutoff <0.01) sorted by *P*-values for ceritinib sample.

Gen	β-score ceritinib	*P*-value ceritinib	β-score lorlatinib	*P*-value lorlatinib
C10orf126	2,63	0,000000	2,88	0,000367
MED30	2,69	0,000000	3,05	0,000157
SNRPF	2,64	0,000000	3,48	0,000052
UBA1	2,66	0,000000	2,93	0,000314
ZNHIT3	2,66	0,000000	2,90	0,000367
C16orf59	2,55	0,0000520	2,97	0,000262
ECD	2,43	0,0000520	2,10	0,00891
ELP4	2,44	0,0000520	2,85	0,000367
FDX1L	2,59	0,0000520	2,47	0,00204
GPN2	2,54	0,0000520	3,07	0,000157
KIAA0754	2,42	0,0000520	2,72	0,000733
NOL7	2,46	0,0000520	2,51	0,00168
RPS27	2,56	0,0000520	3,49	0,000052
ZNF626	2,42	0,0000520	3,11	0,000052
HSPA5	2,41	0,000105	3,19	0,000052
MRPL41	2,41	0,000105	3,56	0,000052
FOXRED1	2,35	0,000157	3,02	0,000210
NHLRC2	2,40	0,000157	2,82	0,000367
HIST1H2BL	2,31	0,000210	2,13	0,00749
MEPCE	2,25	0,000262	2,48	0,00194
C19orf52	2,21	0,000367	2,09	0,00906
CSHL1	2,22	0,000367	2,70	0,000733
NF1	2,19	0,000419	2,60	0,00110
OR7E24	2,20	0,000419	2,83	0,000367
PIAS3	2,20	0,000419	2,67	0,000838
CD3EAP	2,19	0,000471	3,09	0,000157
TSPAN17	2,19	0,000471	2,70	0,000733
SMARCD3	2,18	0,000524	2,81	0,000367
EIF2S3	2,18	0,000576	2,61	0,00110

AURKA	2,15	0,000629	2,41	0,00251
RAD50	2,15	0,000629	2,51	0,00168
RPL18A	2,15	0,000629	2,78	0,000471
DDB1	2,14	0,000681	2,96	0,000262
NUS1	2,13	0,000733	2,75	0,000576
C14orf80	2,12	0,000786	2,79	0,000419
C20orf27	2,13	0,000786	2,39	0,00262
NDUFA2	2,13	0,000786	2,80	0,000419
IFNGR2	2,11	0,00110	2,53	0,00152
MRPL50	2,11	0,00110	2,30	0,00346
CSK	2,08	0,00115	2,39	0,00262
FOS	2,09	0,00115	2,18	0,00650
KIF11	2,09	0,00115	2,20	0,00597
MRPL9	2,10	0,00115	2,60	0,00110
DDX42	2,08	0,00126	2,67	0,000838
CTR9	2,06	0,00141	2,37	0,00288
SLCO6A1	2,06	0,00141	2,46	0,00215
P3H1	2,01	0,00189	2,35	0,00309
ENTHD2	1,99	0,00210	2,68	0,000786
C19orf12	1,98	0,00225	2,47	0,00204
LMNTD2	1,99	0,00225	2,35	0,00309
RUVBL1	1,98	0,00225	2,41	0,00251
ATP13A1	1,97	0,00246	2,25	0,00461
MIPEP	1,96	0,00251	2,12	0,00786
EIF2B5	1,96	0,00257	2,22	0,00555
NDN	1,96	0,00257	2,53	0,00152
FITM2	1,95	0,00272	2,20	0,00582
ZBTB8OS	1,95	0,00278	2,35	0,00309
KRTCAP3	1,95	0,00288	2,26	0,00403
DNLZ	1,94	0,00293	2,30	0,00346
ACAD10	1,93	0,00314	2,23	0,00508
VARS	1,93	0,00314	2,98	0,000262
ZPR1	1,92	0,00330	2,28	0,00377
KIF1BP	1,91	0,00346	2,28	0,00377
NELL1	1,91	0,00346	2,61	0,00110

RC3H1	1,91	0,00346	2,71	0,000733
SPATA17	1,91	0,00346	2,44	0,00231
GBF1	1,90	0,00351	2,18	0,00650
GORASP2	1,90	0,00351	2,51	0,00168
KRT19	1,90	0,00351	2,22	0,00555
RPL38	1,91	0,00351	2,72	0,000733
NSFL1C	1,90	0,00362	2,09	0,00927
BACH1	1,88	0,00409	2,58	0,00121
DRAP1	1,88	0,00419	2,56	0,00121
PPA2	1,87	0,00419	2,09	0,00922
STMN4	1,88	0,00419	2,13	0,00733
SLC39A3	1,87	0,00435	2,50	0,00173
AIMP1	1,86	0,00445	2,17	0,00650
CEP85L	1,86	0,00445	2,13	0,00739
DDX11	1,85	0,00482	2,53	0,00157
CHMP3	1,82	0,00503	2,54	0,00136
PKN2	1,82	0,00503	2,17	0,00660
TBCA	1,82	0,00503	2,23	0,00482
TMEM40	1,82	0,00503	2,50	0,00173
HIST2H3D	1,81	0,00508	2,53	0,00152
GNB2L1	1,81	0,00513	2,31	0,00346
BANP	1,79	0,00550	2,26	0,00419
TBL1X	1,78	0,00571	2,21	0,00566
GRIN2A	1,78	0,00582	2,18	0,00634
GRIA3	1,77	0,00592	2,15	0,00697
KRBOX1	1,77	0,00613	2,26	0,00424
RPP21	1,77	0,00613	2,46	0,00204
PPIL4	1,76	0,00629	2,35	0,00309
PSMD11	1,76	0,00629	2,62	0,000995
USP1	1,76	0,00629	2,26	0,00424
HIRA	1,76	0,00634	2,29	0,00346
GNB1L	1,75	0,00655	2,14	0,00723
OSMR	1,75	0,00676	2,09	0,00922
TANGO6	1,74	0,00707	2,46	0,00215
PEX13	1,73	0,00723	2,15	0,00702

ETV4	1,72	0,00744	2,15	0,00723
RPS14	1,71	0,00760	2,84	0,000367
MYC	1,71	0,00796	2,17	0,00660
TMPRSS6	1,79	0,00828	2,30	0,00346
GRIN2D	1,69	0,00849	2,33	0,00341
TBC1D28	1,69	0,00849	2,10	0,00896
PDCD7	1,69	0,00875	2,17	0,00660
AKTIP	1,67	0,00948	2,44	0,00231
OGT	1,66	0,00959	2,76	0,000576
GOLGA6L2	1,66	0,00974	2,28	0,00377

Table 8.2: Results of a Gene Set Enrichment Analysis (GSEA) using the "c2" gene set listing gene sets enriched in the CRISPR knockout screen derived data.

Name	**NES**	**FDR q-val**	**FWER p-val**
REACTOME_MITOCHONDRIAL_TRANSLATION	2,37	0,00	0,00
REACTOME_TRANSLATION	2,33	0,00	0,00
REACTOME_NONSENSE_MEDIATED_DECAY_NMD	2,14	0,00	0,00
REACTOME_COMPLEX_I_BIOGENESIS	2,14	0,00	0,00
REACTOME_RESPIRATORY_ELECTRON_TRANSPORT	2,13	0,00	0,00
REACTOME_RESPIRATORY_ELECTRON_TRANSPORT_ATP_SYNTHESIS_BY_CHEMIOSMOTIC_COUPLING_AND_HEAT_PRODUCTION_BY_UNCOUPLING_PROTEINS	2,10	0,00	0,0100
REACTOME_MITOCHONDRIAL_TRNA_AMINOACYLATION	2,09	0,00	0,0100
REACTOME_SRP_DEPENDENT_COTRANSLATIONAL_PROTEIN_TARGETING_TO_MEMBRANE	2,09	0,00	0,0100
WP_MITOCHONDRIAL_COMPLEX_I_ASSEMBLY_MODEL_OXPHOS_SYSTEM	2,07	0,00	0,0200
REACTOME_EUKARYOTIC_TRANSLATION_INITIATION	2,06	0,00	0,0200

MALONEY_RESPONSE_TO_17AAG_DN	2,05	0,00	0,0200
BIOCARTA_EIF_PATHWAY	2,04	0,00	0,0300
WP_ELECTRON_TRANSPORT_CHAIN_OXPHOS_SYSTEM_IN_ MITOCHONDRIA	2,04	0,00	0,0300
REACTOME_REGULATION_OF_EXPRESSION_OF_SLITS_AND _ROBOS	2,03	0,00	0,0400
REACTOME_EUKARYOTIC_TRANSLATION_ELONGATION	2,03	0,00	0,0400
RHODES_CANCER_META_SIGNATURE	2,02	0,00	0,0600
REACTOME_TRNA_AMINOACYLATION	2,00	0,00	0,0800
SCHLOSSER_MYC_TARGETS_REPRESSED_BY_SERUM	2,00	0,0100	0,0900
BIOCARTA_PROTEASOME_PATHWAY	1,99	0,0100	0,100